NASA CONTRACTOR REPORT

NASA CR-231

NASA CR-231

DESIGN, DEVELOPMENT, AND FABRICATION OF A SEALED, BRUSHLESS DC MOTOR

Prepared under Contract No. NAS 5-3582 *by*
SPERRY FARRAGUT COMPANY
Bristol, Tenn.
for

NATIONAL AERONAUTICS AND SPACE ADMINISTRATION • WASHINGTON, D. C. • MAY 1965

NASA CR-231

DESIGN, DEVELOPMENT, AND FABRICATION OF A SEALED, BRUSHLESS DC MOTOR

Prepared under Contract No. NAS 5-3582 by
SPERRY FARRAGUT COMPANY
Bristol, Tenn.

for

NATIONAL AERONAUTICS AND SPACE ADMINISTRATION

For sale by the Clearinghouse for Federal Scientific and Technical Information
Springfield, Virginia 22151 – Price $4.00

ACKNOWLEDGMENT

This project has been a cooperative undertaking between the Goddard Space Flight Center and Sperry Farragut Company. The primary responsibility for this work was assigned to Sperry Farragut, but appreciable technical assistance was contributed by Goddard Space Flight Center. Particular acknowledgment is made of the helpful suggestions, checking and special testing contributed by Mr. Philip A. Studer, of Goddard.

CONTENTS

CONTENTS

ILLUSTRATIONS

ILLUSTRATIONS

TABLES

SECTION I

SUMMARY

23143

This final report describes a program, sponsored by Goddard Space Flight Center, to develop and produce a compact, hermetically sealed, brushless motor with true DC motor characteristics.

In this motor, photo-optical detectors and transistorized switches perform the functions of the conventional commutator without physical contact. The rotor is a permanent magnet. Hermetic sealing of the stator and commutator compartments was specified to eliminate the possibility of bearing contamination by outgassing, in hard-vacuum environments, from insulating materials, plastics, and solder fluxes. The motor also features a rotor-bearing assembly that can be removed as a unit from the front of the motor without disturbing its remaining components.

Design goals included a reduction in over-all size to approximately one-third of the volume of a three-watt motor produced previously by Sperry Farragut Company under Contract No. NAS 5-2832. The achieved reduction in volume, to 36.5 percent of that of the previous motor, closely approached the design goal. Also included was a requirement for sufficient improvement in efficiency to offset most of the losses incurred by sealing the motor. The original requirement of 45 percent minimum efficiency was vastly exceeded in the new design, so that the efficiency obtained now exceeds that of a good AC induction motor of comparable performance. Furthermore, the reliability of the motor was to be at least 95 percent for one year. A predicted reliability in excess of 95 percent for one year was achieved as required.

SECTION II

PRINCIPLES OF OPERATION OF MOTORS DEVELOPED ON THIS PROGRAM

These brushless DC motors use a permanent magnet rotor for field excitation and a slotted stator with a conventional direct current winding. The current in each coil of the armature winding is reversed cyclically by a solid-state power-switching network, exactly duplicating conventional commutation.

Figure 1 is a block diagram of an elementary brushless DC motor. The three coils represent a two-pole armature winding which normally would use three commutator segments. The blocks A, B, C, etc. represent six equally spaced, photoelectric devices which conduct current only when illuminated. The aperture in the light shield spans 120 degrees and always illuminates two adjacent photoelectric devices. When the light beam impinges on photoelectric devices A and B, current flows in the path of the solid arrows. This produces a magnetic field in the armature that is in space quadrature with respect to the field of the rotor and also is in the position in which maximum torque is exerted on the rotor. As the rotor turns, the light beam moves with it until photo devices B and C are illuminated. The current now flows in the direction of the broken arrows in Figure 1, and the armature field again is in space quadrature with respect to the rotor field. This process continues and the rotor accelerates as in a conventional DC motor.

The circuit of Figure 1 is functional, but the armature current is limited by the relatively small current capacity of presently available photoelectric devices. To overcome this limitation, the blocks A, B, C, etc. are in reality high-current, solid-state, switching circuits driven by the photo devices.

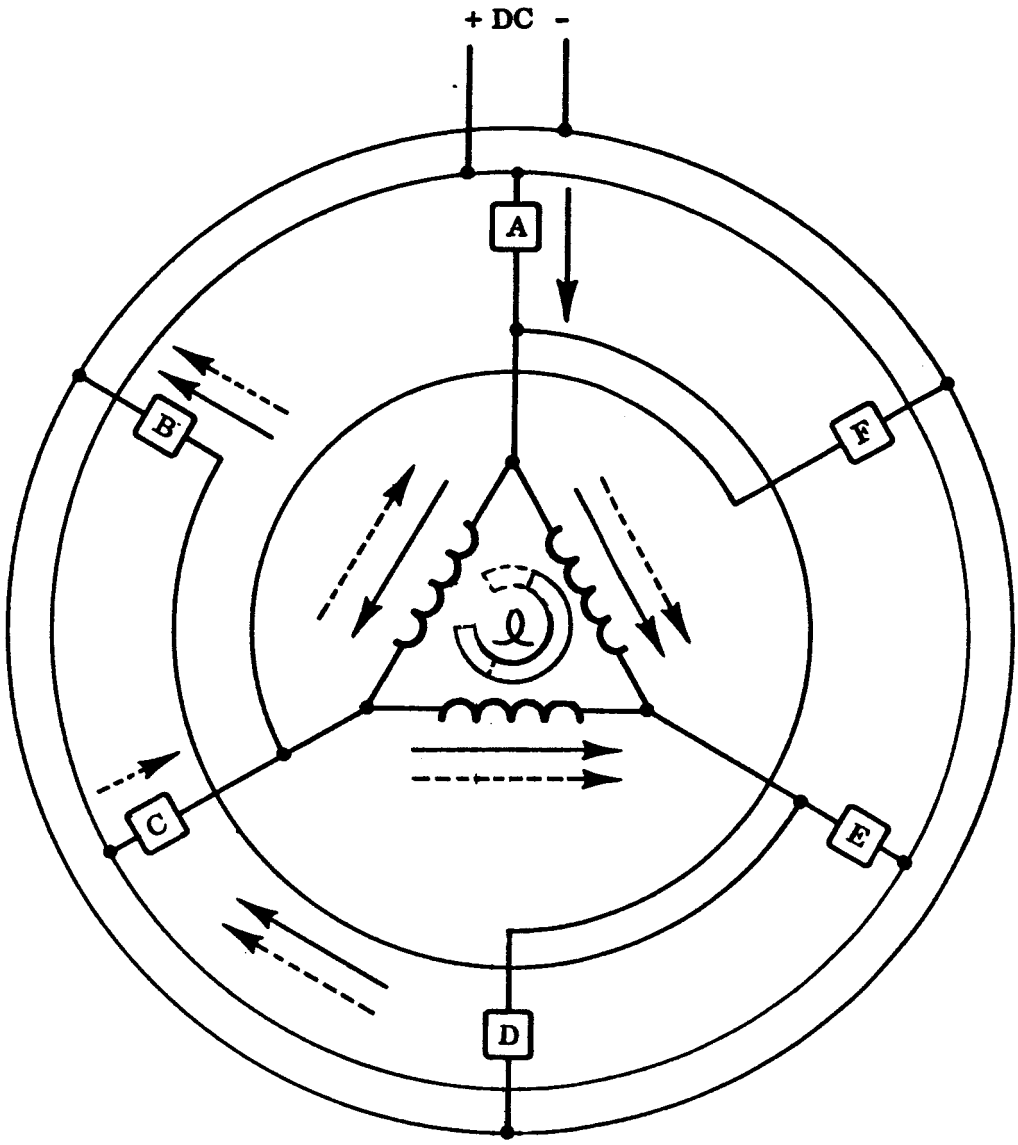

FIGURE 1
BLOCK DIAGRAM OF BASIC CIRCUIT
FOR A BRUSHLESS DC MOTOR

Figure 2 is a simplified schematic of the solid-state circuits associated with blocks A and B of Figure 2. The circuit of Figure 2 represents essentially one-third of the total circuitry required for a complete motor.

The number of stages required for any particular motor is a function of current-switching requirements of the last stage, forced h_{fe} of each device, and current output from the photo-sensor. Each stage is driven into saturation. This results in maximum operational reliability, minimum series voltage drop within the motor, and maximum efficiency/weight ratios.

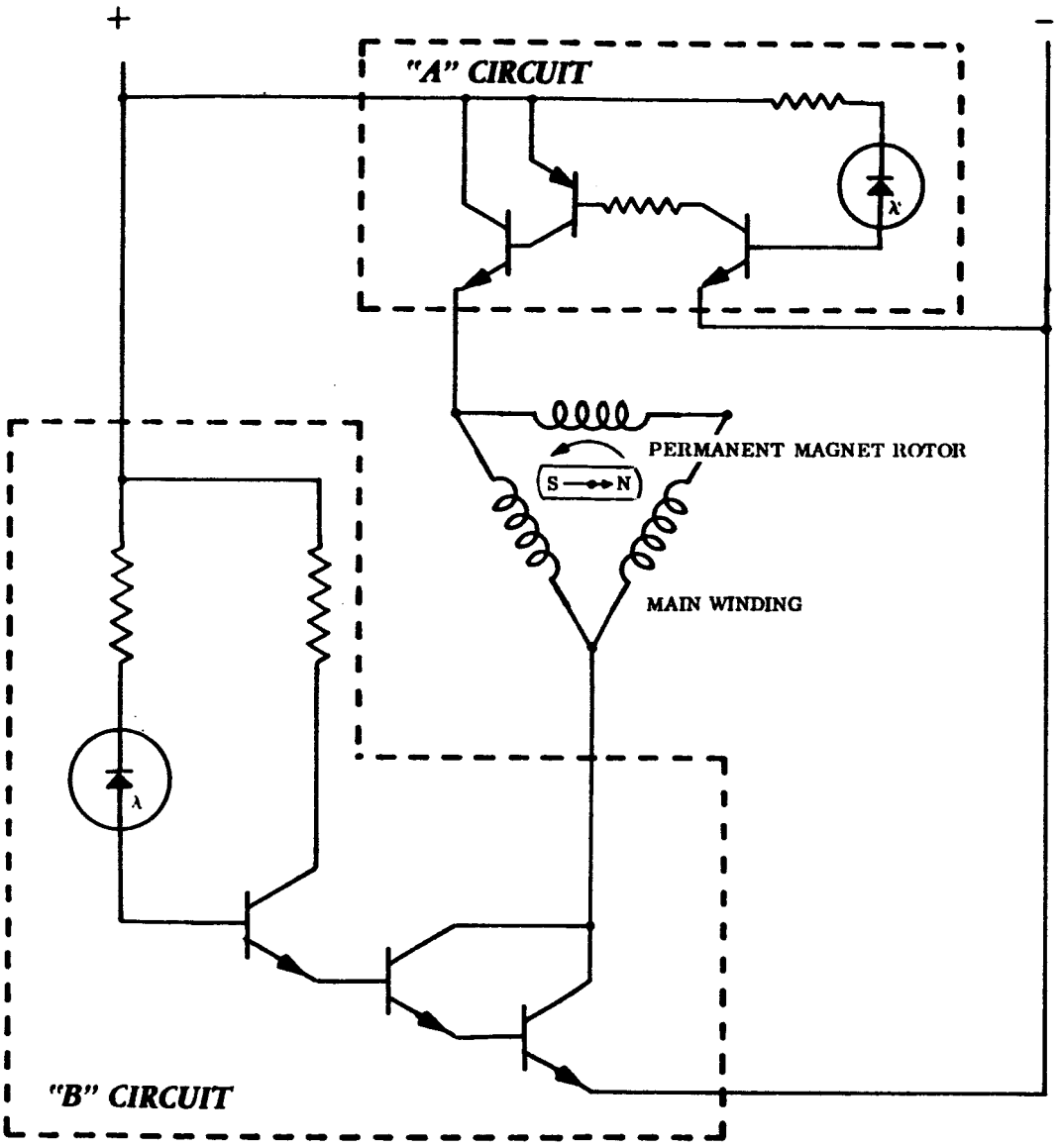

FIGURE 2

SIMPLIFIED COMMUTATING CIRCUIT

SECTION III

STATEMENT OF WORK

A. SCOPE

Phase I: Motor design and development leading to a motor of maximum efficiency and simplicity with the capability of being hermetically sealed.

Phase II: Manufacture of six motors and delivery to Goddard Space Flight Center.

B. TECHNICAL REQUIREMENTS

The following were the original technical requirements of the contract. Deviations agreed to by Goddard Space Flight Center are discussed later in this report.

1. Motor Operational Parameters

Rated Speed:	3000 RPM
Input Voltage:	24 VDC (nominal)
Torque:	The motor was to be capable of being wound for outputs from 0.05 in-oz. to 0.3 in-oz. at 3000 RPM.

2. Motor Design Characteristics

   a. The motor was to be brushless, employ no mechanical contact between stator and rotor, and exhibit true characteristics of a conventional permanent-magnet type (shunt) DC motor.

   b. The electronic commutator was to employ a minimum of components and a conservative derating practice.

   c. The commutation design was to be versatile to permit production of motors with operating speeds from 500 to 10,000 RPM.

d. Optimum circuit packaging techniques were to be employed to minimize size.

e. Optional means were to be provided for completely sealing the stator of the motor to prohibit outgassing from insulating materials, plastics, and solder fluxes.

3. General Specifications

The following specifications applied originally to all motors to be delivered under the contract.

a. Size: As small as possible, not to exceed 1.25" in diameter by 2.5" long. (See paragraph IV.A.1).

b. Weight: As lightweight as possible, not to exceed 8 oz.

c. Commutation: A commutation angle of 60^{o} to 90^{o} was required (for the commutator design envisioned). (See paragraph IV.A.2).

d. Noise: AF and accoustical noise were to be minimized.

e. Environment:

(1) The motors were to operate properly after 50 g, 2 millisecond shock and 5 minutes of random vibration (20 to 2000 cps, 15 g rms) in each of 3 mutually perpendicular planes.

(2) The motors were to operate properly over an ambient temperature range of $-10^{o}C$ to $+70^{o}C$.

(3) The motors were to be capable of operating in a vacuum of 1×10^{-9} mm Hg for a one-year period.

f. All motors were to be capable of withstanding stall current without damage.

g. The motors were to employ SR-2 instrument bearings. (See paragraph IV. A. 3.)

h. The rotors were to be dynamically balanced to reduce undetermined loads on the bearings.

i. Means were to be provided for applying a selectable axial preload from 0 to 1 pound on the outer race of the bearing.

4. Detailed Specifications

Originally, the Sperry Farragut Company was required to design, develop, fabricate, and deliver to Goddard Space Flight Center six brushless DC motors with the following specifications. (See paragraph IV. A. 4.)

a. Two motors as follows:

(1) Torque: 0.27 in-oz. at 3000 RPM

(2) Efficiency: 60% minimum at 3000 RPM

(3) Unsealed stator and solid-state switching system

b. Two motors as follows:

(1) Torque: 0.2 in-oz. at 3000 RPM

(2) Efficiency: 45% minimum at 3000 RPM

(3) Motors to be hermetically sealed except for rotor and bearings.

c. Two motors as follows:

(1) Torque: 0.1 in-oz at 3000 RPM

(2) Efficiency: 45% minimum at 3000 RPM

(3) Motors to be hermetically sealed except for rotor and bearings.

5. Reliability

Reliability was to be maximized by reduction of the number of active components, conservative derating and elimination of components of questionable reliability. A reliability of 95% for an operational life of one year (calculated value based upon accepted component failure rates) was required.

C. SCHEDULE

Delivery of six motors was to be made within eight months from award of contract.

D. DOCUMENTATION

The following documentation was required:

1. Monthly progress reports, each including the design approach, calculations data, and performance.

2. Prints and a reproducible copy of all such drawings as would be made to permit the construction of engineering prototypes.

3. A final report summarizing the advantages and disadvantages of the various design approaches considered and detailing the performance characteristics of the prototype hardware.

SECTION IV

PERFORMANCE OF WORK

A. DEVIATION FROM ORIGINAL SPECIFICATIONS

1. Size

   By using modular miniaturization techniques, major circuit redesign, and demanding minimum package size from each electronic component vendor; Sperry Farragut Company, with invaluable technical assistance from Goddard Space Flight Center was able to produce a motor that met the original requirements for weight and diameter. However, the required length of 2.5 inches was exceeded by 0.25 inches. It would have required a very expensive program and many non-standard components and techniques to have achieved the 0.25-inch reduction in motor length.

2. Commutation Angle

   As the design of the electronic commutator evolved, circuit modifications made mandatory a change in commutation angle from 60^{o} to 120^{o}.

3. Bearings

   Size SR166 instrument bearings were substituted for the smaller sized SR2 bearings called for in the purchase specifications, primarily for ease in assembling the rotor assembly. This ultimately makes rapid bearing substitutions and changes feasible. To use the SR2 bearing would necessitate the removal of the cup which surrounds the lamp each time the bearings were changed.

4. Detailed Specifications

When the original detailed specifications were agreed upon, it was assumed that the efficiency of the 1-watt motors would be around 60 percent without hermetic sealing and 45 percent with sealing. Thus, Goddard Space Flight Center asked for two unsealed 1-watt motors and 2 sealed 1-watt motors. When breadboard tests showed that a substantially higher efficiency could be obtained in a sealed motor, the detailed specifications for the 1-watt motors (see paragraph III. B. 4. a and b) were changed to read: "Four motors shall be supplied as follows:

a. Torque output at 3000 RPM: 25 in-oz.

b. Efficiency at 3000 RPM: 55% minimum

c. Motors to be hermetically sealed except for rotors and bearings."

5. Schedule

The problems encountered in achieving hermetic sealing in each motor made it necessary for Sperry Farragut Company to request a thirty-day postponement of the required delivery date. This was granted, and the new delivery date was met.

B. DEVELOPMENT OF MOTOR

1. Stator

a. Core Laminations

(1) The preliminary design of the core lamination incorporated an increase in slot area from the value of 0. 0198 square inches used in the three-watt motor (NASA Contract NAS 5-2832) to 0. 0326 square inches. This was

made possible by a reduction in the thickness of the wall of the motor housing from 0.060 to 0.030 inch.

(2) This design change was followed by a further increase in slot area of ten percent, approximately. This accompanied a reduction in the wall thickness of the housing to 0.015 inch, which was made possible by a change of material from aluminum to type 303 stainless steel.

(3) When the rotor material was changed from Alnico V to Alnicus USM-75, with its relatively high energy product, it became possible to decrease the outside diameter of the rotor and thus the inside diameter of the stator. Because the original outside diameter of the stator was retained, the decrease in inside diameter gave a further increase in the slot area.

As a result of the three increases in slot area mentioned above, along with changes in the winding configuration that required fewer inductors to achieve the same CEMF, the inductor wire size was increased and the number of turns was decreased to improve efficiency.

A further increase in efficiency was obtained by changing the lamination material from silicone steel to nickel iron and then reducing the thickness of each lamination. The reduction in core losses attributable to this material change was approximately four percent.

All of the changes described above combined to reduce core losses at 3000 RPM from 1.90 watts in the three-watt motor to 1.55 in the one-watt motor and to 0.95 watts in the half-watt motor. Figure 3,

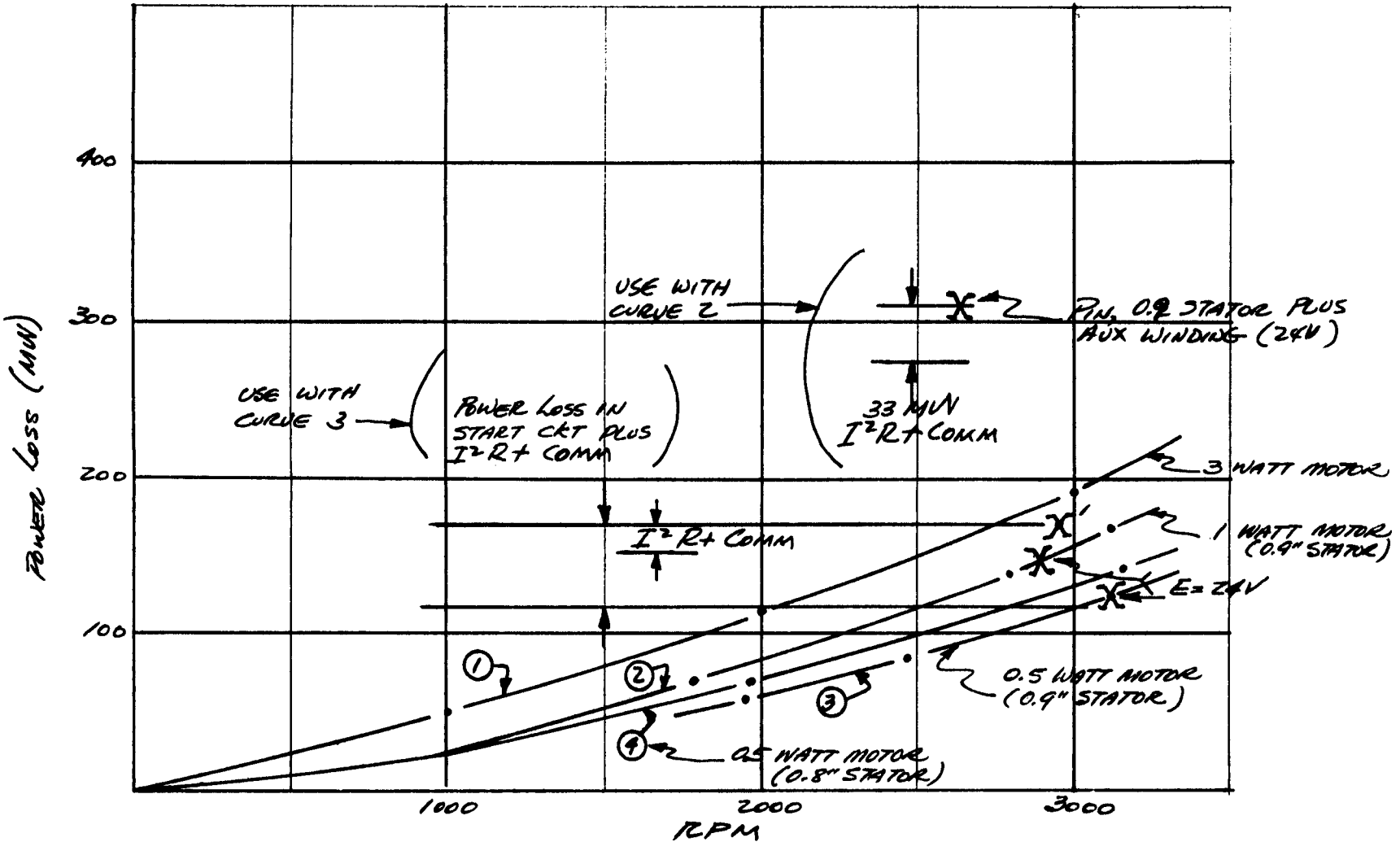

FIGURE 3
SUMMARY OF POWER LOSSES

Stator Lamination

Finished O. D. = 1.192

Finished I. D. = 0.385

Tooth Width b_t = 0.060

Core Width h_c = 0.115

Slot Opening b_o = 0.030

B_g = 4.5 kilogauss (measured maximum air gap flux density)

$$T_{sg} = \frac{\pi D}{12} = \frac{385\pi}{12} = 0.101 \text{ slot pitch}$$

$$B_t = \frac{T_{sg} B_g}{b_t} = \frac{0.101 \times 4.5}{0.06} = 7.6 \text{ kilogauss tooth density}$$

$$B_c = \frac{DB_g}{2h_c} = \frac{0.385 \times 4.5}{2 \times 0.115} = 7.54 \text{ kilogauss core density}$$

Assume g = 0.007 air gap

Carter Factor -

$$K_c = \frac{T_{sg}(5g + b_o)}{T_{sg}(5g + b_o) - b_o^2} = 1.16$$

TABLE 1

MOTOR LAMINATION PARAMETERS

"Evaluation of Power Losses" shows typical values of the various losses in the three motors. Details of the lamination configuration are presented in Table 1.

b. Choice of Main Winding Configuration

A detailed analytical evaluation of various winding techniques is presented in Appendix I, entitled "Armature Winding Analysis for a Brushless DC Motor". The highlights are summarized below, using equation numbers utilized in the Appendix.

The average induced voltage and the effective resistance for the three different windings are:

Ring Winding

(14) $E_{DC} = \frac{Z\phi S}{60} \sin\frac{5\pi}{12} \times 10^{-8}$ volts

(18) $R_{DC} = \frac{\rho L_c}{12A_s}\left(\frac{Z^2}{4}\right) \times 10^{-8}$ ohms

Wye Winding

(25) $E_y = \sqrt{3}\,\frac{Z\phi S}{60} \sin\frac{5\pi}{12} \times 10^{-8}$ volts

(26) $R_y = \frac{\rho L_c}{12A_s}\left(\frac{2Z^2}{3}\right) \times 10^{-8}$ ohms

where Z = total inductors
ϕ = flux
S = speed
ρ = resistivity
L_c = inductor length
A_s = slot area
A_c = coil area

Delta Winding

(28) $E_\Delta = \frac{Z\phi S}{60} \sin\frac{5\pi}{12} \times 10^{-8}$ volts

(29) $R_\Delta = \frac{\rho L_c}{12A_s}\left(\frac{Z^2}{3}\right) \times 10^{-8}$ ohms, per phase

or $R_\Delta = \frac{\rho L_c}{12A_s}\left(\frac{2Z^2}{9}\right) \times 10^{-8}$ ohms between any two terminals

From the analytical study, equations for the earlier motor (3 watts, 6 segments, ring winding) can be reduced to:

$$E_{DC} = \frac{Z\phi S}{60} \sin 75^{o} \times 10^{-8} \text{ volts}$$

and

$$R_{DC} = \frac{\rho L_c}{A_c} \left(\frac{Z}{4}\right) \text{ ohms.}$$

In particular

$Z = 3000$

$Z_s = 250$

$R_{DC} =$ 61 ohms (copper windings)

Using the above equations, R_Δ can now be computed as a ratio which yields:

$$\frac{R_\Delta}{R_{DC}} = \frac{\frac{2}{9}}{\frac{1}{4}} = \frac{2}{9} \times \frac{4}{1} = \frac{8}{9} \text{ from which}$$

$$R_\Delta = \frac{8}{9} \times 61 = 54.2 \text{ ohms}$$

Since the resistance is decreased approximately 11 percent by going to a delta winding from a ring winding certainly the IR drop will decrease and E_Δ will increase. From $E_\Delta = \frac{Z\phi S}{60} \sin 75^{o} \times 10^{-8}$ volts, it can be seen if Z and ϕ do not change then S should increase. Other questions to be answered were: What happens to total motor efficiency, speed-torque curve, power output, etc. ?

To physically evaluate the effect of the delta winding versus the ring winding, Test No. 9 was run (see Figure 4). Test No. 9 should be compared to Test No. 8, shown in Figure 5, which represents duplicate test conditions except the winding change. From this test it was concluded that:

(1) Total efficiency of the motor did not change.

(2) The delta winding provides a slightly higher speed motor for given torque load, thus a slightly higher power output.

(3) Design for future motors, whether ring wound or delta wound, will utilize similar analyses, keeping in mind the effective 11 percent reduction in effective resistance resulting from the delta winding.

(4) The delta winding approach would reduce the total number of electronic components by approximately 50 percent with no appreciable change in commutator characteristics. Figure 6 is a schematic diagram of the delta winding.

Another important conclusion was reached early in the analytical winding investigation. This is shown on pages 1 through 3 of Appendix I. In summary, it shows that a chorded method of winding reduces the effective resistance of the winding approximately 10 percent below the previously used full pitch method.

Continuing with the winding investigation, the following computations were made:

TEST DATA
BRUSHLESS DC MOTOR

Serial No. BREADBOARD
Input Voltage 24

TESTED BY R. KINCER / CARTER TEST DATE 10-24-63

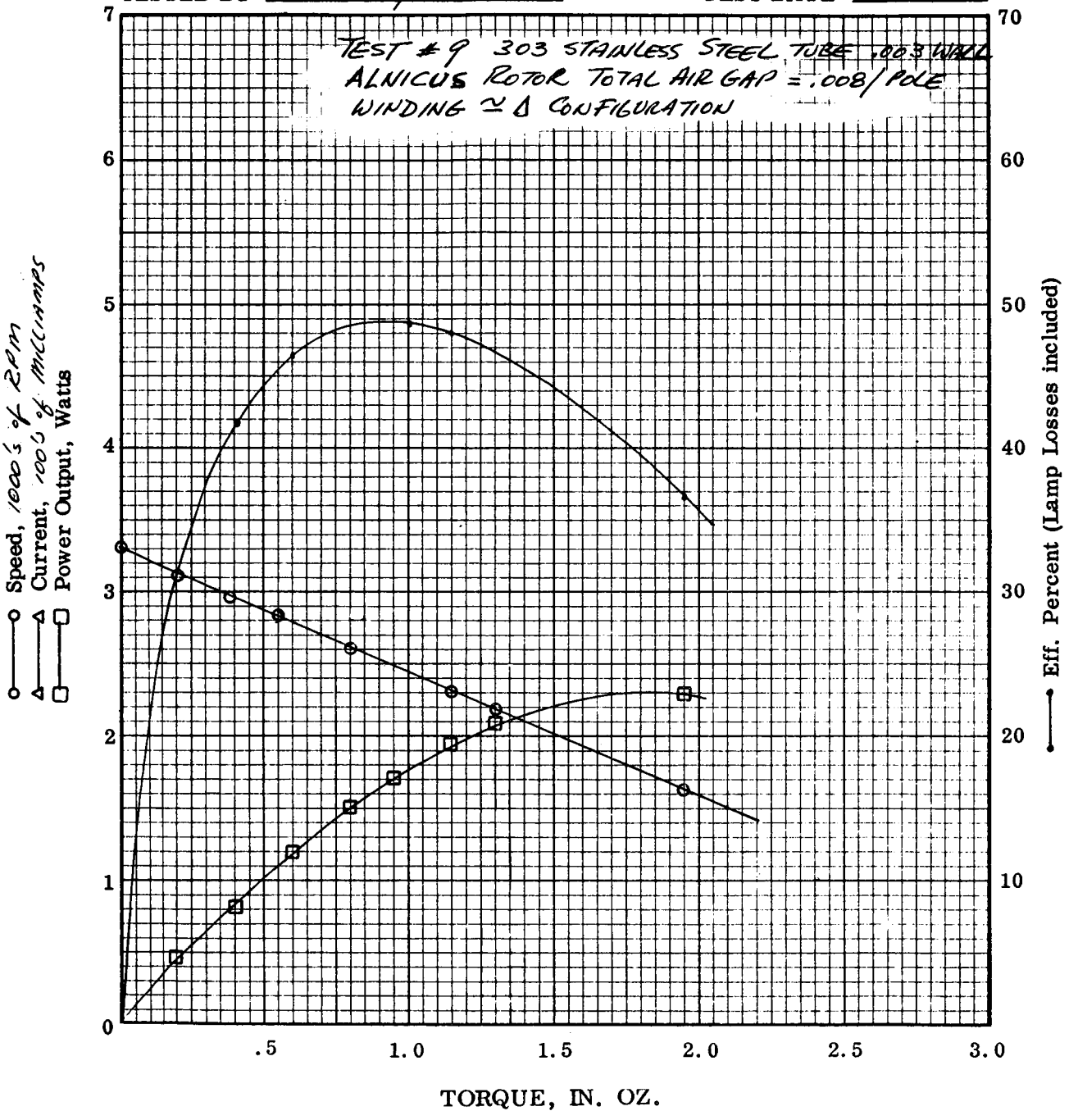

FIGURE 4

TEST DATA
BRUSHLESS DC MOTOR

Serial No. BREADBOARD
Input Voltage 24

TESTED BY R KINCER / CARTER TEST DATE 10-21-63

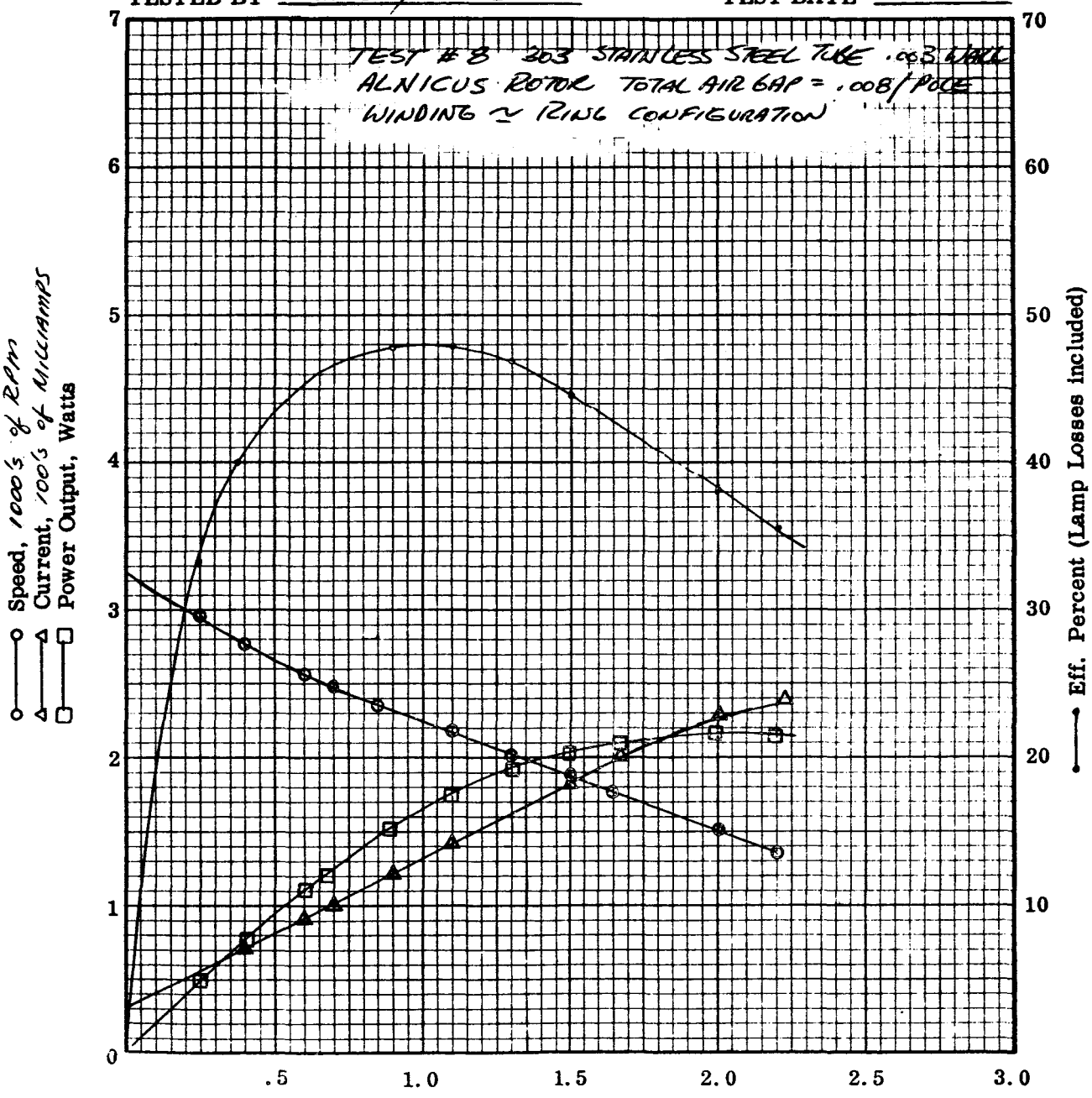

FIGURE 5

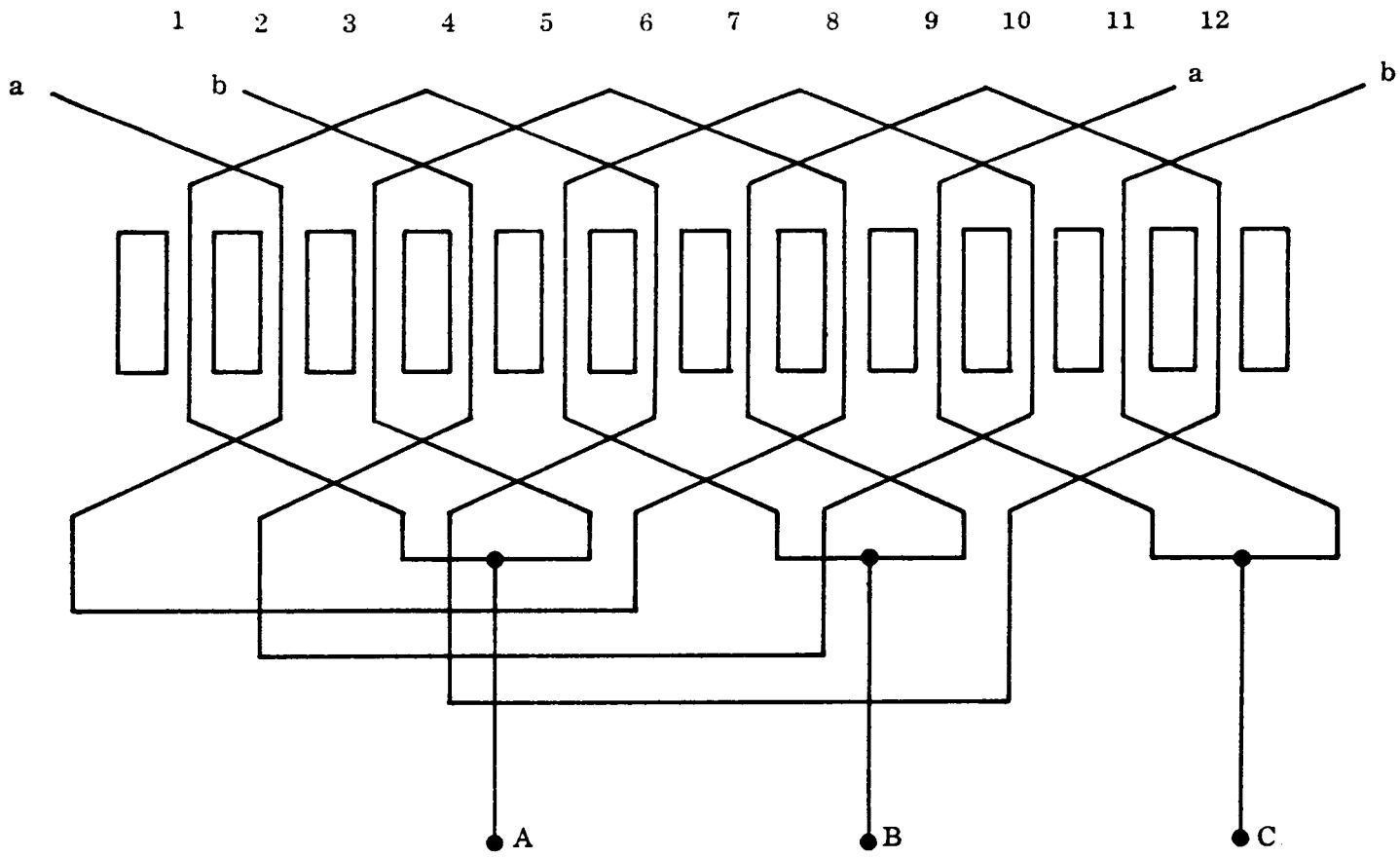

FIGURE 6
DELTA CONNECTED ARMATURE WINDING

Analytically, equations for the wye-wound chorded motor have been proven to be

$$(25)\quad E_y = \sqrt{3}\ \frac{Z\phi S}{60}\ \sin\ 75^{o} \times 10^{-8} \text{ volts}$$

$$(26)\quad R_y = \frac{\rho P L_c}{12 A_s}\left(\frac{2}{3}\ Z^2\right) \times 10^{-8} \text{ ohms}$$

Note that these equations differ from the delta-wound, chorded motor in two details:

(1) The motor equation shows the CEMF to be higher by a factor of $\sqrt{3}$.

(2) The resistance has increased by a factor of 3.

To obtain the same CEMF from the wye-wound motor, the total inductors must be decreased by $\sqrt{3}$ or $\frac{250}{\sqrt{3}}$ = 144 inductors/slot assuming ϕ = constant. Likewise, it would be desirable to reduce the effective resistance to that of the chorded delta-wound motor of 49 ohms. This value of 49 ohms takes into account a reduction in effective resistance as a result of using the chorded method for winding and also winding in delta. To obtain this exact value of effective resistance the wire size would need to be between #32 and #33 AWG. Physically, 144 inductors of #32 wire would not fit into the slot and for this reason #33 AWG was chosen. Schematically, the motor was wound as shown in Figure 7. Calculations show the effective resistance to be 52.6 ohms.

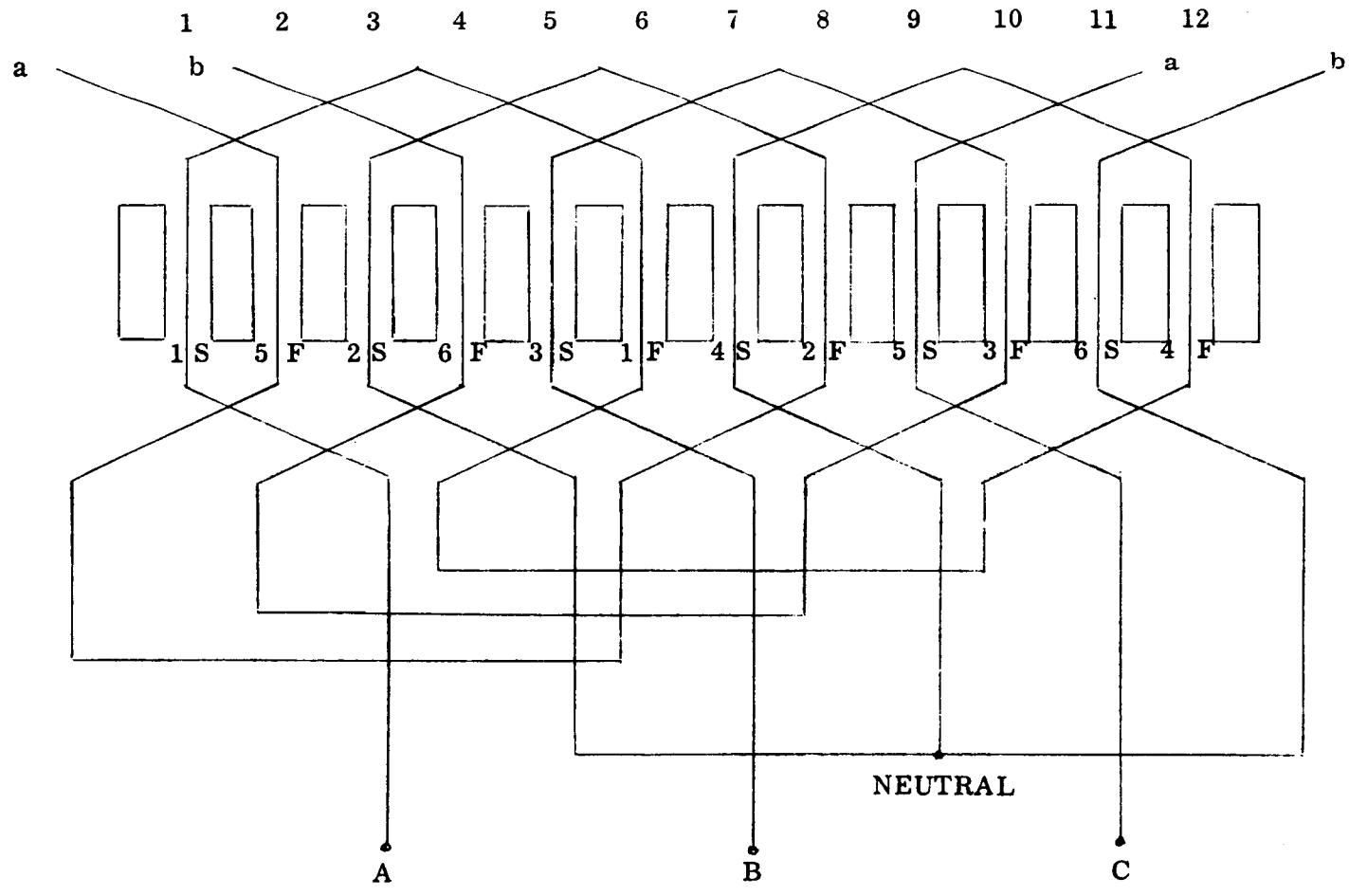

FIGURE 7
WYE-CONNECTED ARMATURE WINDING

Test no. 10 was run to verify the above analysis. See Figure 8 and note the test conditions:

(1) Resistance (effective) equals that computed above.

(2) An Alnico V rotor was used.

(3) Length of gap, lg = 0.0105 in./pole.

(4) No tube (for sealing purposes) was in the air gap.

Resulting from the usage of Alnico V with its relatively lower coercive force, Hc (relative to that of Alnicus 75) and the large lg, the motor was a higher speed motor; this was anticipated. Of particular interest, however, was the loss in total efficiency η_+. From data collected earlier, an increase in η_+ was anticipated.

The chorded-delta winding was selected as the most suitable for the motors for this contract because of its higher CEMF.

c. Auxiliary Winding

For reasons stated in paragraph IV. B. 3. c, it was necessary to add an auxiliary winding that would generate sufficient current to switch out the starting circuit when the motor attained approximately half of rated speed, and to supply enough current to the lamp to give adequate brilliance under no load at rated speed. Using Faraday's Law for DC motors it was determined that 60 turns of #39 magnet wire would be satisfactory. Heavy Formvar insulation was used.

TEST DATA
BRUSHLESS DC MOTOR

Serial No. BREADBOARD
Input Voltage 24

TESTED BY R. KINCER & CARTER TEST DATE 10-28-63

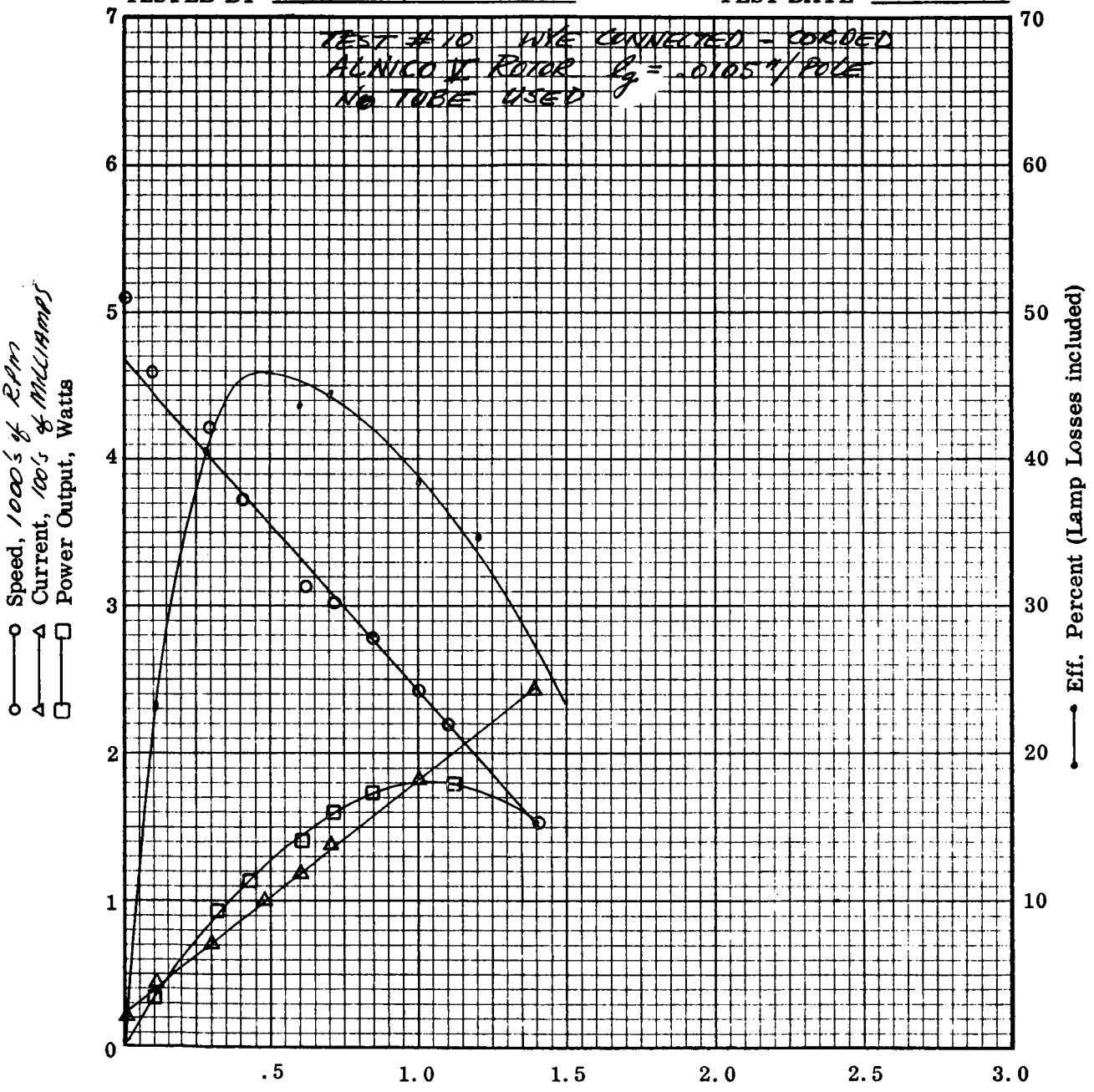

TORQUE, IN. OZ.

FIGURE 8

2. Rotor

a. Material

As recommended by GSFC, Alnicus USM-75 was used for the rotors of the one-watt and half-watt motors instead of Alnico V, which was used in the earlier three-watt motors (NASA Contract NAS 5-2832). The Alnicus has a much higher energy product, residual induction and coercive force than Alnico V, as shown in Table 2.

Property	Alnicus USM-75	Alnico V
Nominal Energy Product, BH maximum, in millions of Gauss-oersteds	7.5	5.5
Residual Induction, B_r, in Gauss	13,900	12,700
Coercive Force, H_c, in Oersteds	740	650
Density (lbs. per cu. in.)	0.265	0.265
Mechanical Properties	Hard, Brittle	Hard, Brittle

TABLE 2
COMPARISON BETWEEN ALNICUS USM-75 AND ALNICO V

As a result, a higher flux density was obtainable without an increase in rotor size. Thus, it was possible to use a larger air gap leaving room for a nichrome tube for hermetic sealing and possibly reducing hysteresis losses and cogging. Even with the larger air gap, the field strength, B, for these motors was essentially that of the earlier 3 watt design. With B fixed and a much larger slot area available, (see paragraph IV. B. 1. a) it was possible to use larger diameter inductors and fewer turns. This was done, decreasing copper losses and increasing efficiency.

Platinum-cobalt was investigated for use as a rotor material also. Although it had over three times the coercive force of Alnicus USM-75 (2,650 vs. 740 oersteds) it had a much lower remanence (4,530 vs. 13,900 gauss). This would adversely affect winding losses in the stator even if the laminations were redesigned for a low flux density. The next paragraph outlines another consideration relating to the use of Platinum-cobalt for the rotor.

An analysis was made of the eddy current losses and accompanying demagnetizing magnetomotive force in the thin nichrome cylinder used to seal off the rotor. (See Appendix I, "DC Brushless Motor with a Metallic Armature Sleeve".) It showed that the added demagnetizing mmf. was small enough to make unnecessary the use of a rotor with a very high coercive force. Although the above-mentioned analysis was prepared for the motor of contract NAS 5-2832, all parameters used applied to this contract except for bore length, which has been reduced by 10%.

b. Shape and Size

The shape and size of the rotor are the same as were used in the earlier 3-watt motor except that the diameter across the pole faces is approximately 0.010 inch smaller in the half-watt motor.

c. Construction

Because Alnicus USM-75 is a hard, but brittle material, a continuous shaft was used to support it. This still left a sufficient volume of Alnicus to provide the necessary flux densities. The method selected for fixing the shaft in the rotor was very simple. An oversized hole,

eloxed through the axis of the cast rotor, was cast full of lead and then drilled for a press fit to the shaft. The shaft was pressed into that hole until its shoulder butted against the rotor. This shoulder was staked into a groove eloxed in the adjacent end of the rotor, and a retaining collar was pressed onto the opposite end. The staking was made necessary by the high shearing stress created between shaft and rotor during the grinding operation on the rotor.

Each rotor was made slightly oversize and "ground-to-order" to give the motor the required speed-torque characteristic. The common center of curvature of the pole faces was not shifted from the axis of the rotor during this operation, so the flux distribution pattern remained sinusoidal. (See "Recommendations.")

d. Preloading

(1) Preloading of the bearings is essential if the lowest practicable level of rotor unbalance is to be obtained.

(2) The rotor is dynamically balanced to leave less than 50×10^{-6} in-oz. of unbalance. The radial play of each bearing before preloading is 0.0001 to 0.0002 inches. Since the rotor weighs 16 grams, the minimum unbalance is given approximately by:

$$\text{Unbalance} = (3.5 \times 10^{-2} \text{ oz.})(0.0002 \text{ in.}) = 7.0 \times 10^{-6} \text{ in-oz.}$$

(3) Bearing preload is to be adjusted by turning a No. 5/8-56 adjusting nut on the front of the motor. The preload nut bears on a Beryllium-copper wavy spring washer. It will develop 3.06 lbs. of preloading,

maximum, if turned through its full range of one turn. Calculations show that the preload will change by 0.316 lbs. in response to a temperature change of 80°C (the maximum ambient temperature change specified for the motor). Before shipment, each motor has its bearing preload set to a nominal pressure of one pound. The resulting power loss is approximately 24 milliwatts at 3,000 RPM.

3. Solid-state Commutator

a. Choice of Lamp and Light Sensor

The search for a suitable combination of lamp and light-sensor for the solid-state electronic commutator yielded many frustrations and revealed that the arts of lamp design, manufacture, and quality control were lagging those of many other electronic components. Conspicuous by their absence were vendor specifications adequate for rendering precise reliability predictions. Seven lamps and four light sensors were investigated:

Lamps: No. 2 (Cal-Glo)

No. 3 (Lamps, Inc.)

327-AS-15 (Chicago Miniature Lamps, Inc.)

546-070-2 (American Cystoscope Makers, Inc.)

540-039 (American Cystoscope Makers, Inc.)

L15-45 (Kay Electric)

No. 9 (Lamps, Inc.)

Sensors: L7A, P-N-P-N Light-triggered Switch (G. E.)

LS400 N-P-N Planar Silicon Photo Device (Texas Inst.)

LS600 N-P-N Planar Silicon Light Sensor (Texas Inst.)

P102 Photosensitive Field-effect Transistor (Siliconix, Inc.)

The following are capsule summaries of Sperry Farragut's findings on this topic:

(1) The L15-45 lamp was investigated for use with the L7A switch. A review of tests made by GSFC showed satisfactory operation at room temperature, but insufficient lamp candlepower for operation 0.1 inch from the sensor at the 0.9 volts operating level required to give the lamp the desired life expectancy. A very thorough study (involving about one man-month of work) was made to see if the P102 sensor could be used with this lamp or if any other useful approach could be found to utilize either the L7A or the P102 as a sensor. No such approach was found. The P102 did prove to be a good field-effect transistor with reasonably low pinch-off voltage when light was prevented from entering its lens, but it required a high resistance in the circuit and current drain through a Zener diode to hold the FET at the required biasing point. The resulting packaging problem and power loss were prohibitive.

(2) The 327-AS-15 lamp was used successfully with the T1-LS400 switch in the earlier 3-watt motors, but consumed excessive power for use in the 1-watt motor, where it would have prevented the attainment of satisfactory efficiency.

(3) The L15-45 lamp was tested in a breadboard motor with the LS400 switch, but each lamp drew too much current for use in series with the stator winding at low torque loading.

(4) The 546-070-2 lamp was tested, but required excessive current also. It was suitable in all other respects.

(5) The 540-039 lamp drew a sufficiently low current for use in series with the stator winding, but was marginal in light output and very unreliable. Since it was operated at 68 percent of its rated voltage, it should have given 96 percent reliability for 10,000 hours, according to the vendor's published data. However, 3 out of 5 of these lamps tested by Sperry Farragut failed after operating for five minutes or less and thus were rejected.

(6) The No. 2 lamp (Cal-Glo) according to Lamps, Inc., is the same as the No. 3 lamp (Lamps, Inc.). See below.

(7) The No. 3 lamp was tested extensively in breadboard motors with the LS400 and LS600 switches at various lamp-to-sensor spacings and in various environments. It was satisfactory from all aspects except reliability (see "Lamp Reliability Tests" below).

(8) Lamp No. 9 had the same envelope size as lamp No. 3, but was rated at 5 volts rather than 1.5 volts. As indicated under "Lamp Reliability Tests" below, the No. 9 lamp showed excellent reliability even at 6.5 volts under all applicable environmental conditions. It was tested extensively in breadboard motors with LS600 sensors with circuit modifications to handle its high current demand. It proved to be excellent in all respects except for its adverse effect on the over-all efficiency of the motor, but the loss in efficiency was considered an acceptable "price" to pay for high reliability. This lamp was selected for use in the deliverable motors.

(9) The CM8-666 lamp was tested in a breadboard motor with the LS600 sensor and performed satisfactorily except for its high current requirement, which exceeded that of the No. 9 lamp, and its loss of candlepower in the accelerated life test (see "Lamp Reliability Tests" below).

(10) The possibility of using a gamma-sensitive GM counter tube as a means of sensing rotor position does exist, but the cost and time required to develop such a system was prohibitive for this program. If, in the future, the need should arise for a low-powered motor such that a saving of 50 milliwatts of power is badly needed, such a system could be developed by Ampex Electronic Corporation, the only one of 10 vendors contacted who submitted a quotation in response to a query from Sperry Farragut Company.

b. Lamp Reliability Tests

(1) Summary

(a) Lamp No. 3

Static tests at room temperature revealed that insufficient control was being exercised over the production of this lamp to give uniform quality and long life. Thus it was rejected without further testing. Similar tests made earlier by Goddard Space Flight Center confirmed these findings.

(b) Lamp No. 9

This lamp showed no failures in static tests at room temperature or elevated temperatures and no failures in dynamic tests at

room temperature. These results were in line with the manufacturer's rating of 100,000 hours life expectancy at 5 volts. Operation of this lamp at 1.1 volts in the deliverable motors is expected to result in a highly reliable light source.

(c) Lamp No. CM8-666

This lamp showed no catastrophic failures in an accelerated life test at room temperature under static conditions. However, all samples developed blackened envelopes and thus an excessive reduction in candlepower. Although operation at 1.1 volts instead of 6.5 volts might produce no noticeable darkening of the envelope in the period of one year, this risk could not be taken and the lamp was rejected without further testing.

(2) Life Tests on Lamp No. 3 (Lamps, Inc.)

(a) Selection and Test

Sperry Farragut subjected 37 of these lamps to static "accelerated" life tests at 2.5 volts at room temperature. They were divided into three lots: Group A - 8 that the vendor claimed were superior.

Group B - 8 others that Sperry Farragut judged to be superior on the basis of microscopic inspection, taken from a lot of 30 purchased expressly for life testing.

Group C - 21 of those remaining from the lot of 30.

These 37 lamps were run in parallel until 76 percent had failed (85.47 hours).

Goddard Space Flight Center subjected 25 No. 3 lamps to static life tests at 2.3 volts at room temperature with no prior microscopic examination. These lamps were run in parallel until 76 percent had failure (94.3 hours).

(b) Failure Rates

Failure rates for the above lamps at 2.5 volts, which is the voltage applied to the lamps during the accelerated life tests, were calculated from the mean time between failures in the test sample by means of Poisson's equation: $R_t = e^{-tr}$

where R_t = % reliability for t hours of operation (i.e. reliability figure), and r = failure rate at voltage V_M used in motor.

The projected failure rates, as they would be at voltages that might be used in the motor, were calculated using the following equation:

$$\text{Failure Rate at } V_M = \left(\frac{V_M}{V_A}\right)^{12} \times \text{Failure Rate at } V_A$$

where V_M = Voltage considered for use in motor

and V_A = Voltage at which accelerated life test was conducted.

These projected failure rates are listed in Table 3 below. As indicated by the test data of Table 4, those lamps that were preselected on the basis of better workmanship did not give better performance. Group A and B combined had as many failures as Group C, and fewer samples.

Test data obtained from Goddard Space Flight Center are shown in Table 5.

Group	Projected Failure Rate in Percent per 1000 Hours				"Accelerated Test Voltage	No. in Group
	@ 1.45 volts	@ 1.4 volts	@ 1.25 volts	@ 1.10 volts		
A		4.55	1.10	0.2405	2.5	8
B & C		1.44	0.352	0.0761	2.5	16
A, B & C		1.46	0.356	0.0772	2.5	37
GSFC	4.725					

TABLE 3

PROJECTED FAILURE RATES OF NO. 3 LAMPS (LAMPS, INC.)

(3) Life Tests on Lamp No. 9 (Lamps, Inc.)

(a) Static Tests at Room Temperature

Eight lamps were operated continuously in parallel at 6.5 volts for 268 hours. Forty more were operated continuously in parallel at 2.3 volts for 264 hours. None of the 48 lamps failed.

Applied Voltage - 2.5 volts	
Failure No.	Time To Failure Hours
7A	9.58
7C	11.50
3A	12.58
1A	13.58
8A	21.33
6A	21.91
1B	28.83
2A	39.58
17C	46.24
3C	46.74
5B	48.07
18C	55.83
20C	61.41
12C	61.49
2C	61.57
14C	62.57
6B	64.73
11C	65.31
4C	66.15
4B	66.48
7B	66.48
19C	68.40
2B	68.82
8B	68.98
13C	69.56
3B	78.81
8C	85.06
15C	85.47
28 Lamps	

TABLE 4

SPERRY FARRAGUT COMPANY LIFE TEST DATA
FOR NO. 3 LAMPS (LAMPS, INC.)

Applied Voltage - 2.3 Volts	
1	0.6
2	3.2
3	9.8
4	16.7
5	23.0
6	30.7
7	32.6
8	38.2
9	41.5
10	41.7
11	42.2
12	53.5
13	53.8
14	58.2
15	75.7
16	84.7
17	87.0
18	88.4
19	94.3

TABLE 5

GODDARD LIFE TEST DATA
FOR NO. 3 LAMPS (LAMPS, INC.)

(b) Vibration

The 48 lamps were vibrated in two mutually perpendicular planes at frequencies ranging from 15 to 2000 cps at a constant acceleration of 50 g. The lamps were submitted to three 10-minute vibration cycles with the lamps operating at 5 volts and to three 10-minute cycles with the lamps off. No failures occurred.

(c) Shock

With no voltage applied, the 48 lamps were subjected to 50 g shocks in two mutually perpendicular planes for 0.5 milliseconds per plane. No failures occurred.

(d) Temperature

Following the shock test, the 48 lamps were subjected to an ambient temperature of 88°C for 15 minutes while operating at 5.0 volts. No failures occurred.

(4) Life Tests on Lamp No. CM 8-666 (Chicago Miniature Lamps, Inc.)

A static test at room temperature was conducted on fifteen of these lamps. They were operated at 6.5 volts for 265.8 hours. Although there were no catastrophic failures, all were considered to have suffered major failures because their envelopes blackened and their candlepower dropped correspondingly. Thus, this type of lamp was rejected without further tests.

(5) Reliability Failure Rate for Lamp No. 9

A reliability failure rate for the No. 9 lamp of 0.075 percent for 1,000 hours of operation at 1.4 volts has been assigned by Sperry Farragut Reliability Engineering Department. This value is very conservative and was based on engineering judgment in the light of the lack of failures during the accelerated life tests.

c. Starting Circuit

(1) The need for designing the starting circuit for these motors was determined by several of the essential lamp characteristics. These included not only long life and ample light output but also small physical size, short filament length, and low power consumption. The latter characteristics necessitated a low operating voltage which was not compatible with a 24-volt supply. Considerations were given to: a resistor in series with the lamp operating from 24 volts DC, an inverter, placing the lamp in series with various circuit elements, operating the lamp from auxiliary (generating) windings, and placing the lamp in series with entire motor. The last approach was chosen because it gave the highest efficiency and greatest simplicity of design.

(2) Figure 9 is a block diagram of the starting circuit, and Figure 10 is the corresponding schematic diagram. Note that the lamp voltage is limited by diodes CR7 and CR8. This voltage during normal operation is approximately 1.2 volts. The lamp must be on before the motor can operate and yet the lamp will not continue to operate unless the motor is operating. Thus it is necessary to provide

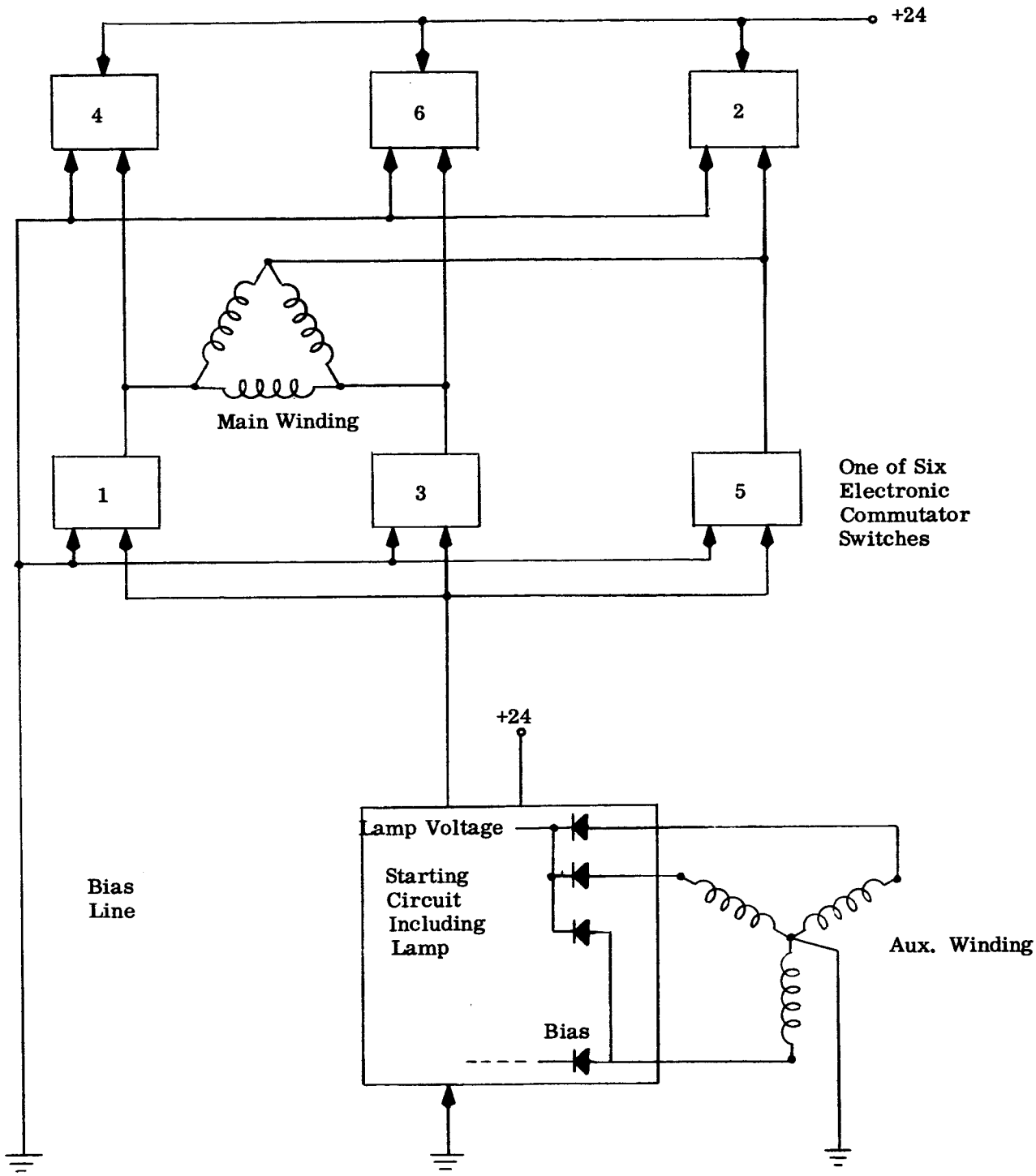

FIGURE 9
BLOCK DIAGRAM OF STARTING CIRCUIT

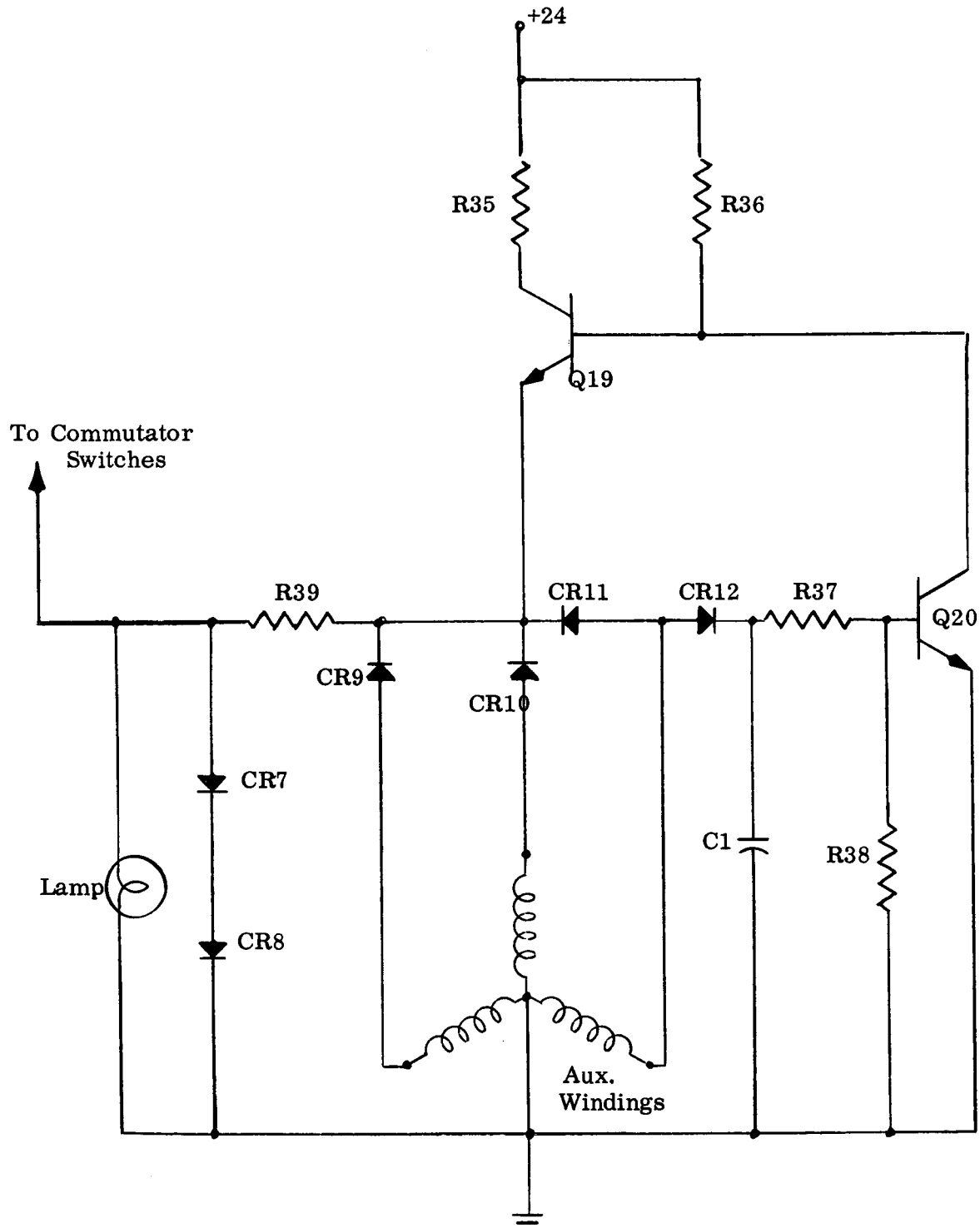

FIGURE 10
SCHEMATIC DIAGRAM OF STARTING CIRCUIT

additional circuitry. Upon application of power to the entire motor, transistor Q19 is forward biased by R36. Transistor Q19 is then switched on and supplies current to the lamp-diode combination. Since the lamp is now illuminated, the commutator circuits operate and additional current is drawn through the lamp-diode combination. The resistance selected for resistor R39 had to be low enough to give consistent starting at low temperatures, yet as high as could be tolerated so as to give reasonable efficiency. When the motor has attained a speed that is approximately 50 percent of rated speed, sufficient voltage is induced in the auxiliary windings to switch on Q20 through R37 and CR12. This action essentially shorts the base of Q19 to ground and back-biases the base-emitter junction of Q19. Transistor Q19 is now off and the lamp is receiving current through the motor circuitry. Capacitor C1 provides filtering while R37 and R38 make up a voltage divider which determines the motor speed at which Q20 is switched on. The no-load current of the motor is equal to or less than the current required for the lamp. This necessitates another source of power during no-load conditions which is supplied by the auxiliary winding in conjunction with CR9, CR10, and CR11.

(3) It was necessary to add CR12 to prevent Q20 from receiving bias current through the commutator switches rather than the auxiliary winding. The value of resistor R36 was chosen to provide only the base-drive current required by Q19 to supply approximately 30 ma of collector current. Again considering efficiency, the resistance

of R36 is kept as high as can be tolerated so as to give reasonable efficiency. The resistance of R35 is such that it limits starting current to an optimum value. Transistor Q19 was selected because of its high h_{FE} at the operating current level, its small physical size, and its capability of supplying starting current under stall conditions. The power dissipation capabilities and h_{FE} of transistor Q20 are not critical since Q20 must supply only microamps. Fortunately, capacitor C1 does not need a high capacitance or high working voltage and thus it is also of small size. Diodes CR7 and CR8 were chosen because of their voltage-current characteristics, their current-handling capability under stall conditions, and their small physical size. Diodes CR9 through CR12 carry little current so diodes of the micro-package type were selected.

(4) In summary, Q19 supplies current to the lamp at starting, but is back-biased and cut off by Q20 during normal operation. Thus, low power is consumed by R36 and Q20 during this period of normal operation. A by-product of the starting circuit is a 1.2 volt back-bias which is applied to the base of the first transistor in each of the 6 commutator switches. This voltage is derived from the voltage across the lamp and insures that the preamp transistors are back-biased and off when their corresponding photodevices are not illuminated. See the entire circuit schematics, Figures 11 and 12.

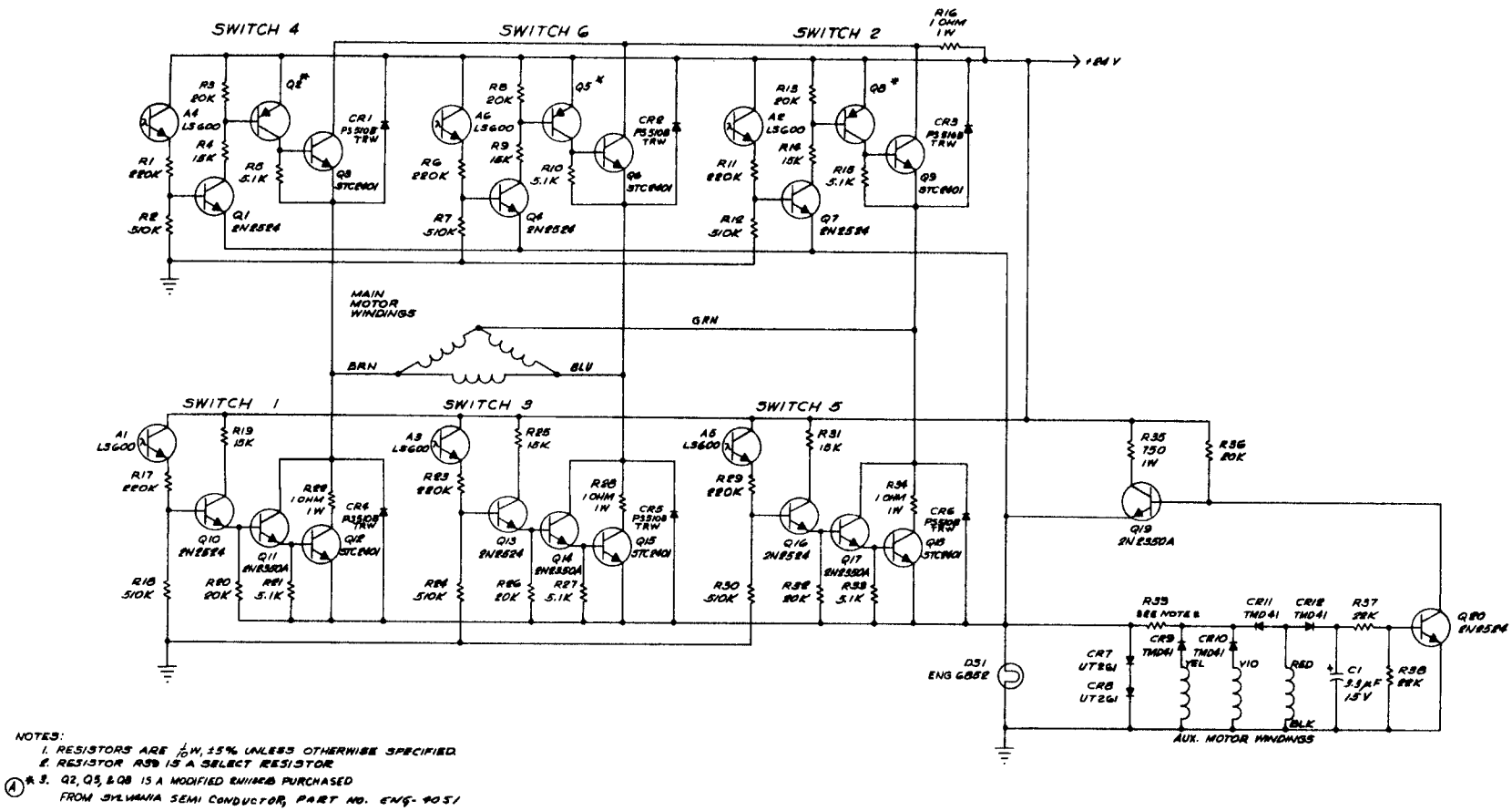

FIGURE 11
SCHEMATIC DIAGRAM OF ONE-WATT MOTOR

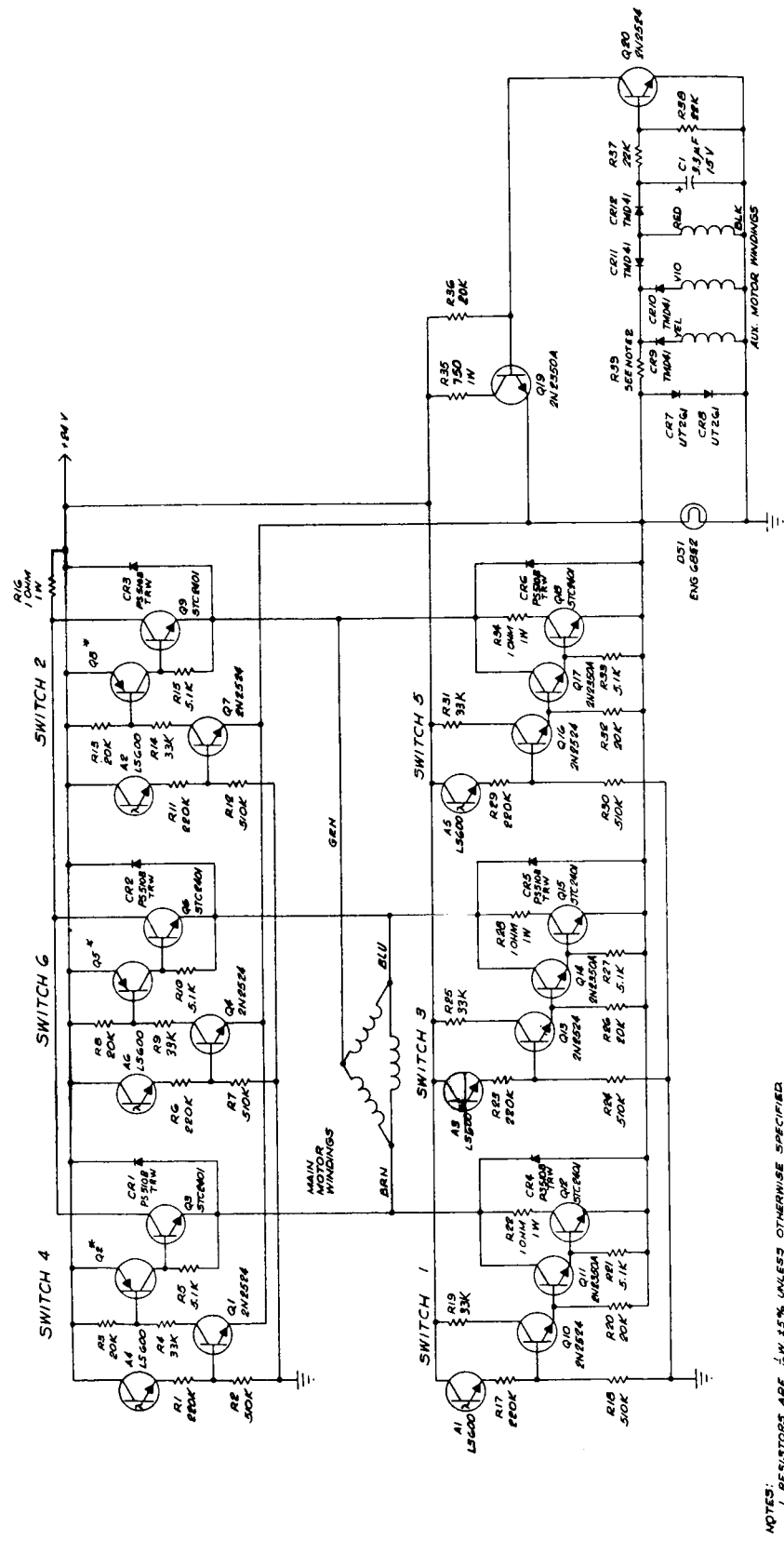

FIGURE 12
SCHEMATIC DIAGRAM OF HALF-WATT MOTOR

d. 120-Degree Commutation

1) Reasons for Adoption

Motor size requirements necessitated a change in commutation angle from 60^{o} to 120^{o}. This reduced the number of commutator components by 50%; but adding a starting circuit left a net reduction of 40%. A net volume reduction of 30% from the size used on Contract NAS 5-2832 was achieved.

2) At least two of the six photosensors, located at 60^{o} intervals around the lamp (DS1 of Figure 12) are illuminated at all times as the light shield's 120^{o} aperture rotates between lamp and sensors in step with the rotor. These must trigger two non-opposite switches, one from the upper row (2, 4, or 6) and one from the lower (1, 3, or 5) simultaneously. If photosensors A1 and A2 are illuminated, current through A1 causes transistors Q10, Q11, and Q12 to conduct, and current through A2 causes Q7, Q8, and Q9 to conduct.

Switches 1 and 2, entirely, are now conducting, allowing current to flow through Q9, Q12, and the main motor winding with little impedance. The current in the main winding sets up a magnetic field at quadrature to that of the permanent-magnet rotor. When the rotor and light shield have turned 60^{o}, A3 and Switch 3 conduct, and Switch 1 turns off.

Current now flows through Q9, Q15, and the main winding, setting up a new magnetic field in quadrature with the new direction of the rotor field, and turning the rotor and light shield again. This switching action continues in the cyclic order: 1, 2, 3, 4, 5, 6, 1, 2, ..., producing continuous rotation while power is applied.

4. Hermetic Sealing

a. Metallic Armature Sleeve

Calculations performed revealed that the minimum wall thickness of the metallic armature sleeve used for hermetic sealing need be only 0.00015 inch based on a differential pressure of 15 psi using standard stress equations for thin-wall tubes of aluminum. Stronger materials would yield correspondingly thinner walls. However, to check for a practical machining capability, a 0.010 inch wall tube was fabricated. With successive grinding operations, a 0.003 wall thickness was arrived at. The 0.003 tube was considered too thin for practical use in a motor since it was questionable if the tube was round when removed from the grinding arbor. Further handling by insertion in the motor caused the tube to split on the ends. A 0.005 inch wall tube appeared much more stable in relation to handling and resistance to bending. It was concluded that a 0.005 inch wall would be the thinnest possible tube for practical use in the motor.

Various materials, listed in Table 6, were considered for usage; however, only those materials tabulated in Table 7 were chosen for further evaluation. Table 7 shows the results of motor efficiency tests made with sealing tubes of these materials.

PROPERTIES	MONEL R	INCONEL (600)	ALUMINUM 6061-T6	NICHROME	STAINLESS STEEL (303)	TITANIUM RC-55	HASTELLOY ALLOY-C
Density lb/in^3	0.305	0.300	0.098	0.298	0.290	0.163	0.323
Thermal Expansion $in/in/^oF$	$7.8x10^{-6}$	$9x10^{-6}$	$13x10^{-6}$	$7.5x10^{-6}$	$9.6x10^{-6}$	$4.8x10^{-6}$	$7.02x10^{-6}$
Modulus of Elasticity (Psi)	$26x10^6$	$31x10^6$	$10x10^6$	$30x10^6$	$30x10^6$	$15.5x10^6$	$28.5x10^6$
Electrical Conductivity % of Copper	4	3.5	45	1.6	32.3	3.1	1.33
Magnetic Permeability μ	1.03	1.0028	1.00	1.0	1.003	1.00005	1.000 1.001
Specific Resistance μ ohm-cm	58.1	98.1	4.31	112	72	48.6	133
NOTES:	Must be silver brazed @ 1175^oF (not weldable)	Can be soldered (Acid Flux)	Can be soldered	Can be soldered	Can be soldered	Fabrication Expensive	Can be soldered

TABLE 6
GENERAL PROPERTIES OF METALS CONSIDERED FOR SEALING-TUBE

MATERIAL	TUBE WALL THICKNESS	ROTOR AIR GAP/POLE	TOTAL AIR GAP PER POLE	MAXIMUM MOTOR EFFICIENCY PERCENT
303 Stainless	0.003	0.003	0.006	44
303 Stainless	0.005	0.003	0.008	50
None	-	0.008	0.008	50.3
Aluminum	0.005	0.003	0.008	35.2
Inconel	0.005	0.003	0.008	50.5
Nichrome	0.003	0.005	0.008	48

TABLE 7

EFFECTS OF SEALING-TUBE MATERIAL AND WALL-THICKNESS ON MOTOR EFFICIENCY

Data shown in Table 7 was extracted from Figures 8 through 12 of the monthly report for October, 1963. From the efficiency data of Table 7 it was concluded that the 0.005 inch stainless tube was better than the 0.003 inch stainless tube. No explanation can be given for this phenomenon at this time. The data indicated that material selection would be relatively unimportant if the resistivity were equal to or above that of stainless steel

b. End-Cap Seal

(1) Sealing Techniques

(a) One of the most important characteristics of the sealed motor housing material is that of solderability. Three materials were chosen to be evaluated for this application, namely: aluminum, stainless steel, and yellow brass. Solderability tests were conducted using sample parts which simulated the shaft end of the motor housing. As was expected, the aluminum

would not solder to the nichrome tube, and the stainless steel specimen would solder only by using high heat and corrosive flux. The brass specimen soldered easily to a pre-tinned nichrome tube.

(b) The next series of tests was conducted using stainless steel and nichrome with a copper flash under tin plating. This combination proved to be extremely easy to solder using a small soldering iron (37-1/2 watt) and Kester "44" solder. Kester "44" resin flux is believed to be the most active resin flux known to soldering. It has been found non-corrosive by MIL-S-6872 and USAF Spec. No. 41065-B, method 31.

(c) Stainless steel was selected for this application because of:

- ★ Ease of plating for solderability
- ★ High strength, which permitted thinner housing walls which, in turn, permitted use of larger laminations for increased efficiency
- ★ Thermal expansion rate, which was closer to that of the laminations and nichrome tube than that of aluminum or brass
- ★ Low galvanic corrosion rating in combination with the nichrome and tin-lead solder combination.

(2) Difficulties Encountered at Assembly

Several end caps failed to solder properly to the housing until

activated flux was applied to the end cap and housing. All possible precautions were taken during this operation to prevent contamination. The parts were made from stainless steel which is not solderable at low temperatures. A copper flash was applied and electroless tin plating was added. The above problem may have been caused by porosity of the copper flash, which would permit galvanic corrosion of the base metal in the tin-plating solution, or by handling during inspection and assembly, which could have resulted in contamination and/or loss of tin plating.

The above causes of poor solderability will be eliminated or minimized on future contracts by the following corrective action:

(a) Special handling procedure during inspection and assembly of all parts that require tin plating.

(b) Increased copper and tin thicknesses from .0002" to .0005".

c. Lamp-to-Base Seal

It was originally planned to seal the lamp to the base with solder glass. In order to obtain proper fusing, the lamp and base assembly must be heated to approximately 450°C. It was experimentally determined that the lamp intensity had decreased after assembly of the lamp to the base with solder glass. A series of tests was performed to determine the magnitude and effect of this change (see Table 8). From this series of tests it became evident that the lamp characteristics were adversely affected. It has been determined that the change in characteristics of the lamp was a result of partial loss of vacuum caused by heat applied during fusing.

Lamp No.	Photo Cell No.	Before Fuzing Lamp to Base		After Fuzing Lamp to Base(oven at 450°C)	
		Sensor Current (μa) At Lamp Voltage of 1.5 volts	Sensor Current (μa) At Lamp Voltage of 1.1 volts	Sensor Current (μa) At Lamp Voltage of 1.5 volts	Sensor Current (μa) At Lamp Voltage of 1.1 volts
1	1	108	107	1.4	0.05
	2	107	46	0.05	0
	3	102	25.6	0.5	0.01
	4	108	48	0.09	0.01
	5	108	51	0.05	0
	6	108	72	1.5	0.09
2	1	108	103	15.5	0.5
	2	107	60	18.2	0.5
	3	107	27.3	11.0	0.5
	4	107	59	8.5	0.2
	5	107	42	8.4	0.2
	6	107	52	15.1	0.5
3	1	107	91	74	7.5
	2	107	42	28	1.1
	3	107	31	30	2.5
	4	107	36	46	3.6
	5	86	20.4	30	2.0
	6	107	46.0	41	3.7

TABLE 8
FIRST LAMP TO BASE SEALING METHOD

The assembly technique was altered in an attempt to minimize or eliminate completely the above condition. Table 9 shows lamp performance after the assembly technique was changed. These results indicate that after the introduction of the new technique, the lamp intensity did not decrease as it did when the original sealing technique was used. Subsequently, several lamp-and-base assemblies fabricated by this method were checked for leaks by means of the Helium Mass Spectrometer. All of the assemblies had very high leak rates. The leakage occurred at the metal-to-glass interface. To obtain sealing at this interface would require that the metal base reach approximately the same temperature required to melt the solder glass ($450^{o}C$). Since the lamp intensity is affected at this temperature, an attempt was made to work with the metal base at a lower temperature, without success.

Another method used for lamp-to-base sealing employed an inorganic silicate-base cement (Sauereisen #1) for heat shielding and mechanical support during the fusing operation. The solder glass was fused over the cement for hermetic sealing. The same problem occurred as before: the metal-to-glass interface leaked. This again appeared to be a result of insufficient heating of the metal base. The next approach for sealing was to use an epoxy with gold vacuum-deposited on the surface to be exposed to a vacuum. The heat produced due to exothermic reaction of the epoxy during the curing cycle was dissipated very quickly. In fact, the lamp-and-base assembly essentially remained at the ambient

Lamp No.	Photo Cell No.	Before Fuzing Lamp to Base		After Fuzing Lamp to Base (Localized Heating)	
		Sensor Current (μa) At Lamp Voltage of 1.5 volts	Sensor Current (μa) At Lamp Voltage of 1.1 volts	Sensor Current (μa) At Lamp Voltage of 1.5 volts	Sensor Current (μa) At Lamp Voltage of 1.1 volts
1	1	110	93	110	100
	2	110	58	110	58
	3	110	58	110	51
	4	110	50	110	50
	5	110	50	110	49
	6	110	72	110	68
2	1	110	81	110	69
	2	110	30	102	21
	3	107	29	90	20
	4	101	24	93	20
	5	100	23	65	15
	6	110	51	110	30

TABLE 9
SECOND LAMP TO BASE SEALING METHOD

temperature during the entire curing cycle. The problem mentioned previously (degradation of lamp characteristics) was eliminated completely by this method.

The Bacon Industries epoxy resin LCA-4 was selected because of its low coefficient of linear expansion, good thermal shock characteristics, and the fact that it does not produce condensible volatiles when heated. The coefficient of linear expansion for LCA-4 epoxy is: 17×10^{-6} inch/inch/^{o}F. The average epoxy has a coefficient of linear expansion of the order of (40 to 75) $\times 10^{-6}$ inch/inch/^{o}F.

This method utilized the epoxy for mechanical support and preliminary sealing. The gold was then vacuum-deposited on the exposed surface to complete the sealing. The subject of vacuum-deposited gold to achieve hermetic sealing was discussed at length with several people familiar with this process. The general opinion was that the film of gold produced by this process would not be continuous over the entire surface. During leak testing with the Helium Mass Spectrometer, a lamp and base assembly (epoxy with vacuum-deposited gold) failed to pump down. It was found that a small void (approximately .0001 to .0005 inches in diameter) was present in the epoxy. This assembly was electroplated to a thickness of .000150 inch, approximately, with gold. The assembly was rechecked for leakage after completion of electroplating. No detectable leak was observed during this check. This indicates that the void was effectively sealed by the electroplating. Unfortunately this does not ensure that the

plating was continuous over the entire surface. A continuous surface of metal over the epoxy is essential if a true hermetic seal is to be obtained. This is necessary due to the permeability of epoxy resin.

Permeability of Epoxy LCA-4 to air

@ $75^{o}F$ 1×10^{-11} cc/sec/cm/atm

@ $200^{o}F$ 1×10^{-9} cc/sec/cm/atm

The permeability of epoxies will increase where exposed to certain compounds, i. e. LCA-4 Epoxy will swell when exposed to toluene, increasing the permeability to air approximately 200 times the original value.

Conclusion:

The epoxy seal cannot be considered a true hermetic seal, since it is permeable to gasses. The vacuum gold deposit with additional electroplated gold may or may not yield an hermetic seal, depending on continuity of the plating. It does appear that this method would not be feasible since a very elaborate inspection technique would be required.

Figure 13 illustrates the sealing technique used on the delivered motors.

d. Leak Rate

Originally it was planned to use the Radiflo method for leak-testing the motors. Subsequently it became apparent that the motors might become contaminated during these tests if such a method were used. Upon mutual agreement between Goddard and Sperry Farragut this method was replaced by the Helium-mass-spectrometer method, and the previously discussed leak-rate of 1×10^{-8} cc/sec. maximum was relaxed to 1×10^{-5} cc/sec maximum.

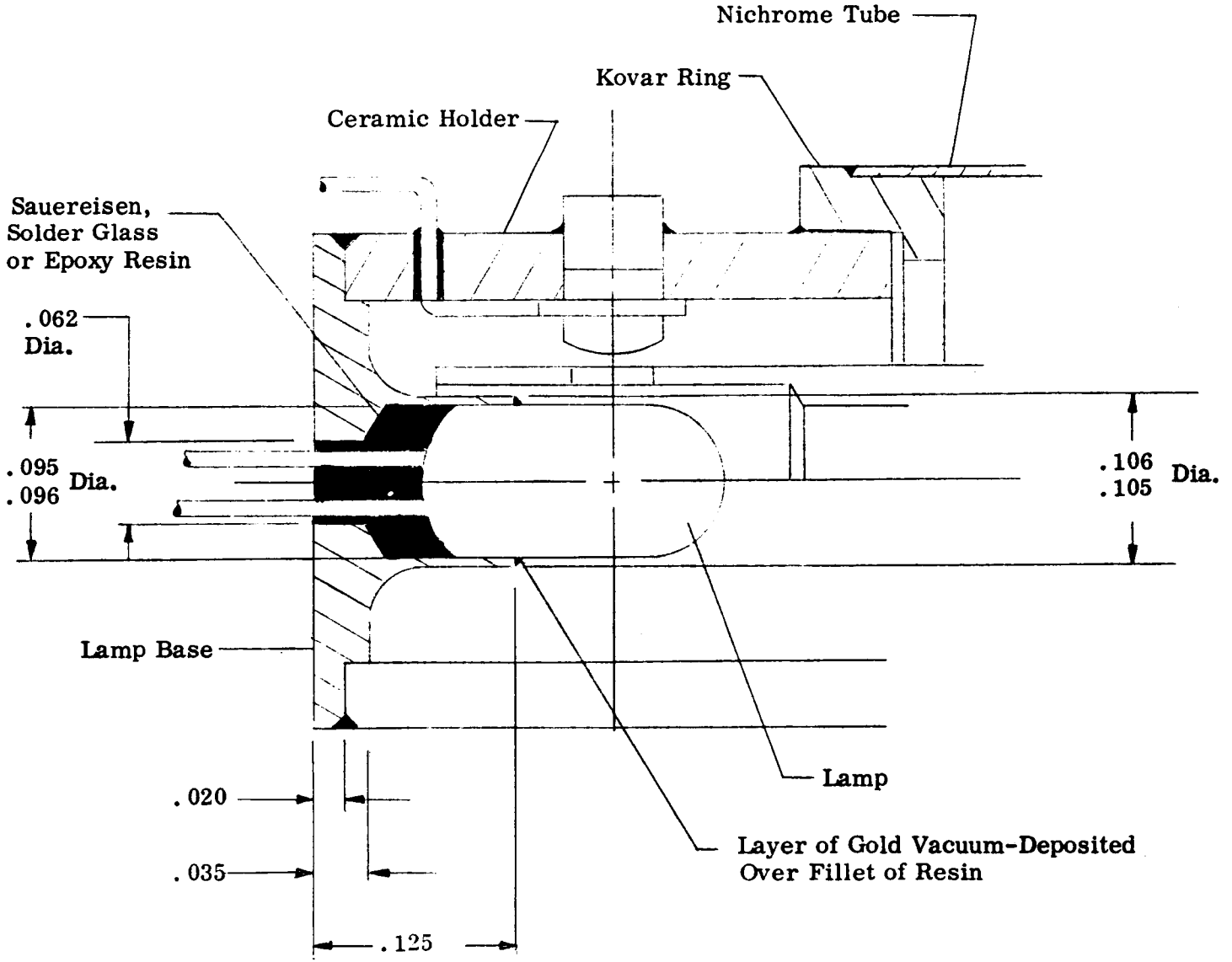

FIGURE 13
TUBE-TO-LAMP HERMETIC SEAL

5. Packaging

a. Electronic Commutator

(1) The electronic commutator package consists of five printed circuit boards TB1 through TB5. Boards TB1, TB2, and TB3 are identical and contain the preamp stages of the 6 commutator switches. Components on these boards are approximately the same height to provide maximum packaging density. Board TB4 contains the power output transistors. Board TB5 contains the starting circuit and monitoring terminals for photo-device leads, main and auxiliary windings, and other wires from each of the other four boards. The starting circuit was placed in its present position at the end of the motor to facilitate final wiring during assembly and for ease of troubleshooting. Another advantage of the position of this board is that it may be removed or replaced by another board if other designs should not require a starting circuit.

(2) The components in the electronic commutator were encapsulated with G. E. RTV-108 silicone rubber sealant. This material was chosen because of its ease of application and its mechanical stability at temperatures ranging from $-75^{\circ}F$ to $+300^{\circ}F$ for extended periods. RTV-108 comes ready-mixed in an application tube and can be applied without a primer or catalyst. The material air-dries in 24 hours without the addition of heat and provides excellent environmental protection, vibration resistance, and transparency (such that the electronic parts remain visible).

If repairs must be made in the electronic package, this encapsulating material can be cut away to expose the faulty component. The hole can be refilled with new material after the circuit has been repaired, without detriment to the remaining encapsulation. This same material was added to the rear of the tube-and-lamp assembly to reduce vibration of the leads from the lamp and sensors.

(3) Stranded wire in the circuit board assembly was replaced by solid bus wire (Alpha Wire Co. 299/3, #30 AWG). Until this change was made, these interconnecting wires were frequently broken or damaged during assembly and test.

(4) Elimination of more than 40 percent of the electronic components that were used in the commutator of the earlier three-watt motor was accomplished by making several innovations. Among these were the change from a full-pitched ring winding in the armature to a chorded-delta winding with an accompanying increase in aperture size in the light shield, the substitution of a half-wave bridge for a full-wave bridge in the starting circuit and the use of micro-packaged diodes and transistors wherever possible. This removed the need for the large separate commutator cover and made it possible for the electronic circuitry to be packaged in the motor housing with only a small increase in housing length.

(5) Over-all Packaging

The over-all packaging layout is shown in Figure 14. The major components and assemblies are shown before final assembly (and

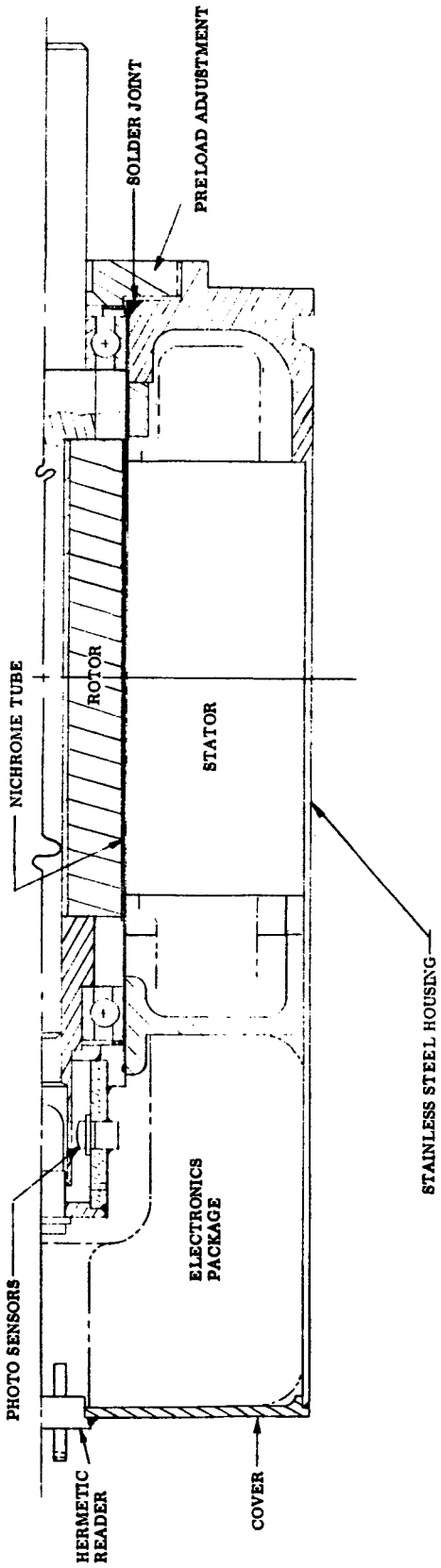

FIGURE 14

PACKAGING LAYOUT

the encapsulation of the circuit board assembly) in Figure 15. The assembled motor is shown in Figure 16.

C. DELIVERABLE MOTORS

1. Configuration

The salient mechanical details and electrical characteristics of each of the six motors delivered to Goddard are listed in Table 10. Because of the developmental nature of the program, there are minor differences between these motors and the final designs represented in the final drawings.

2. Performance

Test data showing the actual performance characteristics of the six motors delivered to Goddard Space Flight Center are presented in graphic form in Figures 17 through 22.

D. RELIABILITY

1. Design Improvements

a. The half-and one-watt motors have a higher reliability than the earlier three-watt motor for several reasons. In addition to standard derating practices recommended by component vendors to allow for ambient temperature extremes, critical components were further derated to ensure longer life. For example, the lamp in the electronic commutator operates at twenty-five percent of its rated voltage, even though it gave every indication of excellent reliability in environmental and accelerated life tests.

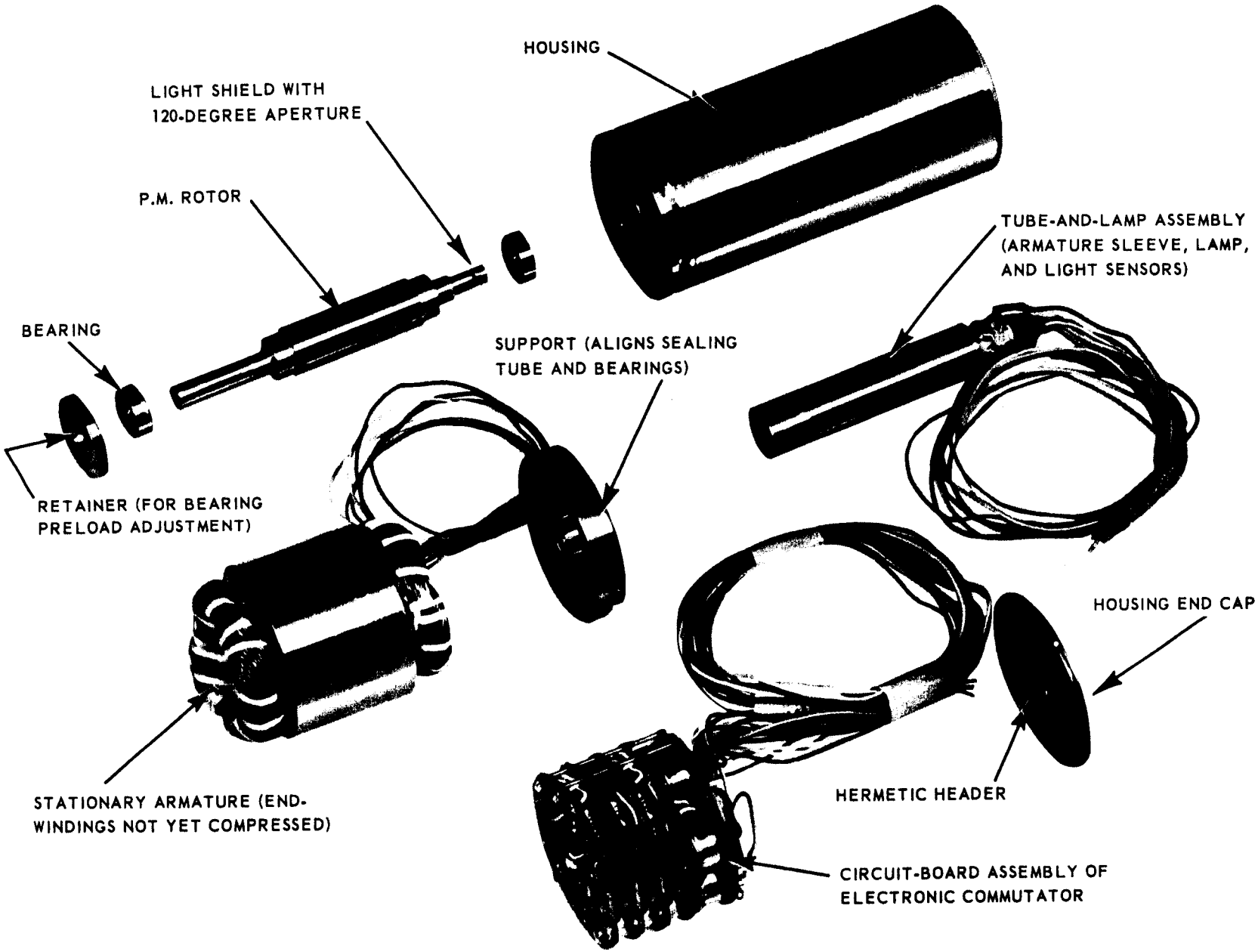

FIGURE 15. MAJOR COMPONENTS AND ASSEMBLIES OF HERMETICALLY SEALED MOTOR

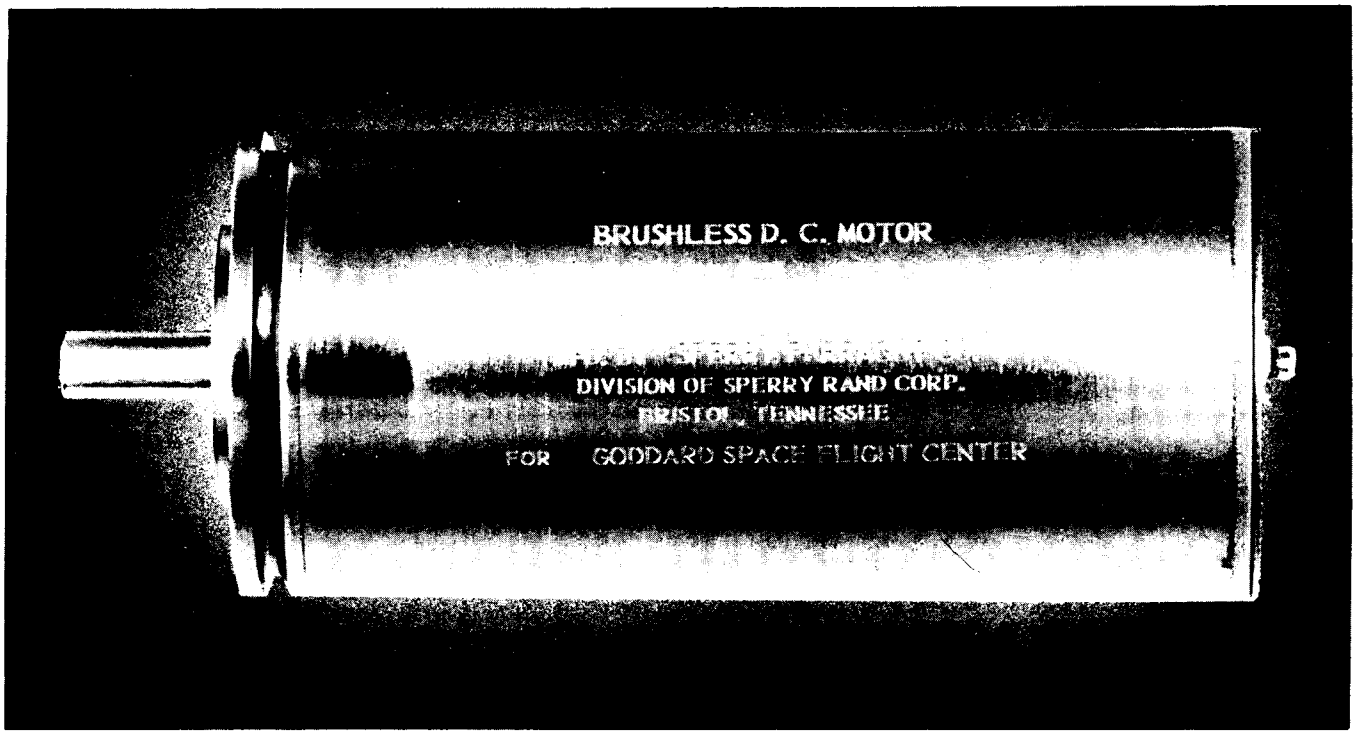

FIGURE 16. ASSEMBLED HERMETICALLY SEALED BRUSHLESS DC MOTOR

P/N	Serial No.	Resistor Value R39 (ohms)	Rotor Size	Total Air Gap/Pole	η_t @ .25 oz-in.	Rotation (Rotor magnetized with slot oriented to the north pole)	Effective resistance of primary winding (ohms)
Eng 9821 1 watt	SF-1	47	.364	.0221	57.7%	ccw	46
	SF-2	22	.365	.0211	57.8%	ccw	46.2
	SF-3	47	.3635	.0226		cw	49
	SF-4	47	.363	.0230	56.3%	ccw (see remarks)	44.9
Eng 9847 1/2 watt	SF-1	0 short circuit	.354	.0321	46.9%	ccw	69.8
	SF-2	0 short circuit	.353	.0330	49%	ccw	67.4

TABLE 10

CHARACTERISTICS OF BRUSHLESS DC MOTORS DELIVERED TO GSFC

S/N	Effective Resistance Auxiliary Winding	Wire Sized Auxiliary Winding	Leak Rate (atmo -cc/sec)	Mechanical Variations		
				Tube & Lamp Assy Eng 9835	Lamp Assy Eng 6891	Spacer Eng 4040
SF-1	40.4	#39	1.04×10^{-7}	Per Print	Per Print	Omitted
SF-2	53.6	#40	Not Sealed	No RTV potting compound	Lamp secured in base by: (a) Sauereisen insa-lute #1 (b) Solder glass	Used
SF-3	45.2	#40	Not Sealed	Per Print	Per Print	Used
SF-4	47.7	#40	Less than 1×10^{-10}	Per Print	Per Print	Omitted
SF-1	34.8	#39	Not Sealed	Per Print	Per Print	Omitted
SF-2	54.5	#40	Not Sealed	Per Print	Vacuum-deposited gold omitted from epoxy resin	Used

TABLE 10

CHARACTERISTICS OF BRUSHLESS DC MOTORS DELIVERED TO GSFC

S/N	Rotor Imbalance			Remarks
	Before Balancing		After Balancing	
	Left End	Right End		
SF-1	200 in-oz.	250 in-oz.	-50 in-oz.	Activated flux used to solder end cap to housing
SF-2			Not Balanced	
SF-3	300 in-oz.	350 in-oz.	-50 in-oz.	Activated flux used to solder end cap to housing
SF-4	300 in-oz.	200 in-oz.	-50 in-oz.	Activated flux used to solder end cap to housing Rotor magnetized 1800 from SF-1 and SF-2
SF-1	450 in-oz.	400 in-oz.	-50 in-oz.	Activated flux used to solder end cap to housing
SF-2			Not Balanced	

TABLE 10

CHARACTERISTICS OF BRUSHLESS DC MOTORS DELIVERED TO GSFC

TEST DATA
BRUSHLESS DC MOTOR

Serial No. SF-1 (1 WATT) ENG 9821
Input Voltage 24

TESTED BY RICHARD SPARKS TEST DATE 6-30-64

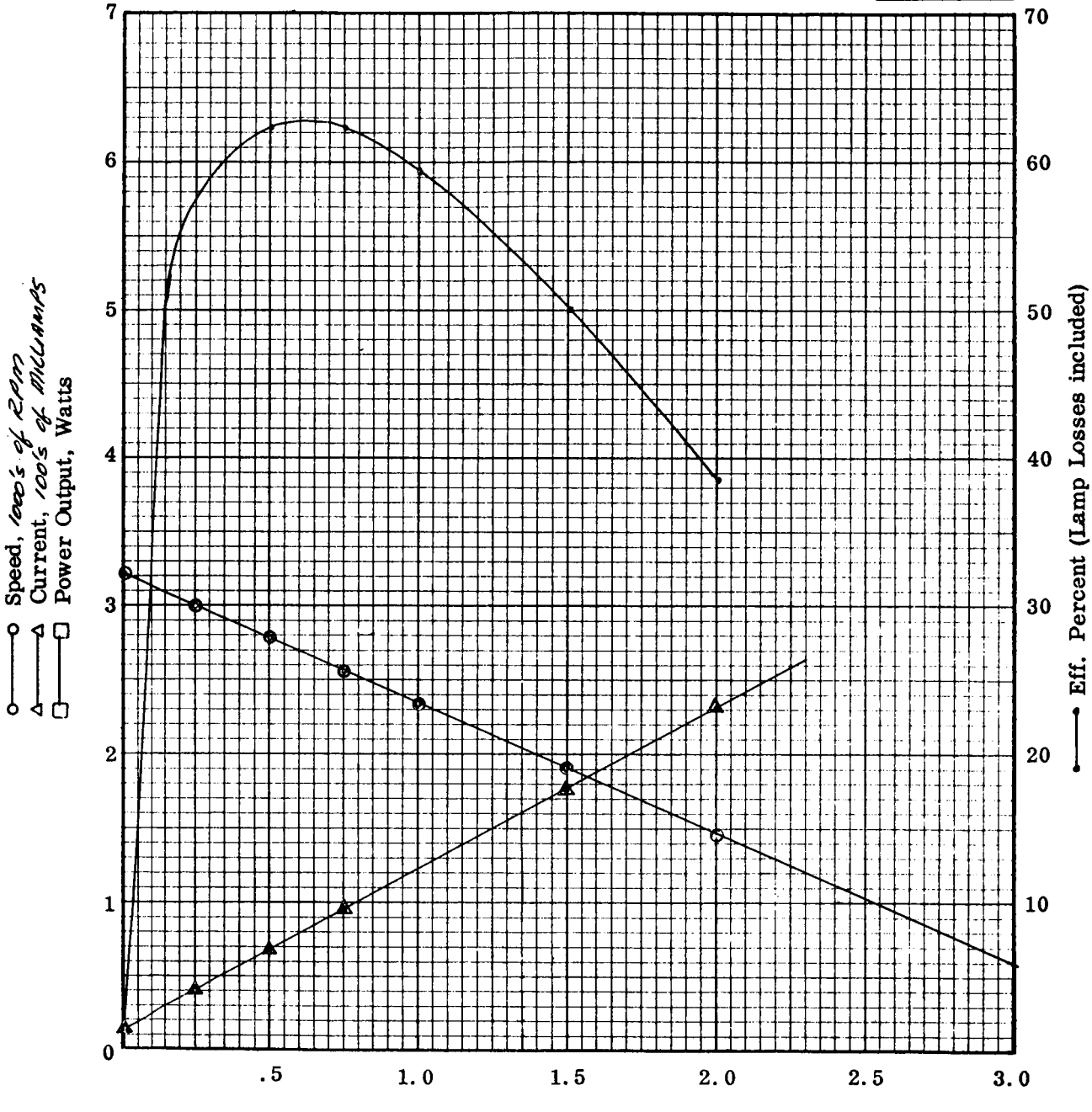

TORQUE, IN. OZ.

FIGURE 17

TEST DATA
BRUSHLESS DC MOTOR

Serial No. SF-2 (1 WATT) ENG 9821

Input Voltage 24

TESTED BY RICHARD SPARKS TEST DATE 6-18-64

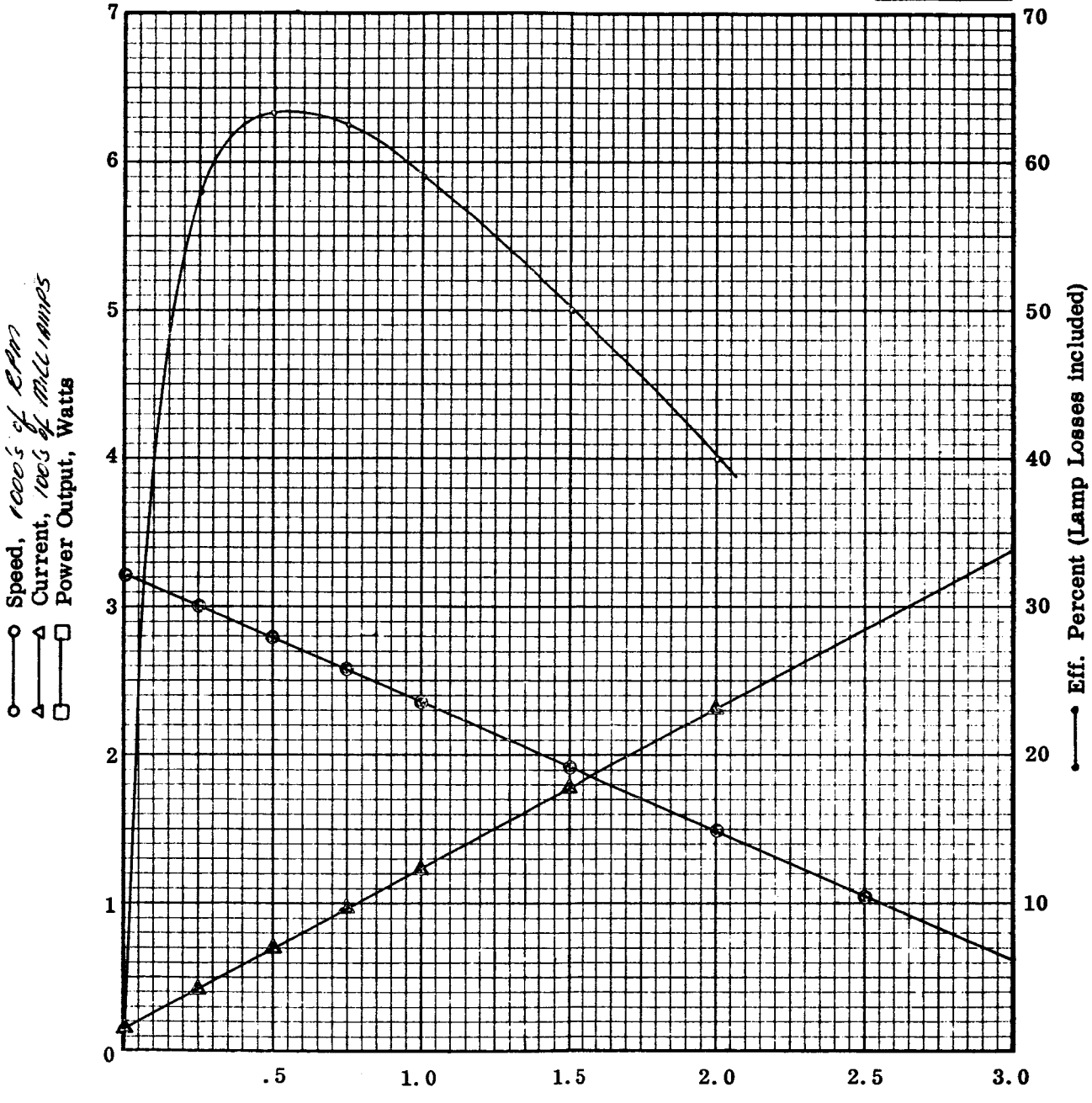

TORQUE, IN. OZ.

FIGURE 18

TEST DATA
BRUSHLESS DC MOTOR

Serial No. SF-3 (1 WATT) ENG 9821

Input Voltage 24

TESTED BY RICHARD SPARKS TEST DATE 7-1-64

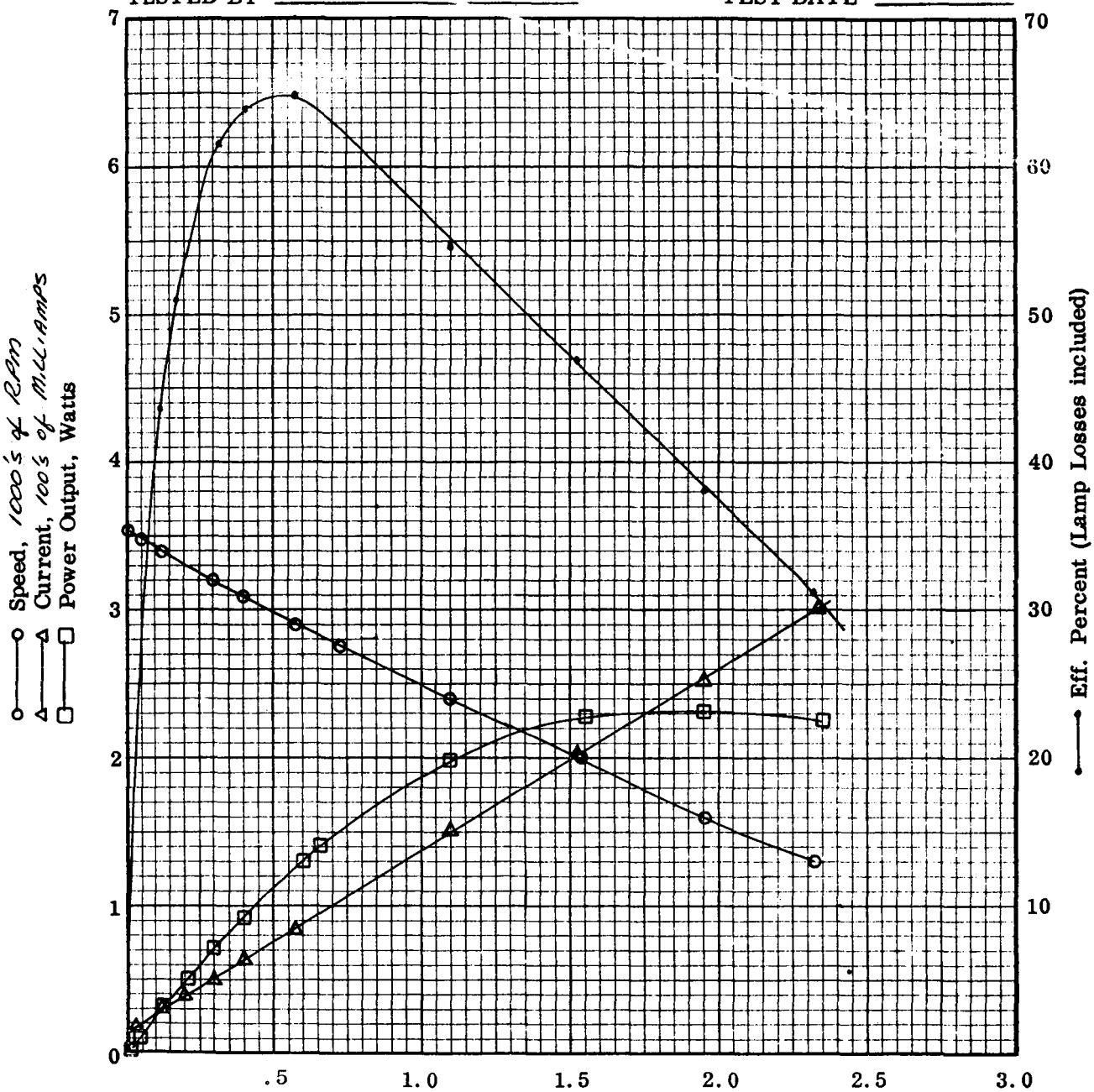

FIGURE 19

TEST DATA
BRUSHLESS DC MOTOR

Serial No. SF-4 (1 WATT) ENG 9821

Input Voltage 24

TESTED BY RICHARD SPARKS TEST DATE 6-30-64

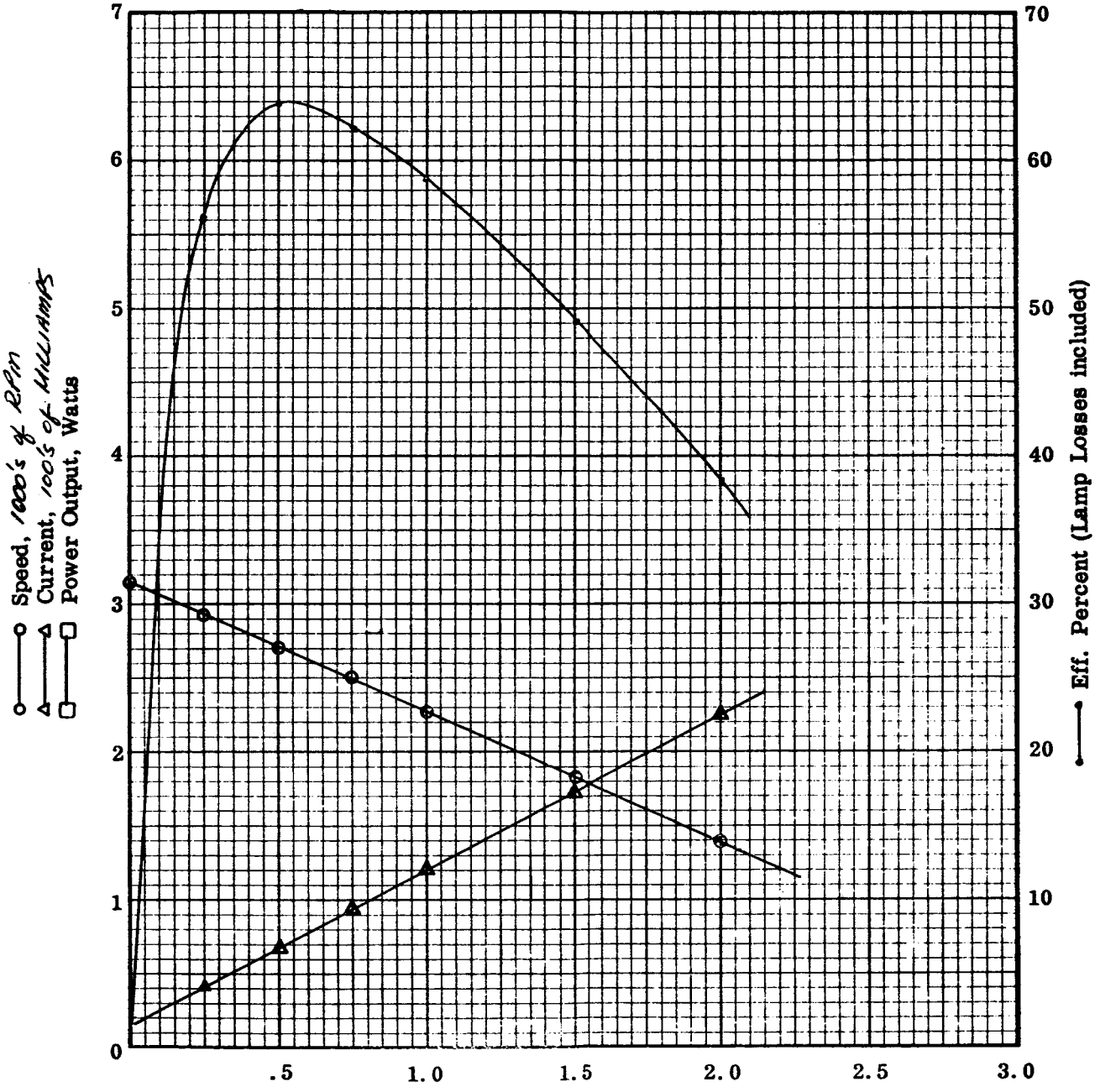

FIGURE 20

TEST DATA
BRUSHLESS DC MOTOR

Serial No. SF-1 (1/2 WATT) ENG 9847

Input Voltage ____

TESTED BY RICHARD SPARKS TEST DATE 7-1-64

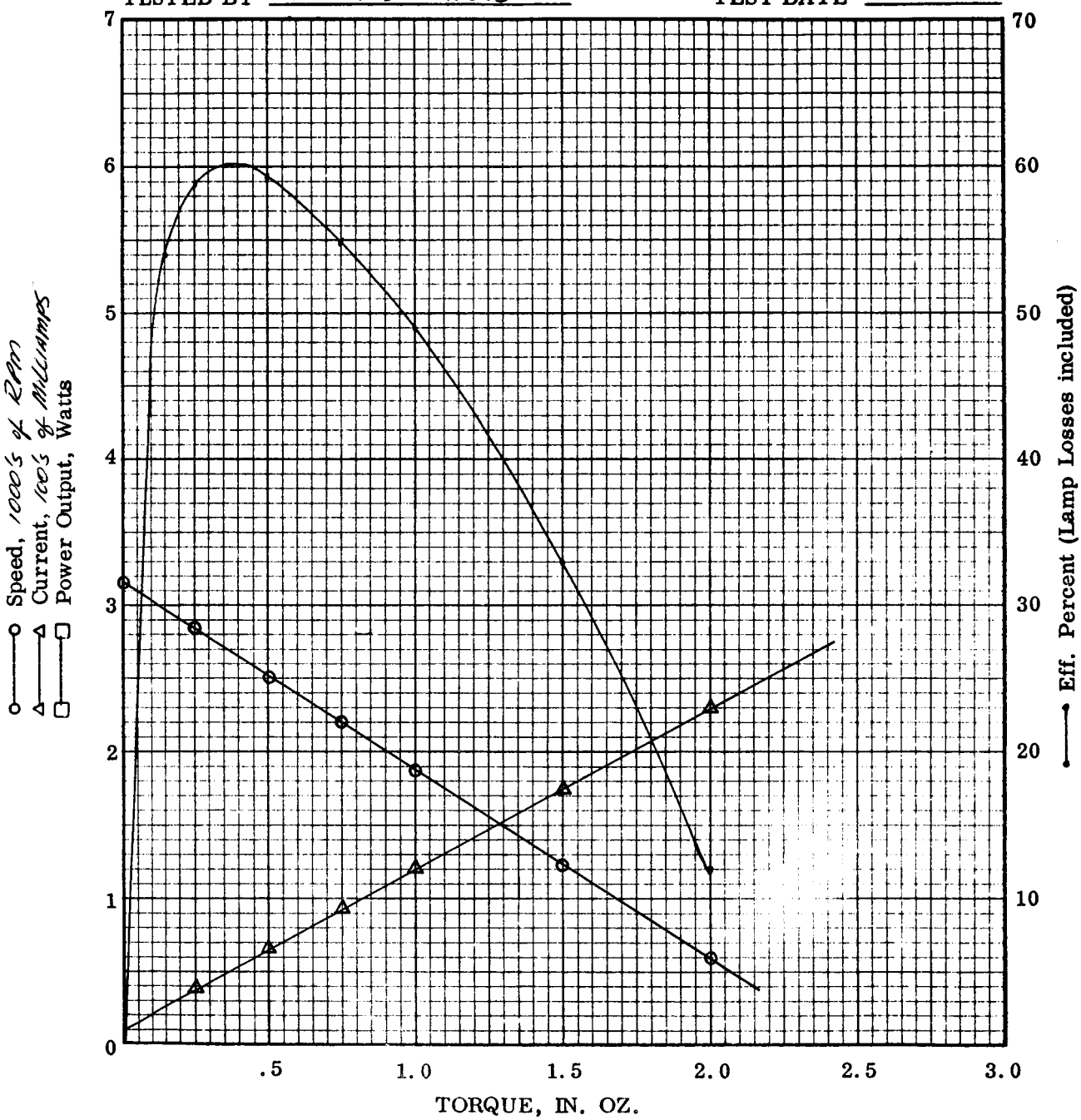

FIGURE 21

TEST DATA
BRUSHLESS DC MOTOR

Serial No. SF-2 (½ WATT) SNG 9847
Input Voltage 24

TESTED BY RICHARD SPARKS TEST DATE 6-18-64

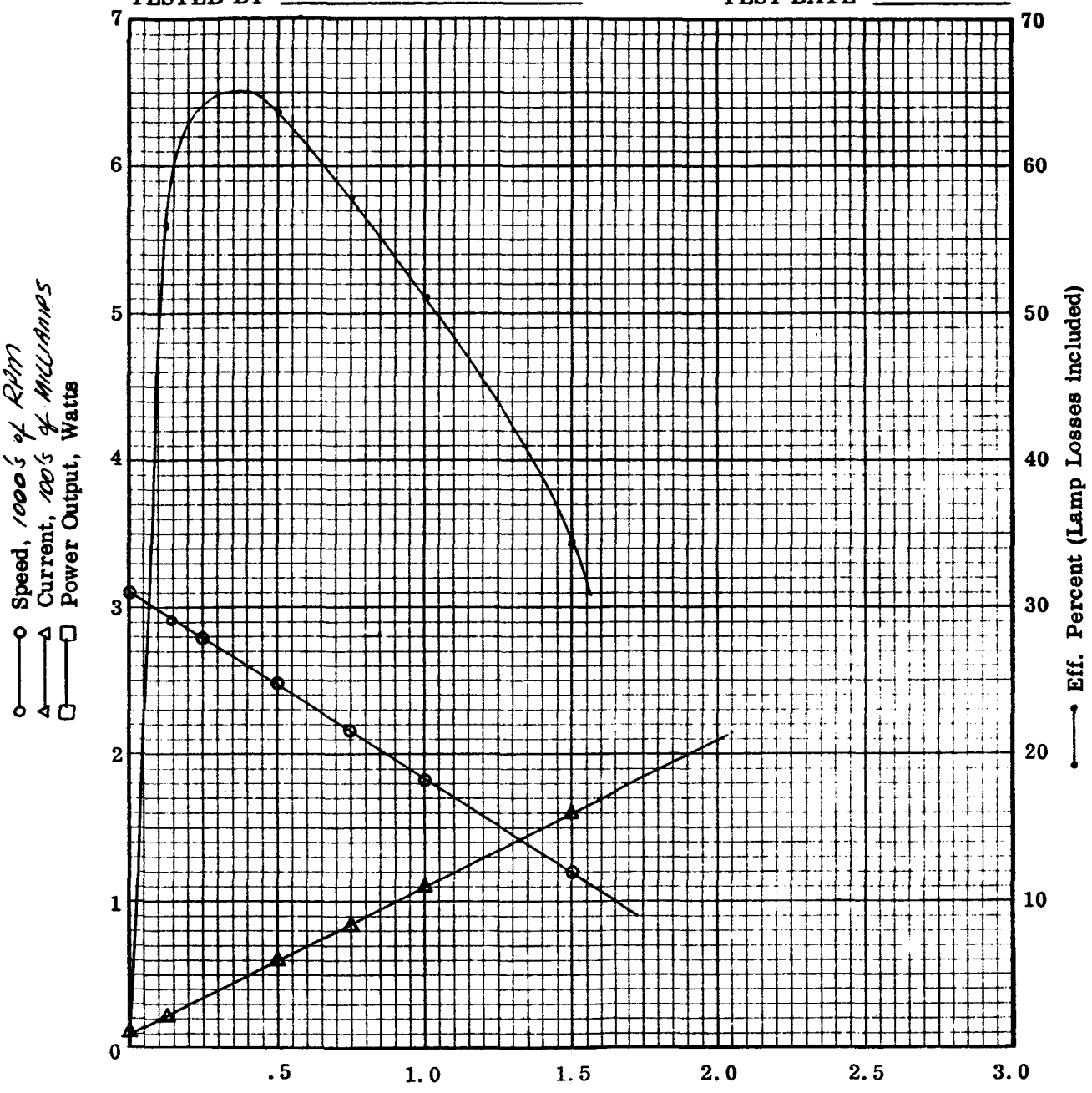

FIGURE 22

b. Ruggedized integrated miniature circuitry was introduced in the commutator. The five hollow-disk circuit boards, stacked with collinear centers, have been braced with three continuous pillars to give greater mechanical rigidity. The entire electronic section of the commutator has been encapsulated in a compound that has good transparency to facilitate final inspection while improving shock and vibration resistance. Hermetic sealing of the commutator has eliminated any danger of bearing contamination that might have resulted from outgassing from the encapsulating material or wiring insulation in a hard-vacuum environment.

c. The reduction of the number of electronic components in the commutator by more than 40 percent gave a substantial increase in the reliability of the half- and one-watt motors over that of the earlier three-watt motor.

d. The reliability tests and calculations described below indicate that a predicted reliability figure in excess of 95 percent for a one year mission was achieved as required.

2. Reliability Analysis of the Half-Watt Motor

a. The reliability of the half-watt motor (P/N 9847) was computed for the four different "minor-fault" modes in which the motor will continue to operate. These modes are included in the test data listed in Table 11. Various numbers of segments were deleted at an ambient temperature of 25^{o}C with a nominal supply voltage of 24 VDC. Figures 23 through 27 are the block diagrams representing these minor-fault operating modes along with the applicable reliability parameters. The reliability figures given in the blocks apply to 10,000 hours of operation. The derivations

	Segment Removed	Current (Ma)	Speed RPM	Light Voltage
1.	0	20	3300	1.34
2.	2	19.5	3130	1.23
3.	2 & 5	18.4	2840	1.04
4.	2, 5 & 3	42.4	2440	1.325
5.	6	35	2450	
6.	3,5 & 4	29	2740	1.11
7.	3 & 5	27.2	2750	1.1
8.	3 & 2	19.1	2920	1.15
9.	2,3 & 6	23.5	2320	1.1
10.	1, 2, 4 & 6			
11.	3, 6 & 4	36	2450	1.21
12.	3 & 4	29.8	2900	1.2
13.	1 & 3	20	2660	1.04
14.	1,3 & 2	19.5	2670	1.02
15.	3, 2, 4 & 1	50	2450	1.39
16.	1 & 6	19.5	2930	
17.	4 & 6		0	

TABLE 11

MOTOR CHARACTERISTICS FOR OPERATION
IN MINOR-FAULT MODES
(HALF-WATT MOTOR)

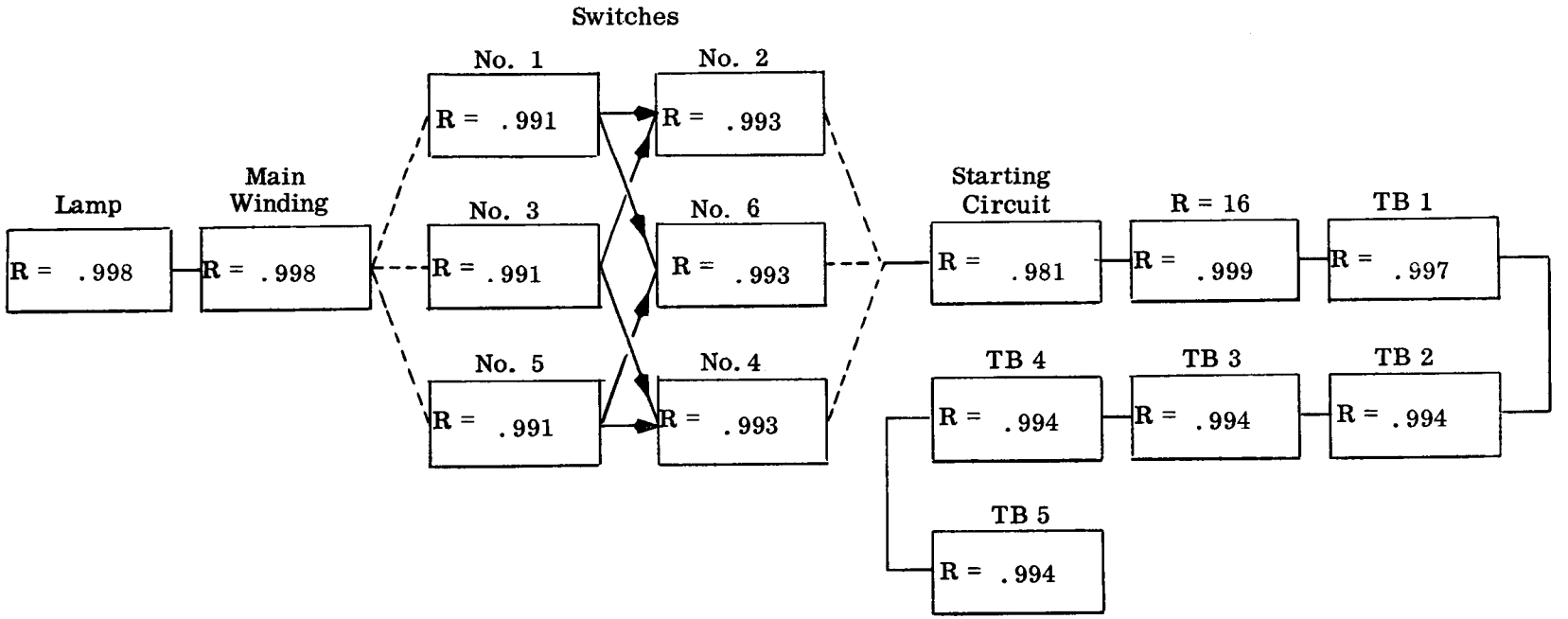

– – – – Redundancy paths provided by flywheel action of rotor

Notes:

1. Failure of four commutator switches acceptable (Failure Mode A).
2. It is assumed here that motor will continue to run so long as its main winding receives current, as indicated by a through path in this diagram.
3. No minimum speed has been specified for this motor
4. Values for reliability figures R apply for 10,000 hours only.

$R_{motor} = 0.94$ for t = 10,000 hours
$R_{motor} = 0.96$ for t = 8,760 hours

FIGURE 23

RELIABILITY DEPENDENCY DIAGRAM FOR HALF-WATT MOTOR
(FAILURE MODE A)

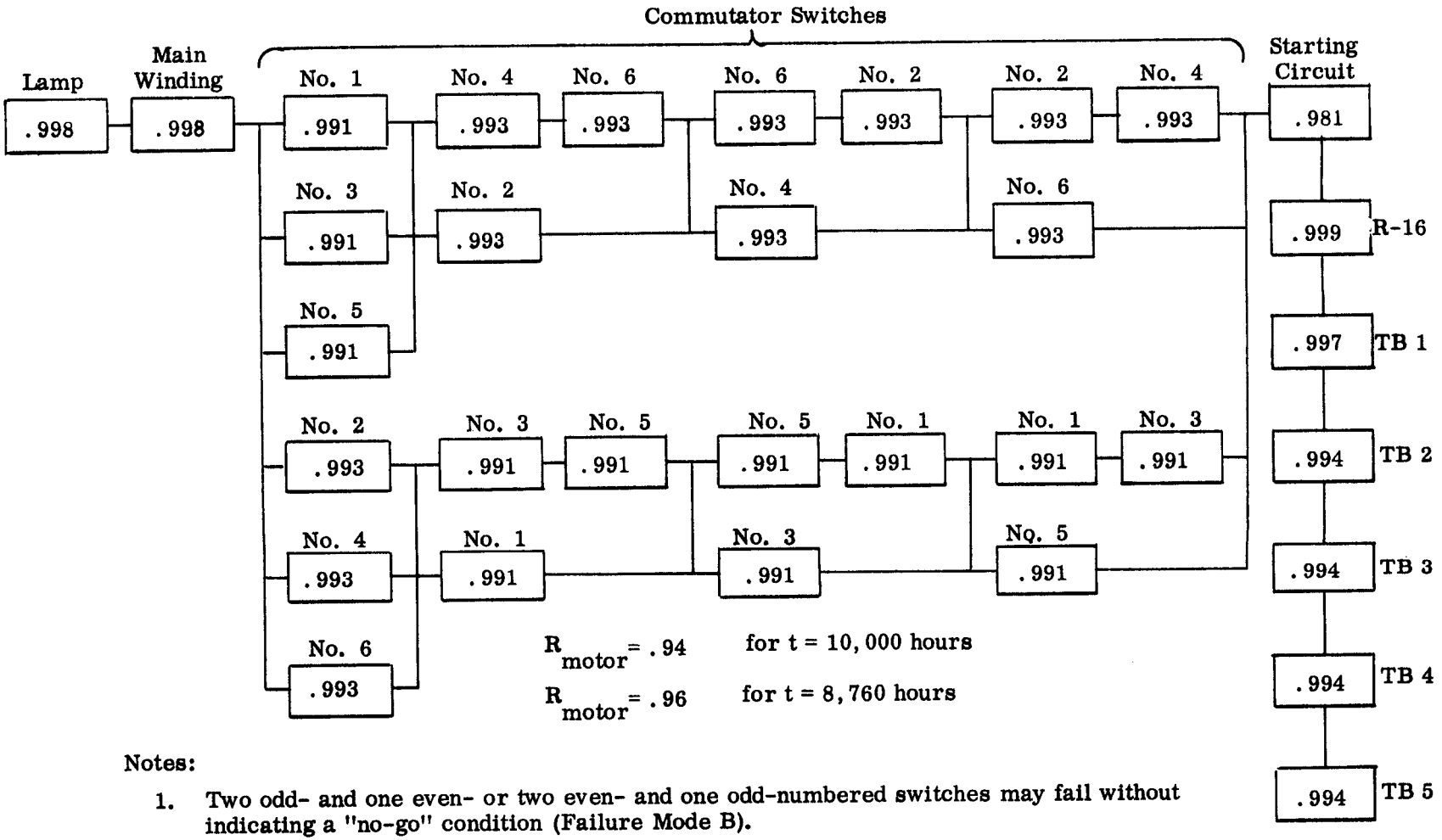

Notes:

1. Two odd- and one even- or two even- and one odd-numbered switches may fail without indicating a "no-go" condition (Failure Mode B).

2. Values shown for reliability figures, in blocks, apply for t = 10,000 hours only.

FIGURE 24

RELIABILITY DEPENDENCY DIAGRAM FOR HALF-WATT MOTOR
(FAILURE MODE B)

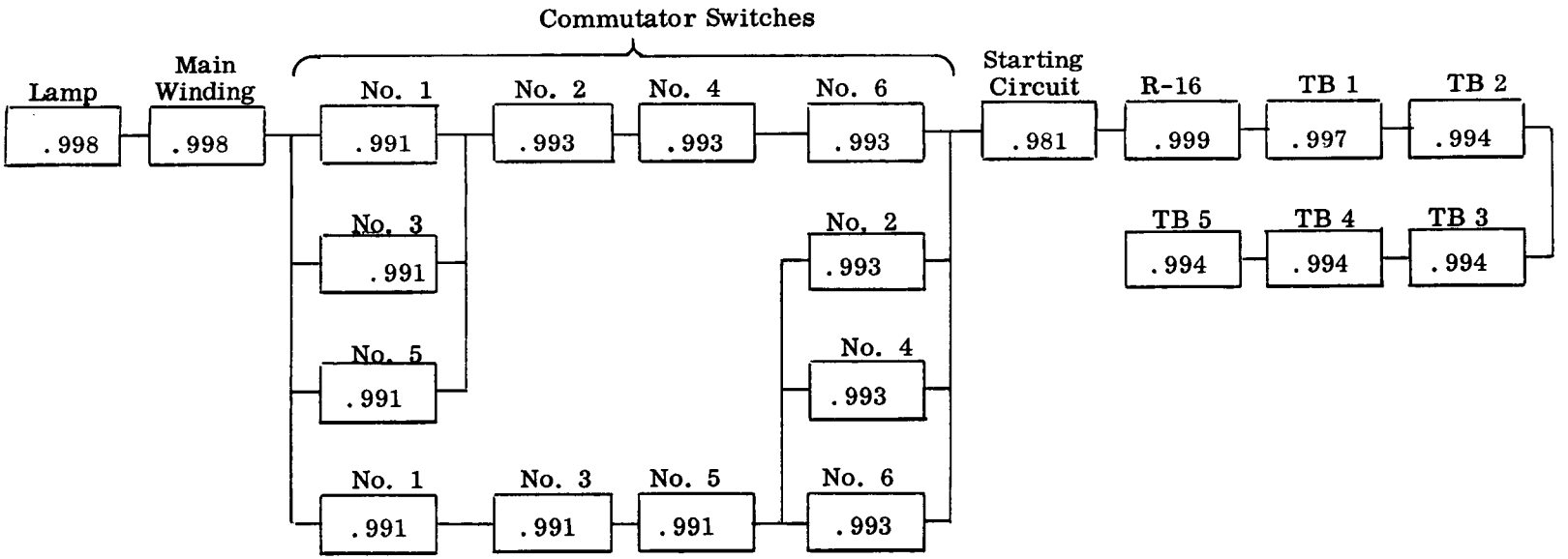

Notes:

1. This diagram applied for failure of two even- or two odd-numbered switches (Failure Mode C).

   $R_{motor} = .93$ for 10,000 hours

   $R_{motor} = .95$ for 8,760 hours

2. Values shown for R in blocks apply for t = 10,000 hours only.

3. This diagram applies to the one-watt motor also.

FIGURE 25

RELIABILITY DEPENDENCY DIAGRAM FOR HALF-WATT MOTOR
(FAILURE MODE C)

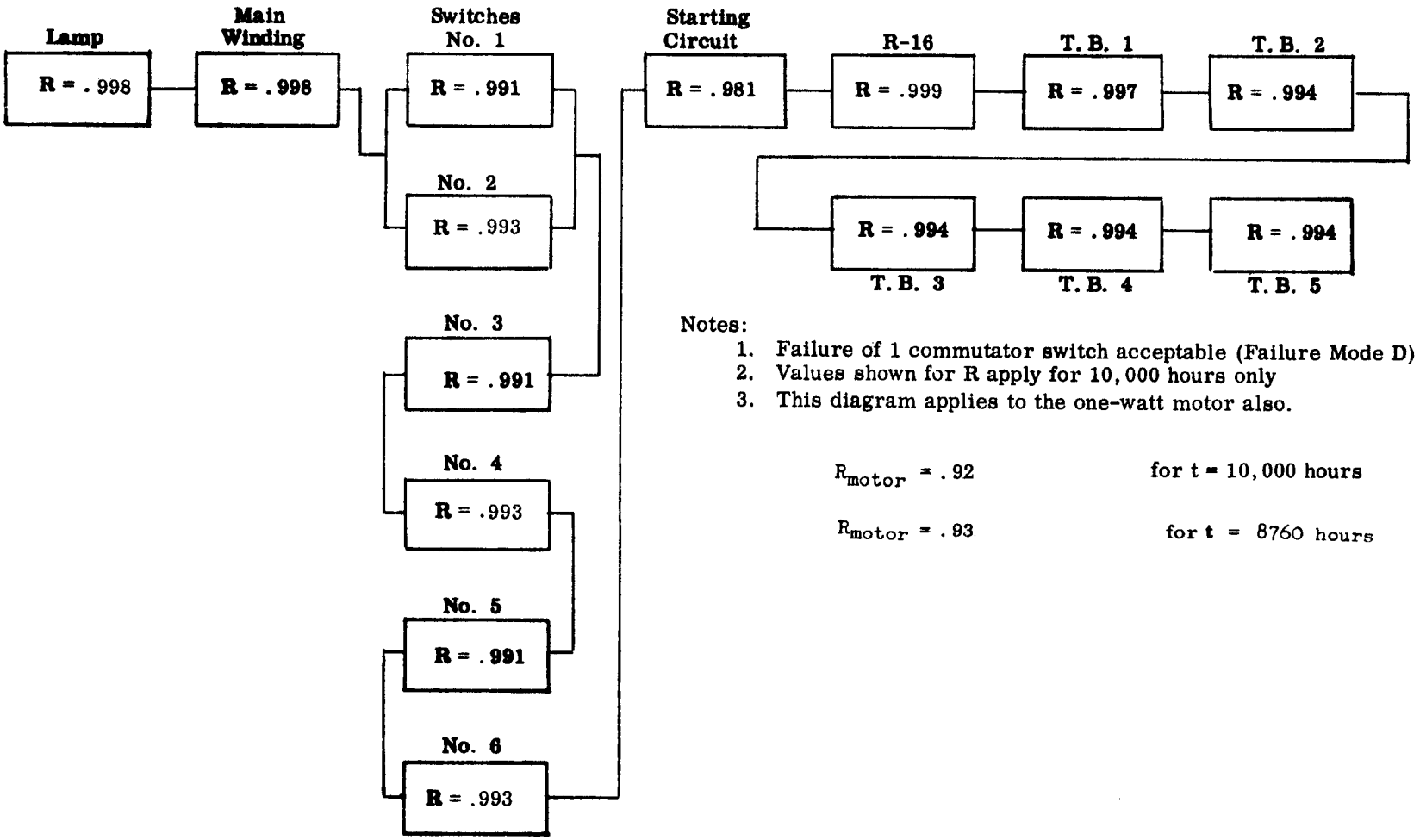

FIGURE 26

RELIABILITY DEPENDENCY DIAGRAM FOR HALF-WATT MOTOR (FAILURE MODE D)

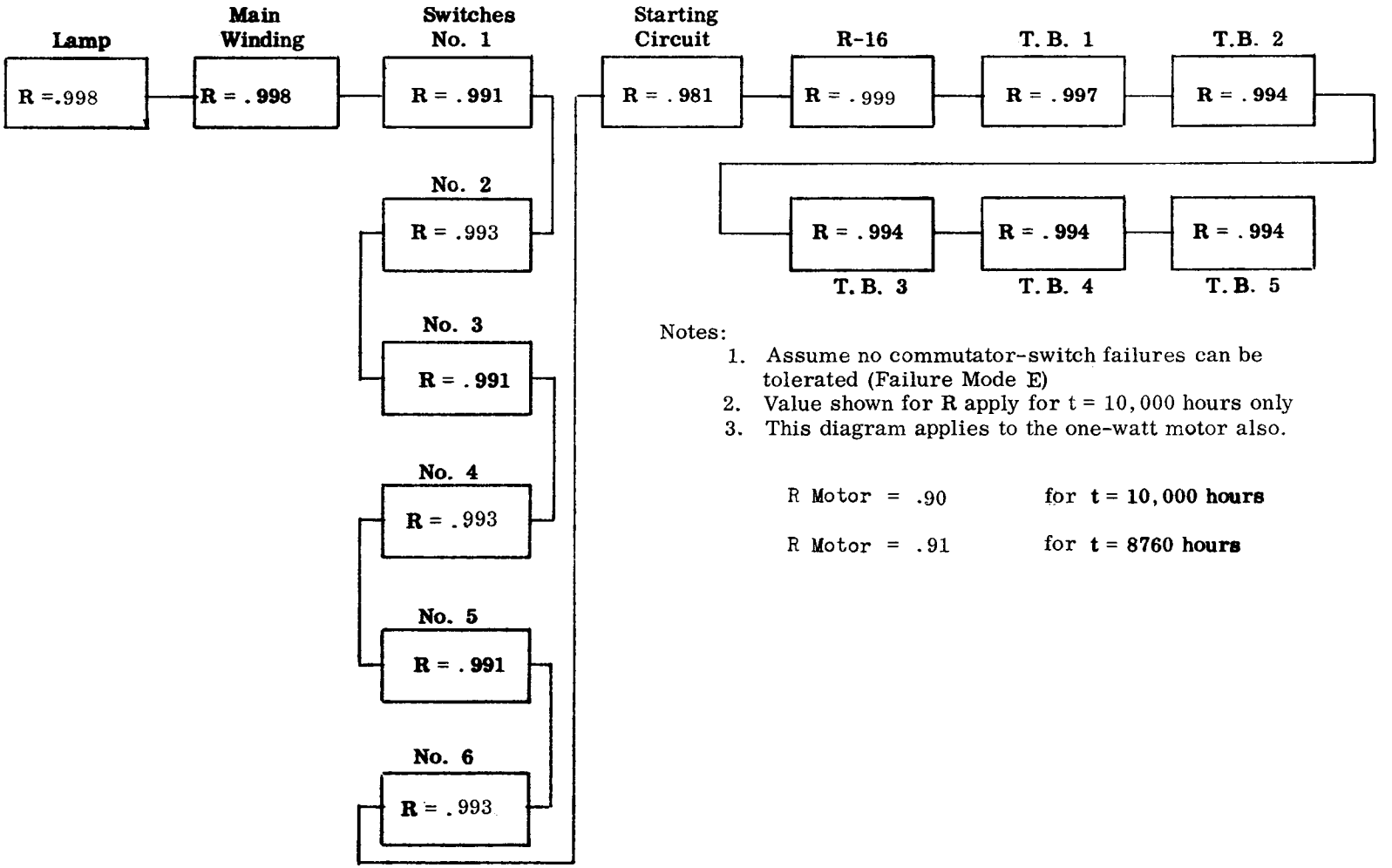

Notes:

1. Assume no commutator-switch failures can be tolerated (Failure Mode E)
2. Value shown for R apply for t = 10,000 hours only
3. This diagram applies to the one-watt motor also.

R Motor = .90 for t = 10,000 hours

R Motor = .91 for t = 8760 hours

FIGURE 27

RELIABILITY DEPENDENCY DIAGRAM FOR HALF-WATT MOTOR (FAILURE MODE E)

of these figures and those applicable to 8,760 hours (one year) of operation are shown in Appendix III, "Reliability Analysis of Components for Half-watt Brushless DC Motor".

b. The motor-reliability calculations were made with the following assumptions:

(1) No mechanical hardware (e.g. bearings) is included in the calculations.

(2) The lamp has been given a failure rate of 0.020 percent per 1000 hours.

(3) It is assumed that the motor will continue to run so long as it has a current path through the winding, as indicated by a through path on the applicable reliability dependency diagram.

(4) The mission reliability figures R_m (for 10,000 hours and for 8,760 hours) for the half-watt motor as shown in Figures 25 through 27 apply to the one-watt motors also.

(5) The reliability figures for each of the four failure modes (0, 1, 2, 3, and 4 commutator switches failing) are based on the assumption that the speed to which the motor will drop in each case is not sufficiently low to represent a catastrophic failure.

(6) In the cases where it is assumed that three or four commutator switches can fail without an excessive loss in speed, the reliability figures did not change significantly.

(7) In the case where it is assumed that two commutator switches can fail without an excessive loss in speed, the choice of these two has been limited for simplicity. The special case presented in Figure 25 is limited to the failure of two odd- or two even-numbered commutator switches.

(8) Switch numbers used in Figures 23 through 27 are taken from the schematic diagram of Figure 12.

c. Data sources utilized for these reliability calculations, other than in-house information, were:

Interservice Data Exchange Program (IDEP)

RADC Reliability Notebook

Defense Documentation Center (DDC)

MIL Handbook 217

E. RECOMMENDATIONS

1. Changes

It is recommended that the following changes be made in any follow-on contract:

a. Sealing Sleeve

Increase plating thicknesses of copper and tin to 0.0005 inch to improve solderability of the end cap to the tube, and use induction heating to accomplish the soldering.

b. Commutator

Re-package the electronic commutator for increased mechanical rigidity.

2. Investigations

It is recommended that future work should include the following investigations:

a. Rotor

(1) Shape the pole faces to make the flux distribution pattern as nearly rectangular as possible instead of sinusoidal.

(2) Adjust the width of the rotor across the flats in an attempt to reduce cogging.

b. Sealing Sleeve and Stator

(1) Investigate the possibility of reducing the amount of sealing required in the motor. This would involve the elimination, wherever possible, of materials from which outgassing might occur and the substitution of new materials.

(2) Determine whether or not the addition of a secondary winding and an accommodating modification of the commutating circuit will result in an appreciable reduction in commutator power loss.

(3) Investigate further the flexibility of existing Sperry Farragut stator designs. An indication of this flexibility has already been obtained by rewinding the stator from a one-watt motor with 62 turns of #28 heavy Formvar wire and driving it with a heavy duty commutator. As shown by the performance curves of Figure 28, the motor reached a peak efficiency of 62 percent at 14,200 RPM. At that speed it developed two in-oz. of torque and drew 1.25 amps. These figures correspond to a power output of 21 watts for a power input of 35 watts.

c. Commutator

(1) Consider a lower-cost replacement for transistor Q20 (Figures 11 and 12).

(2) Seek a smaller, lower cost diode for suppressing transients.

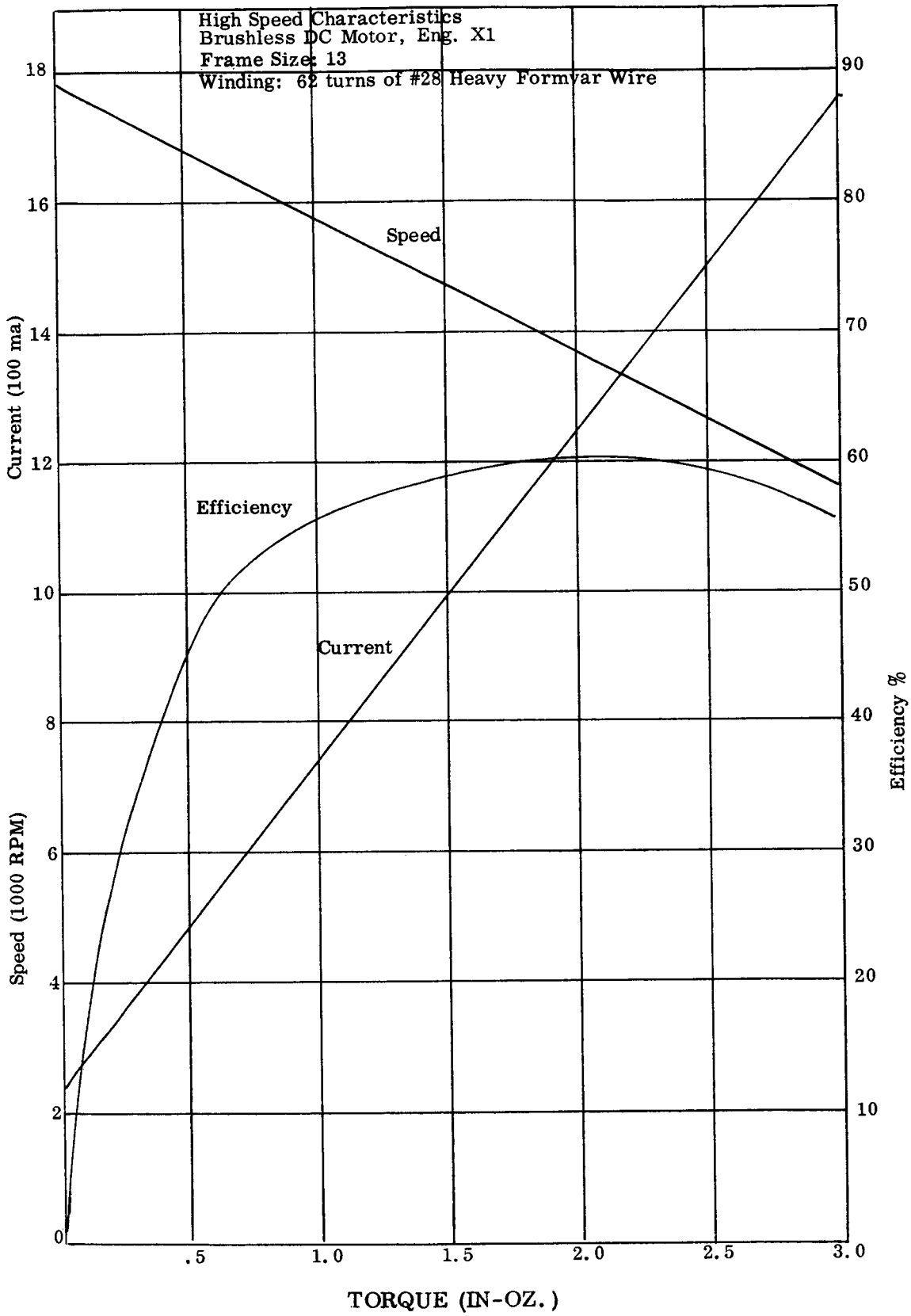
High Speed Characteristics
Brushless DC Motor, Eng. X1
Frame Size: 13
Winding: 62 turns of #28 Heavy Formvar Wire
Speed
Efficiency
Current
Current (100 ma)
Speed (1000 RPM)
Efficiency %
TORQUE (IN-OZ.)
0
2
4
6
8
10
12
14
16
18
10
20
30
40
50
60
70
80
90
.5
1.0
1.5
2.0
2.5
3.0

FIGURE 28

(3) Investigate new techniques for mounting and connecting the photo-devices.

(4) Investigate the possibility of using newly developed electronic components to reduce the size and weight, and raise the efficiency and reliability of the electronic commutator. For example, determine whether micro-packaged transistors could be used in the six preamp stages.

F. DELIVERY OF MOTORS

As mentioned in paragraph IV. A. 5, the revised delivery deadline was met by Sperry Farragut Company. Table 12 shows the date on which each of the motors was shipped to Goddard Space Flight Center.

Part Number	Size	Serial Number	Date Shipped
ENG 9821-A	1 watt	SF-1	6-30-64
ENG 9821-A	1 watt	SF-2	6-18-64
ENG 9821-A	1 watt	SF-3	7-1-64
ENG 9821-A	1 watt	SF-4	6-30-64
ENG 9847	1/2 watt	SF-1	7-1-64
ENG 9847	1/2 watt	SF-2	6-18-64

TABLE 12

DATES OF SHIPMENT OF COMPLETED MOTORS
TO GODDARD SPACE FLIGHT CENTER

G. DOCUMENTATION

1. Progress Reports

Progress on this contract was reported to Goddard by means of monthly progress reports. These included summaries of work accomplished during the reporting period and the effectiveness of such work, statements regarding conformance to the work schedule and the adequacy of funds to complete the task, and statements of the work efforts planned for succeeding reporting periods.

2. Drawings

a. A complete set of drawings for all parts, assemblies, and permanent tooling for this contract was developed and maintained at Sperry Farragut. One set of brownline reproducibles and one set of blueline prints of the final engineering drawings were shipped to Goddard shortly after the motors had been shipped. Many of these drawings were common to both the one-watt and the half-watt motors. Drawings such as those portraying the top assemblies, circuit boards and stator-winding assemblies were, of necessity, kept separate for the two motor types.

b. Motors made to the above-mentioned drawings will incorporate the best features of the engineering developmental models already delivered to Goddard. All differences between the delivered motors and those represented by the final drawings have been tested in Table 10.

c. Final Report

This report is the Final Report required under Contract NAS 5-3582.

APPENDIX I

ARMATURE WINDING ANALYSIS FOR A BRUSHLESS DC MOTOR
(Written in terms of the original 60-degree commutation angle)

LIST OF FIGURES

ARMATURE WINDING ANALYSIS FOR A BRUSHLESS DC MOTOR

OPTIMUM MOTOR PERFORMANCE IS OBTAINED WHEN THE AVERAGE VALUE OF THE COUNTER EMF INDUCED IN THE ARMATURE WINDING IS MAXIMIZED AND THE ARMATURE WINDING RESISTANCE IS MINIMIZED. THE FOLLOWING ANALYSIS IS AN INVESTIGATION OF VARIOUS WINDINGS WHICH MAY BE USED IN A TWO POLE BRUSHLESS MOTOR WITH 12 ARMATURE SLOTS.

A. FULL PITCH LAP WINDING

THE 3-WATT GSFC MOTOR USED THE FULL PITCH WINDING SHOWN BELOW.

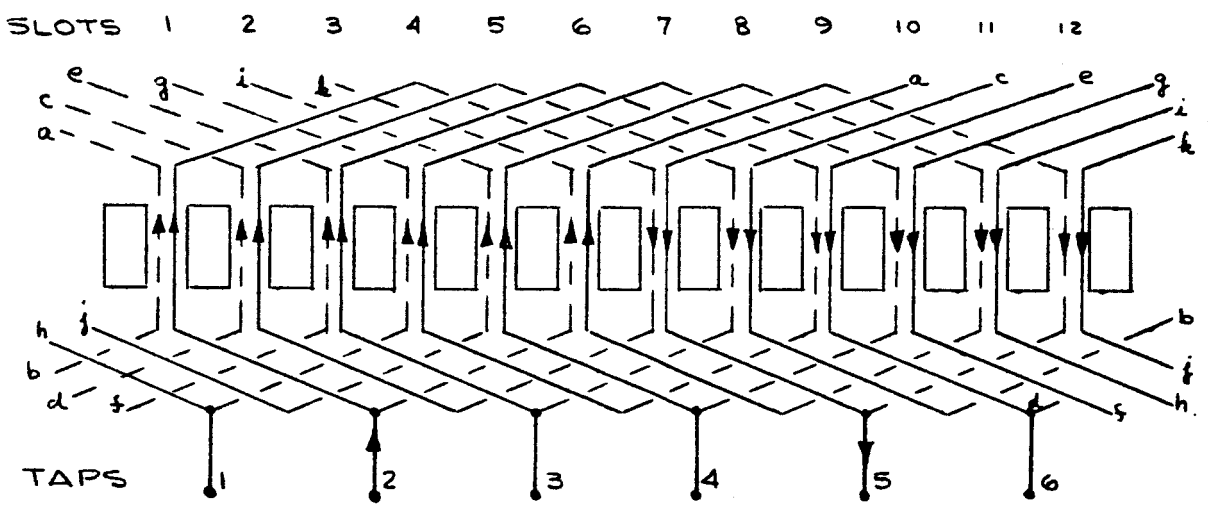

FULL PITCH LAP WINDING
FIGURE 1

THE DIRECTION OF CURRENT IN THE ARMATURE CONDUCTORS IS SHOWN FOR THE

COMMUTATION PERIOD DURING WHICH THE TERMINAL VOLTAGE IS APPLIED BETWEEN COMMUTATING TAPS 2 AND 5. THIS PERIOD EXISTS FOR ONE SIXTH OF A REVOLUTION OF THE ROTOR.

B MODIFIED LAP WINDING

THE WINDING OF FIGURE 1 HAS TWO FULL PITCH COILS BETWEEN ADJACENT COMMUTATING TAPS. ONE SET OF THESE COILS IS SHOWN IN FIGURE 2A, BUT FIGURE 2B SHOWS TWO FRACTIONAL PITCH COILS (CHORDED COILS) THAT PRODUCE THE SAME MAGNETIC EFFECT WITH LESS END WINDING LENGTH

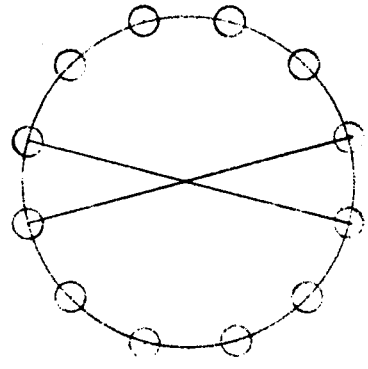

FULL PITCH COILS
FIGURE 2A

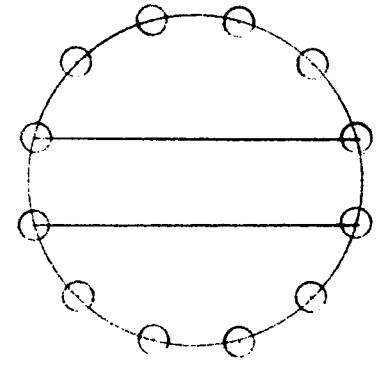

CHORDED COILS
FIGURE 2B

A COMPLETE WINDING USING THE CHORDED COILS IS SHOWN IN FIGURE 3. THIS WINDING IS EXACTLY EQUIVALENT TO FIGURE 1 EXCEPT THAT EACH COIL SPANS ONLY 5 SLOT PITCHES INSTEAD OF 6. THIS RESULTS IN ABOUT A 17 PERCENT REDUCTION IN END WINDING VOLUME AND A 10 PERCENT REDUCTION IN ARMATURE RESISTANCE.

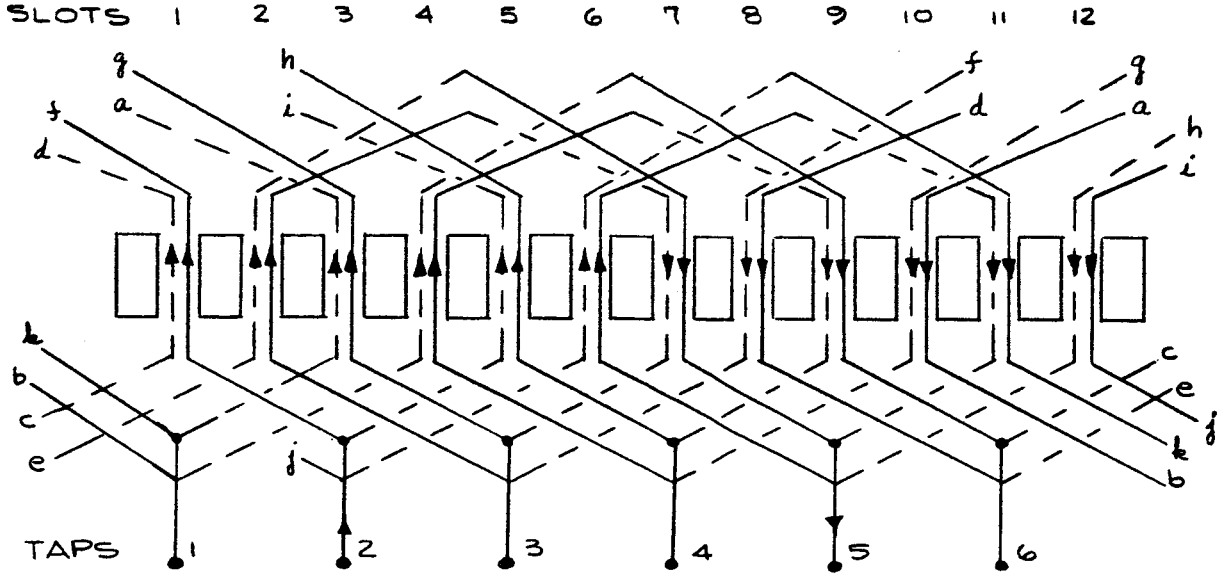

MODIFIED DC WINDING
FIGURE 3

FIGURE 3 IS A HYBRID FULL PITCH WINDING USING CHORDED COILS. IT IS NOT A CONVENTIONAL CHORDED LAP WINDING. AS IN FIGURE 1 THE DIRECTION OF CURRENT FLOW IS THE SAME IN ALL CONDUCTORS OF EACH SLOT DURING EVERY PERIOD OF COMMUTATION. THE CONDITIONS OF CURRENT FLOW IN FIGURE 3 MAY BE REPRESENTED IN FIGURE 4 WHICH IS MORE SUITABLE FOR ANALYSIS OF THE VOLTAGE INDUCED IN THE WINDING BY THE FIELD FLUX.

SEARCH COIL MEASUREMENTS OF THE AIR GAP FLUX IN THE EXISTING GSFC BRUSHLESS MOTORS SHOW THAT THE FIELD FLUX DISTRIBUTION IS NEARLY SINUSOIDAL. FOR THIS ANALYSIS IT WILL BE ASSUMED THAT THE AIR GAP FLUX DISTRIBUTION MAY BE GIVEN WITH RE—

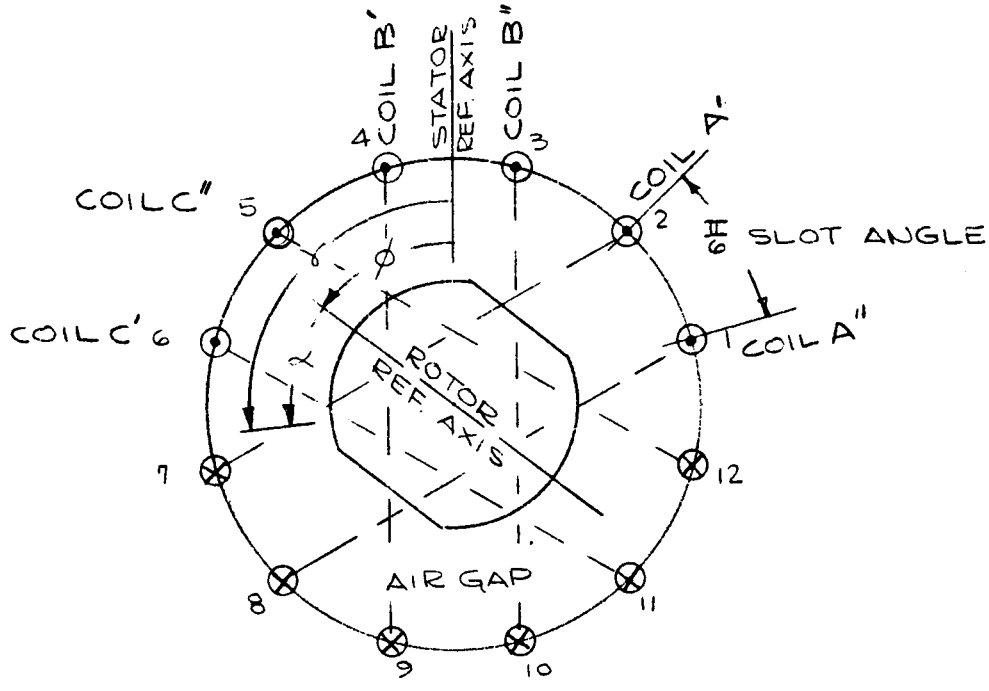

FIGURE 4

SPECT TO THE ROTOR AXIS BY -

① $B(\alpha) = B_0 \cos\alpha$ GAUSS

WHERE α IS AN ANGLE MEASURED AROUND THE AIR GAP FROM THE ROTOR REFERENCE AXIS. THE FLUX MAY BE REFERRED TO THE STATOR (ARMATURE) AXIS BY USING THE RELATIONSHIP -

② $\gamma = \alpha + \phi$

WHERE γ IS AN ANGLE MEASURED AROUND THE AIR GAP FROM THE STATOR REFERENCE AXIS AND ϕ IS THE ROTOR POSITION ANGLE.

③ $\therefore \quad B(\gamma) = B_0 \cos(\gamma - \phi)$ GAUSS

THE WINDING CONTAINS 12 COILS (TWO EACH IN THE SAME SLOTS) OF N_c TURNS

EACH AND EACH SLOT CONTAINS $Z_s = 2N_c$ CONDUCTORS ALL CARRYING CURRENT IN THE SAME DIRECTION. FIGURE 3 SHOWS THAT THERE ARE TWO PARALLEL CURRENT PATHS THROUGH THE WINDING. THE FLUX WHICH LINKS WITH COIL "A'" IN FIGURE 4 IS-

④ $$\Phi'_A = RL\int_{-\frac{3\pi}{12}}^{+\frac{7\pi}{12}} B_0 \cos(\gamma-\phi)\,d\gamma$$

$$= 2RLB_0 \sin\tfrac{5\pi}{12}\cos\left(\phi-\tfrac{\pi}{6}\right) \text{ MAXWELLS}$$

WHERE R= AIR GAP RADIUS (CM.)
L= " " AXIAL LENGTH (CM.)

COIL A' CONTAINS $N_c = Z_s/2$ TURNS AND THE FLUX LINKAGES WITH COIL A' ARE -

⑤ $$\Psi'_A = RLB_0 Z_s \sin\tfrac{5\pi}{12}\cos\left(\phi-\tfrac{\pi}{6}\right) \text{ MAXWELL-TURNS}$$

BY SYMMETRY THE SAME FLUX LINKS WITH COIL "A" AND THE TOTAL FLUX LINKAGES WITH BOTH SERIES CONNECTED COILS IS -

⑥ $$\Psi_A = 2RLB_0 Z_s \sin\tfrac{5\pi}{12}\cos\left(\phi-\tfrac{\pi}{6}\right) \text{ MAXWELL-TURNS}$$

SIMILARLY, THE FLUX LINKAGES FOR THE B AND C COIL SETS ARE -

⑦ $$\Psi_B = 2RLB_0 Z_s \sin\tfrac{5\pi}{12}\cos\left(\phi-\tfrac{\pi}{2}\right)$$

$$\Psi_C = 2RLB_0 Z_s \sin\tfrac{5\pi}{12}\cos\left(\phi-\tfrac{5\pi}{6}\right) \text{ MAXWELL-TURNS}$$

AND THE TOTAL FLUX LINKAGES FOR ALL COILSINTHIS CURRENT PATH ARE -

⑧ $$\Psi = 4RLB_0 Z_s \sin\tfrac{5\pi}{12}\sin\phi \text{ MAXWELL-TURNS}$$

IF THE ROTOR ROTATES AT CONSTANT ANGULAR VELOCITY (ω) IT FOLLOWS THAT

(9) $$\omega = \frac{d\phi}{dt} \quad \text{RAD/SEC}$$

AND THE VOLTAGE INDUCED IN THE ARMATURE IS

(10) $$e = -\frac{\partial \psi}{\partial t} = -\frac{\partial \psi}{\partial \phi}\frac{\partial \phi}{\partial t} = -\omega \frac{\partial \psi}{\partial \phi}$$

OR $$e = -4\omega R L B_0 Z_s \sin\frac{5\pi}{12}\cos\phi \quad \text{ABVOLTS}$$

THIS EQUATION MAY BE SIMPLIFIED BY INTRODUCING THE TOTAL FIELD FLUX PER POLE

(11) $$\Phi = RL\int_{-\frac{\pi}{2}}^{+\frac{\pi}{2}} B_0 \cos\alpha \, d\alpha = 2RLB_0 \quad \text{MAXWELLS}$$

THEN –

(12) $$e = -2\omega Z_s \Phi \sin\frac{5\pi}{12}\cos\phi \quad \text{ABVOLTS}$$

THE OBJECTIVE IS TO OBTAIN THE MAXIMUM AVERAGE INDUCED VOLTAGE OVER A 60 DEGREE COMMUTATION ZONE. EVIDENTLY THIS OCCURS FOR THE ROTOR ANGLE $-\pi/6 < \phi < +\pi/6$ FOR WHICH THE AVERAGE VOLTAGE IS

(13) $$|E_{AVE}| = \left|\frac{3}{\pi}\int_{-\frac{\pi}{6}}^{+\frac{\pi}{6}} e\, d\phi\right| = \frac{6}{\pi}\omega Z_s \Phi \sin\frac{5\pi}{12} \quad \text{ABVOLTS}$$

LET $$n = \frac{30\omega}{\pi} \quad \text{RPM}$$

AND $Z = 12 Z_s$ TOTAL ARMATURE CONDUCTORS

THEN

(14) $$E_{AVE} = \frac{Z\Phi n}{60}\sin\frac{5\pi}{12} = .0161\, Z\Phi n \quad \text{ABVOLTS}$$

THE RESISTANCE OF A SINGLE CONDUCTOR IS -

(15) $$r_c = \frac{\rho L_c}{A_c} \text{ ABOHMS}$$

WHERE ρ = RESISTIVITY OF WIRE (ABOHM-CM)

L_c = LENGTH OF CONDUCTOR (CM)

A_c = AREA OF CONDUCTOR (SQ.CM)

IF THE SLOTS ARE FILLED TO CAPACITY THE FOLLOWING EQUATION IS VALID

(16) $$A_c Z_s = \frac{A_c Z}{12} = A_s \quad \text{SQ. CM.}$$

WHERE A_s = AREA OF ONE SLOT.

THEN -

(17) $$r_c = \frac{\rho L_c Z}{12 A_s} \text{ ABOHMS}$$

THE RESISTANCE OF THE ENTIRE WINDING WITH TWO PARALLEL CURRENT PATHS IS -

(18) $$R_{DC} = \frac{Z r_c}{4} = \frac{\rho L_c}{12 A_s}\left(\frac{Z^2}{4}\right) \text{ ABOHMS}$$

IT IS ASSUMED HERE THAT IT IS ALWAYS POSSIBLE TO OBTAIN A WIRE SIZE WHICH COMPLETLY FILLS THE SLOTS FOR ANY REQUIRED NUMBER OF CONDUCTORS.

C. WYE WINDING

A 2 POLE, 12 SLOT DC ARMATURE MAY ALSO BE WOUND WITH A THREE PHASE WYE WINDING AS REPRESENTED IN FIGURE 5

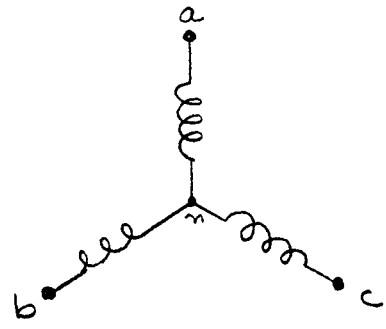

WYE WINDING
FIGURE 5

A SIMPLE FULL PITCH LAP WINDING MAY BE USED HAVING 4 COILS PER PHASE, BUT ALL 4 COILS WOULD OCCUPY ONLY 4 SLOTS AS IN FIGURE 2A. EVIDENTLY THE WINDING RESISTANCE CAN BE REDUCED BY USING THE CHORDED COIL ARRANGEMENT OF FIGURE 2B.

THE WYE WINDING IS COMMUTATED SIX TIMES PER REVOLUTION BY APPLYING VOLTAGE BETWEEN TERMINALS a & b, a & c, b & c, b & a, ETC. ONLY TWO PHASES CARRY CURRENT AT ANY INSTANT. FIGURE 6 REPRESENTS THE WYE WOUND STATOR AND ROTOR WITH THE STATOR REFERENCE AXIS TAKEN ALONG THE MAGNETIC AXIS OF PHASE a. THE FLUX LINKING COIL a_1 OF PHASE a IS -

(15) $$\Phi_{a_1} = RL\int_{-\frac{5\pi}{12}}^{+\frac{5\pi}{12}} B_0 \cos(\gamma-\phi)\,d\gamma$$

$$= 2RLB_0 \sin\tfrac{5\pi}{12}\cos\phi \quad \text{MAXWELLS}$$

AND THE FLUX LINKAGES WITH COIL a_1

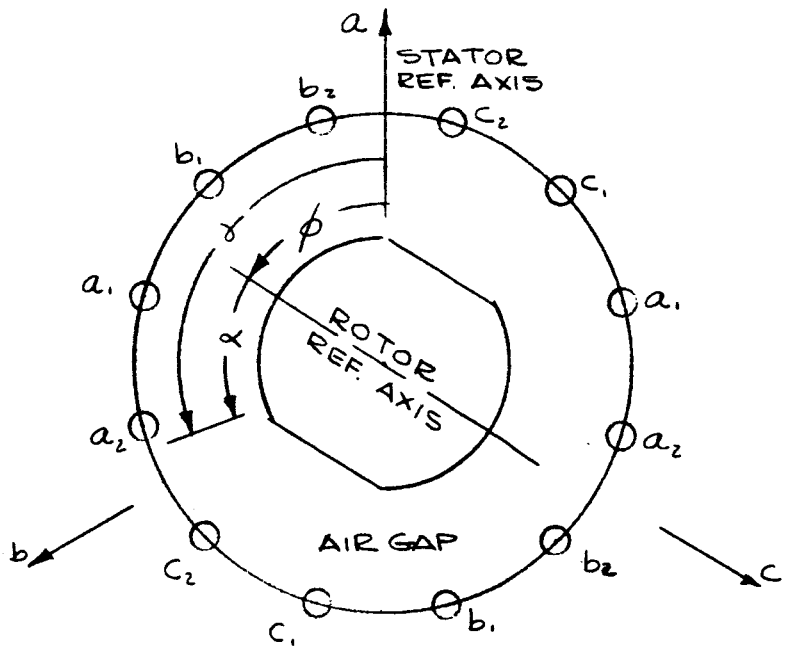

FIGURE 7

WHICH HAS Z_s TURNS (OR CONDUCTORS PER SLOT) ARE -

(20) $\psi_{a_1} = Z_s \Phi_{a_1} = 2RLB_0 Z_s \sin\frac{5\pi}{12}\cos\phi$ MAXWELL-TURNS

BY SYMMETRY THE FLUX LINKAGES WITH COIL a_2 ARE THE SAME AS FOR COIL a_1 AND SINCE THESE COILS ARE IN SERIES THE TOTAL FLUX LINKAGES WITH PHASE a ARE

(21) $\psi_a = 4RLB_0 Z_s \sin\frac{5\pi}{12}\cos\phi$

OR $\psi_a = 2Z_s\Phi \sin\frac{5\pi}{12}\cos\phi$ MAXWELL-TURNS

WHERE $\Phi = 2RLB_0$, THE TOTAL FLUX PER POLE.

SIMILARLY FOR PHASES b AND C

(22) $\psi_b = 2Z_s\Phi \sin\frac{5\pi}{12}\cos\left(\phi - \frac{2\pi}{3}\right)$

$\psi_c = 2Z_s\Phi \sin\frac{5\pi}{12}\cos\left(\phi + \frac{2\pi}{3}\right)$ MAXWELL-TURNS

THE VOLTAGES INDUCED IN EACH PHASE WITH RESPECT TO THE NEUTRAL ARE -

(23) $e_a = 2\omega Z_s \Phi \sin\frac{5\pi}{12} \sin\phi$

$e_b = 2\omega Z_s \Phi \sin\frac{5\pi}{12} \sin\left(\phi - \frac{2\pi}{3}\right)$

$e_c = 2\omega Z_s \Phi \sin\frac{5\pi}{12} \sin\left(\phi + \frac{2\pi}{3}\right)$ ABVOLTS

AND THE VOLTAGES INDUCED BETWEEN TERMINALS ARE

(24) $e_{ab} = e_b - e_a = 4\omega Z_s \Phi \sin\frac{5\pi}{12} \sin\frac{\pi}{3} \cos\left(\phi + \frac{2\pi}{3}\right)$

$e_{bc} = e_c - e_b = 4\omega Z_s \Phi \sin\frac{5\pi}{12} \sin\frac{\pi}{3} \cos\phi$

$e_{ca} = e_a - e_c = 4\omega Z_s \Phi \sin\frac{5\pi}{12} \sin\frac{\pi}{3} \cos\left(\phi - \frac{2\pi}{3}\right)$ ABVOLTS

CONSIDER VOLTAGE e_{bc}. FOR A MAXIMUM AVERAGE VOLTAGE COMMUTATION MUST OCCUR DURING $-\pi/6 < \phi < +\pi/6$ FOR WHICH -

(25) $|E_{AVE}| = \frac{3}{\pi}\left[4\omega Z_s \Phi \sin\frac{5\pi}{12} \sin\frac{\pi}{3}\right]$

$= \frac{\sqrt{3}}{60} Z \Phi n \sin\frac{5\pi}{12}$

OR $E_{AVE} = .0279\, Z \Phi n$ ABVOLTS

THE WYE WINDING USES THE SAME COIL SPAN AS THE MODIFIED DC WINDING AND THE LENGTH OF A CONDUCTOR IS THE SAME FOR BOTH. SINCE ONLY TWO PHASES OF THE WYE WINDING ARE IN SERIES AT ANY INSTANT THE ARMATURE RESISTANCE IS -

(26) $R_Y = \frac{2}{3} Z r_c = \frac{\rho L_c}{12 A_s}\left(\frac{2Z^2}{3}\right)$ ABOHMS.

D DELTA WINDING

THE THREE PHASES OF FIGURE 7 MAY ALSO BE CONNECTED IN DELTA AS IN FIGURE 8 BELOW.

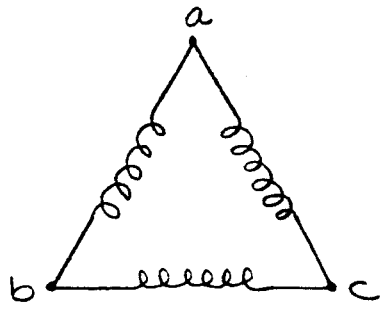

DELTA WINDING
FIGURE 8

IN THIS CASE THE PHASE VOLTAGES OF EQUATION (23) ARE ALSO THE TERMINAL VOLTAGES.

(27) $$e_{ab} = 2\omega Z_s \Phi \sin\frac{6\pi}{12} \sin\phi$$

$$e_{bc} = 2\omega Z_s \Phi \sin\frac{5\pi}{12} \sin\left(\phi - \frac{2\pi}{3}\right)$$

$$e_{ca} = 2\omega Z_s \Phi \sin\frac{5\pi}{12} \sin\left(\phi + \frac{2\pi}{3}\right) \quad \text{ABVOLTS}$$

AND THE MAXIMUM AVERAGE VOLTAGE IS -

(28) $$E_{AVE} = \frac{Z\Phi n}{60} \sin\frac{5\pi}{12} \quad \text{ABVOLTS}$$

WHICH IS THE SAME AS FOR THE DC WINDING

THE DELTA WINDING HAS TWO PARALLEL PATHS WHICH GENERATE THE SAME INDUCED VOLTAGE, BUT DO NOT HAVE THE SAME

RESISTANCE. THE RESISTANCE OF ONE PHASE IS -

(29) $$R_\phi = \frac{\rho L_c}{12 A_s}\left(\frac{Z^2}{3}\right) \quad \text{ABOHMS}$$

THE DELTA WINDING MAY BE REPRESENTED BY THE CIRCUIT OF FIGURE 9 DURING THE PERIOD THAT A VOLTAGE IS APPLIED ACROSS TERMINALS a & b.

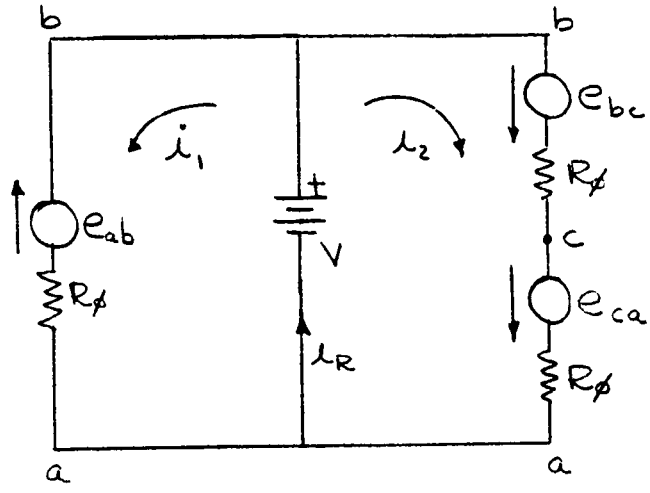

FIGURE 9

THE CIRCUIT EQUATIONS ARE

(29) $$V = e_{ab} + i_1 R_\phi \quad \text{OR} \quad i_1 = \frac{V - e_{ab}}{R_\phi}$$

$$V = -(e_{bc} + e_{ca}) + i_2(2R_\phi) = e_{ab} + 2 i_2 R_\phi$$

$$\text{OR} \quad i_2 = \frac{V - e_{ab}}{2R_\phi}$$

THE TOTAL INPUT CURRENT IS

(30) $$i_R = i_1 + i_2 = \frac{V - e_{ab}}{\frac{2}{3} R_\phi}$$

AN EQUIVALENT DELTA WINDING RESISTANCE MAY BE DEFINED BY –

(31) $$I_R = \frac{V - e_{ab}}{R_\Delta}$$

COMPARING EQUATIONS (30) AND (31) LEADS TO

(32) $$R_\Delta = \frac{2}{3} R_\phi = \frac{\rho L_s}{12 A_s}\left(\frac{2Z^2}{9}\right) \quad \text{ABOHMS}$$

SUMMARY

THE AVERAGE INDUCED VOLTAGE AND THE EFFECTIVE RESISTANCE FOR THE THREE WINDINGS ARE

DC WINDING

$$E_{DC} = \frac{Z\Phi n}{60} \sin\frac{5\pi}{12} \quad \text{ABVOLTS}$$

$$R_{DC} = \frac{\rho L_c}{12 A_s}\left(\frac{Z^2}{4}\right) \quad \text{ABOHMS}$$

WYE WINDING

$$E_Y = \sqrt{3}\,\frac{Z\Phi n}{60} \sin\frac{5\pi}{12} \quad \text{ABVOLTS}$$

$$R_Y = \frac{\rho L_c}{12 A_s}\left(\frac{2Z^2}{3}\right) \quad \text{ABOHMS}$$

DELTA WINDING

$$E_\Delta = \frac{Z\Phi n}{60} \sin\frac{5\pi}{12} \quad \text{ABVOLTS}$$

$$R_\Delta = \frac{\rho L_c}{12 A_s}\left(\frac{2Z^2}{9}\right) \quad \text{ABOHMS}$$

DISCUSSION

THE DELTA WINDING GENERATES THE SAME VOLTAGE AS THE DC WINDING FOR AN EQUAL NUMBER OF CONDUCTORS, BUT THE RESISTANCE OF THE DELTA IS 11 PERCENT LOWER. THE WYE WINDING GENERATES THE HIGHEST VOLTAGE, BUT IT ALSO HAS THE HIGHEST RESISTANCE. THE VOLTAGE OF THE WYE WILL BE THE SAME AS FOR THE DC AND DELTA WINDINGS IF THE NUMBER OF WYE CONDUCTORS IS REDUCED TO $Z/\sqrt{3}$. IN THIS CASE THE WYE RESISTANCE BECOMES –

(33) $$R_Y' = \frac{\rho L_c}{12 A_s} \frac{2}{3}\left(\frac{Z}{\sqrt{3}}\right)^2 = \frac{\rho L_c}{12 A_s}\left(\frac{2Z^2}{9}\right) \quad \text{ABOHMS}$$

WHICH IS THE SAME AS FOR THE DELTA.

THE ANALYSIS SHOWS THAT THE WYE AND DELTA WINDINGS HAVE LOWER RESISTANCE THAN THE 6 TAP DC WINDING. THEY ALSO REQUIRE ABOUT HALF AS MANY SOLID STATE COMMUTATING DEVICES.

APPENDIX II

DC BRUSHLESS MOTOR WITH A METALLIC ARMATURE SLEEVE

LIST OF FIGURES

BRUSHLESS DC MOTOR WITH METALIC ARMATURE SLEEVE

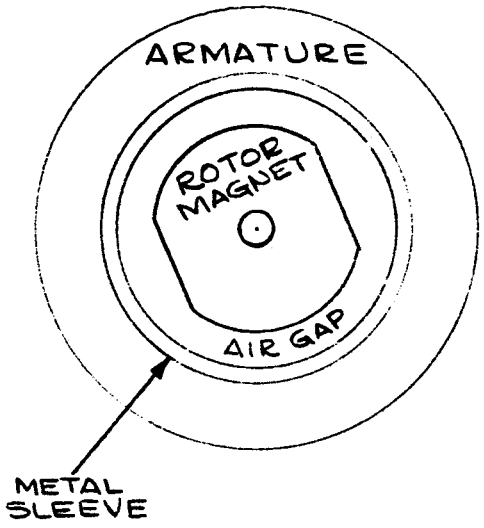

FIGURE 1

FIGURE 1 REPRESENTS A BRUSHLESS DC MOTOR WITH A STATIONARY METAL SLEEVE IN THE AIR GAP. DURING ROTATION THE AIR GAP FLUX INDUCES EDDY CURRENTS IN THE SLEEVE WHICH CAUSE POWER LOSSES.

A MATHEMATICAL ANALYSIS OF FIGURE 1 USING CYLINDRICAL COORDINATES WOULD INVOLVE BESSEL FUNCTIONS. AS AN ESTIMATE THE SIMPLIFIED GEOMETRY OF FIGURE 2 WILL BE ANALYZED

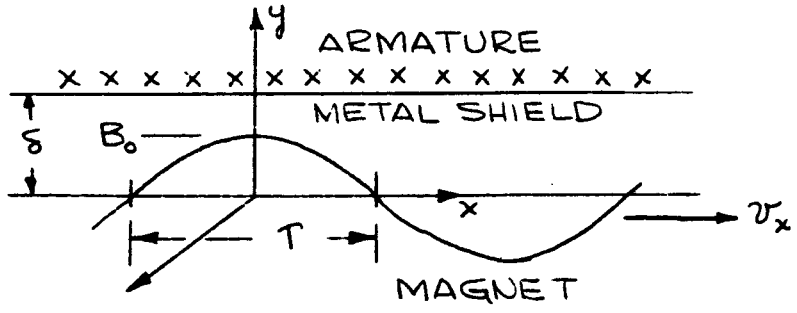

FIGURE 2

IN FIGURE 2 A THIN, NON-FERROUS SHIELD OF THICKNESS δ IS ATTACHED TO A LAMINATED, IRON ARMATURE. THE PERMEABILITY OF THE SHIELD IS UNITY

AND IN COMPARISON THE PERMEABILITY OF THE IRON ARMATURE IS INFINITE, THE RESISTIVITY OF THE LAMINATED ARMATURE IS ALSO ESSENTIALLY INFINITE AS COMPARED TO THE SHIELD.

FOR SIMPLICITY THE AIR GAP WILL BE NEGLECTED AND AS THE ROTOR TURNS AT A CONSTANT VELOCITY v_x THE RADIAL FLUX AT THE SURFACE OF THE SHIELD MAY BE GIVEN BY -

$$\text{①} \qquad \underline{B_y}\Big|_{y=0} = B_0 \cos\left[\frac{\pi}{\tau}(v_x t - x)\right] \quad \text{GAUSS}$$

WHERE τ = POLE PITCH (CM.)
v_x = SURFACE VELOCITY OF FLUX (CM/SEC.)

ELECTROMAGNETIC CONDITIONS WITHIN THE SHIELD ARE DESCRIBED BY MAXWELL'S FIELD EQUATIONS FOR THE QUASI-STATIONARY STATE IN A CONDUCTING MEDIUM.

$$\text{②} \qquad \nabla \times \underline{H} = 4\pi \underline{G} \qquad \nabla \cdot \underline{B} = 0$$

$$\nabla \times \underline{E} = -\frac{\partial B}{\partial t} \qquad \text{(IN CGS SYSTEM)}$$

ALSO $\underline{B} = \mu \underline{H}$ AND $\underline{E} = \rho \underline{G}$

WHERE

$\underline{B}$ = VECTOR INDUCTION (GAUSS)

$\underline{H}$ = VECTOR FIELD INTENSITY (OERSTEDS)

$\underline{G}$ = VECTOR CURRENT DENSITY (ABAMPERES/CM^2)

$\underline{E}$ = VECTOR VOLTAGE GRADIENT (ABVOLTS/CM)

μ = PERMEABILITY

ρ = RESISTIVITY (ABOHM-CM)

THESE EQUATIONS MAY BE REDUCED TO A SINGLE VECTOR EQUATION -

$$\textcircled{3} \qquad \nabla^2 \underline{B} - \frac{4\pi\mu}{\rho} \frac{\partial \underline{B}}{\partial t} = 0$$

WHICH FOR THE y COORDINATE YIELDS -

$$\textcircled{4} \qquad \frac{\partial^2 B_y}{\partial x^2} + \frac{\partial^2 B_y}{\partial y^2} - \frac{4\pi\mu}{\rho} \frac{\partial B_y}{\partial t} = 0$$

EQUATION ① MAY BE WRITTEN -

$$\textcircled{5} \qquad \underline{B_y}\big|_{y=0} = \text{REAL PART OF } B_0 \varepsilon^{j\left[\frac{\pi}{\tau}(v_x t - x)\right]} \text{ GAUSS}$$

OR IN COMPLEX FORM -

$$\textcircled{6} \qquad \vec{B}_y\big|_{y=0} = B_0 \varepsilon^{j\left[\frac{\pi}{\tau}(v_x t - x)\right]}$$

THE GENERAL SOLUTION FOR OTHER VALUES OF y WILL BE

$$\textcircled{7} \qquad \vec{B}_y = \vec{B}\, \varepsilon^{j\left[\frac{\pi}{\tau}(v_x t - x)\right]} .$$

WHERE $\vec{B}$ IS A COMPLEX FUNCTION OF y ONLY, THEN

$$\textcircled{8} \qquad \frac{\partial \vec{B}_y}{\partial t} = j\frac{\pi}{\tau} v_x \vec{B}_y$$

AND $\dfrac{\partial^2 \vec{B}_y}{\partial x^2} = -\left(\dfrac{\pi}{\tau}\right)^2 \vec{B}_y$

EQUATION ④ MAY NOW BE WRITTEN –

$$⑨ \qquad \frac{\partial^2 \vec{B}_y}{\partial y^2} - \vec{k}^2 \vec{B}_y = 0$$

WHERE $\vec{k} = u + jv = \sqrt{\alpha + j\beta} = \left[\frac{\sqrt{\alpha^2+\beta^2}+\alpha}{2}\right]^{\frac{1}{2}} + j\left[\frac{\sqrt{\alpha^2+\beta^2}-\alpha}{2}\right]^{\frac{1}{2}}$

$$\alpha = \left(\frac{\pi}{T}\right)^2 \qquad \beta = \frac{4\pi\mu v_x}{T\rho} = \frac{4\mu T v_x \alpha}{\rho}$$

THE GENERAL SOLUTION IS –

$$⑩ \qquad \vec{B}_y = \left[A_1 \cosh \vec{k}y + A_2 \sinh \vec{k}y\right] \varepsilon^{j\sqrt{\alpha}(v_x t - x)}$$

FROM THE DIVERGENCE THEOREM –

$$⑪ \qquad \vec{B}_x = -j\frac{\vec{k}}{\sqrt{\alpha}}\left[A_1 \sinh \vec{k}y + A_2 \cosh \vec{k}y\right] \varepsilon^{j\sqrt{\alpha}(v_x t - x)}$$

FROM ⑥ AND ⑩ $A_1 = B_0$ AT $y = 0$. AT $y = \delta$ $B_x = \mu H_x = 0$ $(\mu \to \infty)$. THIS LEADS TO –

$$⑫ \qquad \vec{B}_y = B_0 \frac{\cosh[\vec{k}(\delta - y)]}{\cosh(\vec{k}\delta)} \varepsilon^{j\sqrt{\alpha}(v_x t - x)} \quad \text{GAUSS}$$

$$\vec{B}_x = j\frac{\vec{k}}{\sqrt{\alpha}} B_0 \frac{\sinh[\vec{k}(\delta - y)]}{\cosh(\vec{k}\delta)} \varepsilon^{j\sqrt{\alpha}(v_x t - x)}$$

ALSO

$$⑬ \qquad \underline{G} = \frac{1}{4\pi\mu} \nabla \times \underline{B}$$

OR $\vec{G}_3 = \frac{1}{4\pi\mu}\left[\frac{\partial \vec{B}_y}{\partial x} - \frac{\partial \vec{B}_x}{\partial y}\right] = -\frac{v_x B_0}{\rho} \frac{\cosh[\vec{k}(\delta - y)]}{\cosh(\vec{k}\delta)} \varepsilon^{j\sqrt{\alpha}(v_x t - x)}$

$$= -\frac{v_x}{\rho} \vec{B}_y \quad \text{ABAMPS/CM}^2$$

AND

$$⑭ \qquad \vec{E}_3 = \rho \vec{G}_3 = -v_x \vec{B}_y \quad \text{ABVOLTS/CM}$$

THE POYNTING VECTOR IS -

(15) $\underline{P} = \frac{1}{4\pi}[\underline{E} \times \underline{H}] = \frac{1}{4\pi\mu}[\underline{E} \times \underline{B}]$ ERGS/SEC/CM²

POWER FLOWS INTO THE SHIELD NORMAL TO THE x_3 PLANE, HENCE

(16) $P_y = \frac{1}{4\pi\mu} \underline{E_3 B_x}\Big|_{y=0}$

THE REAL PARTS OF $\vec{E}_3$ AND $\vec{B}_x$ AT $y=0$ ARE -

(17) $\underline{E_3}\Big|_{y=0} = -v_x B_0 \cos[\sqrt{\kappa}\,(v_x t - x)]$ ABVOLTS/CM

$$\underline{B_x}\Big|_{y=0} = -\frac{B_0}{\sqrt{\kappa}} \frac{[v\sinh 2u\delta + u\sin 2v\delta]\cos[\sqrt{\kappa}(v_x t - x)] + [u\sinh 2u\delta - v\sin 2v\delta]\sin[\sqrt{\kappa}(v_x t - x)]}{\cosh 2u\delta + \cos 2v\delta}$$

GAUSS

AND THE AVERAGE POWER DENSITY ACROSS THE x_3 PLANE IS -

(18) $P_{y(AVE)} = \frac{v_x B_0^2}{8\pi\mu\sqrt{\kappa}} \frac{v\sinh 2u\delta + u\sin 2v\delta}{\cosh 2u\delta + \cos 2u\delta}$ ERGS/SEC/CM.²

IF THE MOTOR HAS k POLE PAIRS AND EACH POLE SPAN IS T CM. LONG, THE AVERAGE POWER PER CM. OF SHIELD LENGTH IN THE 3 DIRECTION IS -

(19) $P_{AVE} = 2kT P_{y(AVE)} = \frac{v_x k B_0^2}{4\mu\alpha} \frac{v\sinh 2u\delta + u\sin 2v\delta}{\cosh 2u\delta + \cos 2v\delta}$

ERGS/SEC/CM.

FOR $\delta \ll 1$,

(20) $P_{AVE} = \frac{kT v_x^2 B_0^2}{\rho} \varepsilon\left[1 - \frac{2}{3}\alpha\delta^2 + \frac{2}{15}(3\alpha^2 - \beta^2)\delta^4 - \cdots\right]$

THE FLUX DENSITY AT THE ARMATURE SURFACE ($y = \delta$) IS

(21) $$B_y|_s = \frac{\sqrt{2}\, B_0 \cos[\alpha(v_x t - x) - \phi]}{\sqrt{\cosh 2u\delta + \cos 2v\delta}} \quad \text{GAUSS}$$

WHERE $\tan\phi = \tanh u\delta \tan v\delta$

THUS, THE FLUX EXPERIENCES A CHANGE IN AMPLITUDE AND PHASE IN PASSING THROUGH THE SLEEVE. THE FRACTIONAL CHANGE IN AMPLITUDE IS —

(22) $$\frac{|B_{y=\delta}|}{|B_{y=0}|} = \frac{\sqrt{2}}{\sqrt{\cosh 2u\delta + \cos 2v\delta}}$$

FOR $\delta \ll 1$

(23) $$\frac{|B_{y=\delta}|}{|B_{y=0}|} = 1 - \frac{\alpha}{2}\delta^2 + \frac{1}{24}(5\alpha^2 - 2\beta^2)\delta^4 - \cdots$$

APPENDIX III

RELIABILITY ANALYSIS OF COMPONENTS FOR HALF-WATT BRUSHLESS DC MOTOR (SFCo P/N Eng 9847)

LIST OF TABLES

Switch No. 1

Part Number	Schematic Symbol	Part Nomenclature	Type	Failure Rate λ	No. of Parts n	nλ
Eng 4050	A1	Photo Device	LS-600	.010	1	.010
	R17	Resistor	Mil-R-11 220K .1w	.001	1	.001
	R18	Resistor	Mil-R-11 510K .1w	.001	1	.001
	R19	Resistor	Mil-R-11 33K .1w	.001	1	.001
	Q10	Transistor	2N2524	.020	1	.020
	R20	Resistor	Mil-R-11 20K .1w	.001	1	.001
	Q11	Transistor	2N2350A	.020	1	.020
	R21	Resistor	Mil-R-11 5.1K .1w	.001	1	.001
	Q12	Transistor	STC 2401	.020	1	.020
	R22	Resistor	Mil-R-26 1 .1w	.015	1	.015
	CR4	Diode	PS510B 1N645	.00012	1	.00012
			Component failure rate, %/1000 hours			.09012

$R = e^{-\lambda t}$ $\quad t = 10,000$ hours

$R = e^{-.09012 \times 10000 \times 10^{-5}}$

$R = .9910$ or 99.1%

$R = e^{-.00789}$ $\quad t = 8760$

$R = .9921$

TABLE 1
SWITCH 1 FAILURE RATE

Switch No. 2

Part Number	Schematic Symbol	Part Nomenclature	Type	Failure Rate λ	No. of Parts n	nλ
Eng 4050	A2	Photo Device	LS-600	.010	1	.010
	R11	Resistor	Mil-R-11 220K .1w	001	1	.001
	R12	Resistor	Mil-R-11 510K .1w	.001	1	.001
	R13	Resistor	Mil-R-11 20K .1w	.001	1	.001
	R14	Resistor	Mil-R-11 33K .1w	.001	1	.001
	Q7	Transistor	2N2524	.020	1	.020
	R15	Resistor	Mil-R-11 5.1K .1w	.001	1	.001
Eng 4051	Q8	Transistor	2N1132B	.020	1	.020
	Q9	Transistor	STC 2401	.020	1	.020
	CR3	Diode	PS510B 1N645	.00012	1	.00012
				Component failure rate, %/1000 hours		.07512

$R = e^{-\lambda t}$ $\quad t = 10{,}000$ hours

$R = e^{-.07512 \times 10000 \times 10^{-5}}$

$R = .9925$ or 99.25%

$R = e^{-.00658}$ $\quad t = 8760$ hours

$R = .99342$

TABLE 2
SWITCH 2 FAILURE RATE

Switch No. 3

Part Number	Schematic Symbol	Part Nomenclature	Type	Failure Rate λ	No. of Parts n	nλ
Eng 4050	A3	Photo Device	LS-600	.010	1	.010
	R23	Resistor	Mil-R-11 220K .1w	.001	1	.001
	R24	Resistor	Mil-R-11 510K .1w	.001	1	.001
	R25	Resistor	Mil-R-11 33K .1w	.001	1	.001
	Q13	Transistor	2N2524	.020	1	.020
	R26	Resistor	Mil-R-11 20K .1w	.001	1	.001
	Q14	Transistor	2N2350A	.020	1	.020
	R27	Resistor	Mil-R-11 5.1K .1w	.001	1	.001
	Q15	Transistor	STC 2401	.020	1	.020
	R28	Resistor	Mil-R-26 1 1w	.015	1	.015
	CR5	Diode	P5510B 1N645	.00012	1	.00012
			Component failure rate, %/1000 hours			.09012

$R = e^{-\lambda t}$ $\quad t = 10,000$ hours

$R = e^{-.09012 \times 10000 \times 10^{-5}}$

$R = .9910$ or 99.1%

$R = .9921$ $\quad t = 8760$ hours

TABLE 3
SWITCH 3 FAILURE RATE

Switch No. 4

Part Number	Schematic Symbol	Part Nomenclature	Type	Failure Rate λ	No. of Parts n	nλ
Eng 4050	A4	Photo Device	LS-600	.010	1	.010
	R1	Resistor	Mil-R-11 220K .1w	.001	1	.001
	R2	Resistor	Mil-R-11 510K .1w	.001	1	.001
	R3	Resistor	Mil-R-11 20K .1w	.001	1	.001
	R4	Resistor	Mil-R-11 33K .1w	.001	1	.001
	Q1	Transistor	2N2524	.020	1	.020
	R5	Resistor	Mil-R-11 5.1K .1w	.001	1	.001
Eng 4051	Q2	Transistor	2N1132B	.020	1	.020
	Q3	Transistor	STC 2401	.020	1	.020
	CR1	Diode	PS510B 1N645	.00012	1	.00012
				Component failure rate, %/1000 hrs.		.07512

$R = e^{-\lambda t}$ $\quad t = 10,000$ hours

$R = e^{-.07512 \times 10000 \times 10^{-5}}$

$R = .9925$ or 99.25%

$R = .99342$ $\quad t = 8760$

TABLE 4
SWITCH 4 FAILURE RATE

Switch No. 5

Part Number	Schematic Symbol	Part Nomenclature	Type	Failure Rate λ	No. of Parts n	nλ
Eng 4050	A5	Photo Device	LS-600	.010	1	.010
	R29	Resistor	Mil-R-11 220K .1w	.001	1	.001
	R30	Resistor	Mil-R-11 510K .1w	.001	1	.001
	R31	Resistor	Mil-R-11 33K .1w	.001	1	.001
	Q16	Transistor	2N2524	.020	1	.020
	R32	Resistor	Mil-R-11 20K .1w	.001	1	.001
	Q17	Transistor	2N2350A	.020	1	.020
	R33	Resistor	Mil-R-11 5.1K .1w	.001	1	.001
	Q18	Transistor	STC 2401	.020	1	.020
	R34	Resistor	Mil-R-26 1 1w	.015	1	.015
	CR6	Diode	1N645	.00012	1	.00012
					Component failure rate, %/1000 hrs.	.09012

$R = e^{-\lambda t}$ $\quad t = 10{,}000$ hours

$R = e^{-.09012 \times 10000 \times 10^{-5}}$

$R = .9910$ or 99.10%

$R = .9921$ $\quad t = 8760$

TABLE 5
SWITCH 5 FAILURE RATE

Switch No. 6

Part Number	Schematic Symbol	Part Nomenclature	Type	Failure Rate λ	No. of Parts n	nλ
Eng 4050	A6	Photo Device	LS-600	.010	1	.010
	R6	Resistor	Mil-R-11 220K .1w	.001	1	.001
	R7	Resistor	Mil-R-11 510K .1w	.001	1	.001
	R8	Resistor	Mil-R-11 20K .1w	.001	1	.001
	R9	Resistor	Mil-R-11 33K .1w	.001	1	.001
	Q4	Transistor	2N2524	.020	1	.020
	R10	Resistor	Mil-R-11 5.1K .1w	.001	1	.001
Eng 4051	Q5	Transistor	2N1132B	.020	1	.020
	Q6	Transistor	STC 2401	.020	1	.020
	CR2	Diode	1N645	.00012	1	.00012
				Component failure rate, %/1000 hrs.		.07512

$R = e^{-\lambda t}$ $\quad t = 10,000$ hours

$R = e^{-.07512 \times 10000 \times 10^{-5}}$

$R = .9925$ or 99.25%

$R = .99342$ $\quad t = 8760$

TABLE 6
SWITCH 6 FAILURE RATE

Starting Circuit

Part Number	Schematic Symbol	Part Nomenclature	Type	Failure Rate λ	No. of Parts n	nλ
	R35	Resistor	Mil-R-26 1K 1w	.015	1	.015
	Q19	Transistor	2N2350A	.020	1	.020
	R36	Resistor	Mil-R-11 20K .1w	.001	1	.001
	Q20	Transistor	2N2524	.020	1	.020
	R37	Resistor	Mil-R-11 22K .1w	.001	1	.001
	R38	Resistor	Mil-R-11 22K .1w	.001	1	.001
	C-1	Capacitor	150D335 x 0015A2	.008	1	.008
	CR7	Diode	Unitrode UT 261	.010	1	.010
	CR8	Diode	Unitrode UT 261	.010	1	.010
	CR9	Diode	TMD 41	.010	1	.010
	CR10	Diode	TMD 41	.010	1	.010
	CR11	Diode	TMD 41	.010	1	.010
	CR12	Diode	TMD 41	.010	1	.010
	R39	Resistor	Mil-R-11	.001	1	.001
		Aux. Winding		.060	1	.060
				Component failure rate, %/1000 hrs.		.187

$R = e^{-\lambda t}$ $t = 10{,}000$ hours

$R = e^{-.187 \times 10000 \times 10^{-5}}$

$R = .981$ or 98.1%

$R = .984$ $t = 8760$

TABLE 7
STARTING CIRCUIT FAILURE RATE

Miscellaneous Series Parts

Part Number	Schematic Symbol	Part Nomenclature	Type	Failure Rate λ	No. of Parts n	nλ
		Main Winding		.020	1	.020
		Lamp	Lamps Inc. No. 9	.020	1	.020
Eng 9839	T. B. 1			.028	1	.028
Eng 9839	T. B. 2			.036	1	.036
Eng 9841	T. B. 4			.036	1	.036
Eng 9840	T. B. 5			.036	1	.036
	R-16	Resistor	Mil-R-26 1 1w	.015	1	.015

t = 10,000 hours t = 8760

$R_{mw} = e^{-\lambda t} = e^{-.020 \times 10000 \times 10^{-5}} = .998$ .9983

$R_{l} = e^{-\lambda t} = e^{-.075 \times 10000 \times 10^{-5}} = .9980$ .998

$R_{tb1} = e^{-\lambda t} = e^{-.028 \times 10000 \times 10^{-5}} = .997$ .9976

$R_{tb2-5} = e^{-\lambda t} = e^{-.036 \times 10000 \times 10^{-5}} = .994$ .99685

$R_{r16} = e^{-\lambda t} = e^{-.015 \times 10000 \times 10^{-5}} = .9985$ .9987

TABLE 8
MISCELLANEOUS SERIES PARTS FAILURE RATE